



**University of
Zurich** ^{UZH}

Harmonizing the processing chain of water measurements with a data exploitation platform

Tested with in situ radiometric measurements of optically complex waters

GEO 511 Master's Thesis

Author

Alicia Hug
15-721-210

Faculty representative

Prof. Dr. Alexander Damm

Supervised by

Prof. Dr. Alexander Damm
Dr. Daniel Odermatt

30.09.2020

Department of Geography, University of Zurich

1 Abstract

In situ spectral measurements of water are used to monitor water systems, validate, and calibrate satellite data and gain understanding of the processes between radiation and the water body.

Above-water measurements are used to derive the water-leaving radiance, respectively the remote sensing reflectance, which is used to derive spectral information about a water body. A lot of approaches regarding the execution of such measurements exist, starting on how should be measured (measurement protocol), how the data should be processed, and which instruments should be used to acquire the data. These different approaches lead to high differences in the output data. Such differences should be minimized by harmonizing the processing chain and a defined standard to gain a higher comparability of the data. The harmonization of the processing chain is achieved by using a data exploitation platform, e.g. SPECCHIO, which helps with the data handling, recording of metadata, data exchange between scientists and the standardization and consolidation of the measurement methods.

For the case study, measurements were conducted on Greifensee with the instrument RAMSES TriOS. The azimuth angles between the single measurements are unknown and the instrument was fixed to a $\theta = 40^\circ$ zenith viewing angle.

Tests about the prevailing measurement conditions – hazy vs. clear – sky showed no significant difference. Also, no divergence between the two measurement positions could be seen. Tests about the measurement protocols showed that the output data of the different azimuth angles had a high divergence and that azimuth angles too far away from the sun result in outliers (also supported by the mean average error (MAE)). The MAE was applied to the zenith viewing angles and showed that the difference was higher for shorter than for longer wavelengths. The MAE was also applied to the four different processing methods, but the resulting values were not significant enough to suggest a ‘best’ working approach.

A requirement analysis was conducted in the end, which shows what needs to be considered when conducting water measurements

The findings in the literature review and the case study suggest that in the field of spectral water measurements, there is still a need to find a more consistent and standardized processing chain to reduce differences in the data.

2 Acknowledgements

First, I would like to thank my supervisors Alexander Damm and Daniel Odermatt for their support and patience with my questions, the regular meetings, and the understanding with the difficult situation due to COVID-19 and my accident in February.

I would also like to thank the members from the RSWS group for their inputs and help, Jasmin Kesselring, Remika Gupana, Joan Tracy Sturm, Rifat Ahmed and especially Bastian Buman, who helped me with the Python scripts and my questions regarding SPECCHIO.

I would also like to thank the members from the Eawag group for their inputs and help, again Remika Gupana, James Runnalls, Nico Mölg and especially Abolfazl ‘Fazel’ Irani Rahaghi for his help with the scripting in Python.

In addition, I would like to thank my family and friends for their support, especially my friend from University Michelle Müller.

Table of Contents

1	ABSTRACT	II
2	ACKNOWLEDGEMENTS	III
3	LIST OF FIGURES	VIII
4	LIST OF TABLES	XI
5	LIST OF ABBREVIATIONS	XII
6	INTRODUCTION	1
6.1	Importance and challenges of in situ radiometric measurements	1
6.2	Research Gap	2
6.3	Research question and hypothesis	2
7	BACKGROUND	3
7.1	Optical properties of water	3
7.1.1	Definitions radiometric quantities.....	4
7.1.2	Apparent optical properties	5
7.1.3	Inherent optical properties.....	7
7.2	Field spectroscopy vs. imaging spectroscopy	7
7.3	Terrestrial and aquatic reflectance measurements	8
7.3.1	Above-water measurements	8
7.3.1.1	Above-water radiometry with sky radiance measurement and skylight removal	8
7.3.1.2	On-water radiometry with skylight blocked	8
7.3.2	Below water measurements.....	9
7.3.2.1	Underwater radiometry using fixed-depth measurements	9
7.3.2.2	Underwater radiometry using vertical profile.....	10
7.3.2.3	Underwater radiometry with three sensors	10
7.4	Spectral libraries and databases / data exploitation platforms	11
7.4.1	Spectral libraries	11

7.4.2	Spectral databases / data exploitation platforms	12
7.4.2.1	USGS Spectral Library	12
7.4.2.2	SpectraProc	12
7.4.2.3	SPECCHIO	13
8	METHODS	14
8.1	Measurement protocols.....	15
8.1.1	NASA Ocean Optics protocols	15
8.1.2	ESA FRM4SOC protocols.....	15
8.2	Processing.....	16
8.2.1	Fresnel reflectance factor by Ruddick et al. (2019a)	17
8.2.2	Clear / cloudy sky by Ruddick et al. (2006).....	17
8.2.3	Spectral ‘fingerprint’ by Simis & Olsson (2013).....	17
8.2.4	3C model by Groetsch et al. (2017)	18
8.3	Sensors / Measurement instruments.....	19
8.3.1	WISP-3.....	19
8.3.2	RAMSES TriOS.....	20
8.3.3	ASD FieldSpec.....	21
8.3.4	AC-S	21
8.3.5	ECO-VSF 3	22
8.3.6	Data Handling	23
8.3.6.1	WISPweb	23
8.3.6.2	TriOS MSDA_XE.....	25
8.4	Case Study.....	26
8.4.1	Study Site	26
8.4.2	Instrument and Methods.....	26
8.4.3	Data	27
8.4.4	Processing	27
8.4.5	Data evaluation	28
8.4.5.1	Outlier determination.....	28
8.4.5.2	Mean average error (MAE).....	29
9	RESULTS	29
9.1	Measurements Greifensee.....	29

9.1.1	Outliers.....	29
9.1.2	Measurement conditions	34
9.1.3	Measurement protocols	36
9.1.4	Processing schemes.....	38
9.2	Similarities and differences of the sensors	41
9.2.1	Sensor accuracy.....	42
9.3	Requirement analysis.....	43
9.3.1	Measurement setup	43
9.3.2	Sensors	43
9.3.3	Data	44
9.3.4	Measurement protocols	44
9.3.5	Processing schemes.....	44
9.3.6	Data exploitation platform	45
9.3.7	Standardization.....	46
9.3.8	Data quality	47
9.4	Gaps.....	47
10	DISCUSSION	48
10.1	Processing chain components and their impact on reflectance retrievals	48
10.1.1	Measurement protocols	48
10.1.2	Instruments.....	48
10.1.3	Processing schemes.....	49
10.2	Reliability of case study	51
10.2.1	Measurement setup and sensor.....	51
10.2.2	Measurement protocols and processing	51
10.2.3	Requirement analysis for spectral measurements on lakes	52
10.3	Towards harmonized in situ measurements using a data exploitation platform..	52
11	CONCLUSION.....	53
12	REFERENCES	54
13	APPENDIX	57

13.1	Outliers	57
13.2	Measurement conditions	60
13.3	Processing schemes	61
	PERSONAL DECLARATION	66

3 List of figures

Figure 1: A schematic diagram of the interaction between radiation, the atmosphere, water body and the sensor. Important here is the incident solar radiation which gets either reflected at the water surface or refracted at the bottom of the lake. In the water body itself it can get absorbed or scattered at particles like phytoplankton, cyanobacteria, colored dissolved organic matter (CDOM) or suspended matter (SPM). The remaining signal gets absorbed or scattered in the atmosphere and then reaches the sensor (Modified after Dörnhöfer & Oppelt (2016)).....	3
Figure 2: Illustration of definitions of water-leaving radiance, L_w , above and below water upwelling radiances, $Lu_0 +$ and $Lu_0 -$, above-water downwelling (sky) radiance, L_d , above-water upwelling radiance from reflection at the air-water interface ('skylint'), L_r , and downwelling irradiance, $Ed_0 +$. With θ_v as the viewing zenith angle. (Modified after Ruddick et al. (2019a)).....	4
Figure 3: Viewing nadir angle θ measured from downward vertical axis (left) and azimuth viewing angle φ and relative azimuth angle $\Delta\varphi$ measured clockwise from North and sun (right) (Modified after Ruddick et al. (2019a))	5
Figure 4: Schematic of 'Above-water radiometry with sky radiance measurement and skylint removal' (Modified after Ruddick et al. (2019a)).....	9
Figure 5: Schematic of 'On-water radiometry with skylight blocked' (Modified after Ruddick et al. (Ruddick et al., 2019a)).....	9
Figure 6: Schematic of 'Underwater radiometry using fixed-depth measurements' (Modified after Ruddick et al. (2019a)).....	11
Figure 7: Schematic of 'Underwater radiometry using vertical profile' (Modified after Ruddick et al. (2019a)).....	11
Figure 8: Schematic (lower illustration) of 'Underwater radiometry with three sensors' (Modified after Dev & Shanmugam (2014)).....	11
Figure 9: SpectraProc Windows Application with the input interface, spectral database and output interface (left) and the spectral data processing in the database shown by the operations and data stored in the memory (right). (Modified after Hueni & Tuohy (2006)).....	13
Figure 10: Basic layout of SPECCHIO, showing the data sources and the data retrieval. Spectral files are fed into the SPECCHIO database. (Modified after Bojinski et al. (2003))	14
Figure 11: Handling of WISP-3 (left) and an overview of the three radiometers (right) (Modified after Hommersom et al. (2012)).....	20
Figure 12: Setup of RAMSES TriOS with the three sensor Lu , $Lsky$ and Ed (from left to right) (Picture by Alicia Hug).....	20
Figure 13: Possible field setup of ASD Fieldspec, for measuring a terrestrial surface. (Modified after Malvern Panalytical (2019))	21

Figure 14: AC-S Sensor (Modified after Sea-Bird Scientific (2018))	21
Figure 15: Sensor ECO-VSF 3 (Modified after WET Labs (2006)).....	22
Figure 16: Screenshot of the user interface of WISPweb from the Eawag account. The measurements are sorted by the region Greifensee and by the starting and end date. Each measurement has an ID, date, region and station name. For each measurement water quality parameters are derived from the optical information (Chlorophyll-a (Chl-a), Total Suspended Particulate Matter (TSM), Phycocyanin (CPC) and a measure for Transparency (Kd)). Comments about the floating layer, GPS coordinates and cloud cover can be added. (Screenshot taken from https://wispweb.waterinsight.nl/ , 19.07.2020)	23
Figure 17: Screenshots of the downwelling irradiance (Ed), downwelling radiance (Ld) and upwelling radiance (Lu) from the first measurement from Figure 16. The irradiance reads on the right y-axis and both radiance read on the left y-axis. (Screenshot taken from https://wispweb.waterinsight.nl/ , 19.07.2020)	24
Figure 18: Screenshot of the Subsurface Irradiance Reflectance (R0-) from the first measurement from Figure 16. (Screenshot taken from https://wispweb.waterinsight.nl/ , 19.07.2020).....	24
Figure 18: Screenshot of the software MSDA_XE, with the charts for the three sensors on the left side window and the control panels on the three window on the right side. The sampling can be executed over any of the three ‘Sample’ buttons. Pressure and inclination can be seen in the SAMIP_510A window and also the integrationtime can be set in this window. (Screenshot by Alicia Hug).....	25
Figure 19: Measurement setup of the first position with the approximate positions of the eight measurement points (azimuth angles unknown). The dark orange line resembles the sunset, the yellow line the sunbeam for the current time, and the light orange line the sunrise. For the second position the setup was the same, where 1 = 9, 2 = 10, 3 = 11, 4 = 12, 5 = 13, 6 = 14, 7 = 15 and 8 = 16. (Screenshot taken from https://www.sonnenverlauf.de/#/47.3651,8.6654,14/2020.01.21/10:46/1/3 , 13.06.2020).....	27
Figure 20: A 360° view (left) of the second measurement position, where the haze is not visible (photo by Daniel Odermatt) and a picture from the first measurement position (right), where the haze can be seen (photo by Alicia Hug).....	28
Figure 21: Remote sensing reflectance [sr^{-1}] from measurements 1-4 per wavelength [nm], with the outlier measurement number 4 in yellow. Shown are the results from the processing schemes from Ruddick et al. (2019a) and from Simis & Olsson (2013) (all graphs from the other methods can be found in the Appendix 13.1).	30
Figure 22: Remote sensing reflectance [sr^{-1}] from measurements 5-8 per wavelength [nm], with the outlier measurement number 8 in yellow. Shown are the results from the processing schemes from Ruddick et al. (2019a) and from Simis & Olsson (2013) (all graphs from the other methods can be found in the Appendix 13.1).	31

Figure 23: Remote sensing reflectance [sr^{-1}] from measurements 9-12 per wavelength [nm], with the outlier measurement number 12 in yellow. Shown are the results from the processing schemes from Ruddick et al. (2019a) and from Simis & Olsson (2013) (all graphs from the other methods can be found in the Appendix 13.1).	32
Figure 24: Remote sensing reflectance [sr^{-1}] from measurements 13-16 per wavelength [nm], with the outlier measurement number 16 in yellow. Shown are the results from the processing schemes from Ruddick et al. (2019a) and from Simis & Olsson (2013) (all graphs from the other methods can be found in the Appendix 13.1).	33
Figure 25: Comparison of two measuring positions (two top graphs vs. two bottom graphs) and of the ‘sunny’ (measurements 1-3 & 9-11) and the ‘hazy’ side (measurements 5-7 & 13-15) (all graphs from the other methods can be found in the Appendix 13.2).	36
Figure 26: Remote sensing reflectance of measurements 2, 6, 10 and 14 with different zenith viewing angles, 35° , 38° , 39° , 40° , 41° , 42° and 45° , processed with the method by Ruddick et al. (2019a).	37
Figure 27: Comparison of the four processing schemes of measurements 1-3 (all graphs from the other methods can be found in the Appendix 13.3).	40

4 List of tables

Table 1: Overview of the five introduced sensors with the suggested measurement protocols and parameter estimation (Dev and Shanmugam, 2014; Hommersom et al., 2012; Sea-Bird Scientific, 2013; Simis and Olsson, 2013; Tilstone et al., 2017; TriOS Mess- und Datentechnik GmbH, 2013; WET Labs, 2007).	22
Table 2: Mean average error [$\div 1000$] of the observed values of all four processing schemes (between 0 and 1). The modeled values are the chosen ‘best’ measurements 2, 6, 10 and 14. Values in red symbolize the highest values.....	34
Table 3: Mean average error [$\div 1000$] between all four methods for the best measurements 2, 6, 10 and 14. Red values symbolize the highest and green the lowest values.....	40
Table 4: Intercomparison of WISP-3, RAMSES TriOS and ASD FieldSpec (Modified after Hommersom et al. (2012)).	42

5 List of abbreviations

AC-S	Absorption and attenuation sensor
AOPs	Apparent optical properties
ASD	Analytical Spectral Devices
CDOM	Colored dissolved organic matter
DBMS	Database management system
E_d	Downwelling irradiance
ESA	European Space Agency
FOV	Field of view
IOPs	Inherent optical properties
LIMNADES	Lake Bio-optical Measurements and Matchup Data for Remote Sensing
L_r	Water surface-reflected radiance
L_{sky} / L_d	Downwelling sky radiance
L_u / L_t	(Total) Upwelling water radiance
L_w	Water-leaving radiance
MAE	Mean average error
MERMAID	Envisat MERis MATCHUP In situ Database
MSDA_XE	Multi Sensor Data Acquisition System – Extended Edition
NASA	National Aeronautics and Space Administration
NIR	Near-infrared
OCDB	Copernicus Ocean Colour In situ Database
OMS	Optical monitoring systems
ρ_F	Fresnel reflection coefficient factor
ρ_{sky}	Air-water surface reflectance coefficient
RCR	Remote cosine receptor
R_{rs}	Remote sensing reflectance
SeaBASS	SeaWiFS bio-optical archive and storage system
SPM	Suspended particulate matter
SWIR	Short-wave infrared
TACCS	Tethered Attenuation Coefficient Chain Sensor
USGS	United States Geological Survey
UV	Ultraviolet
VIS	Visible spectrum
VSF	Volume scattering function
VSWIR	Visible-to-shortwave infrared wavelength range
WISP	Water Insight Spectrometer

6 Introduction

Remote sensing is a convenient method to monitor inland and coastal water systems, because it covers large areas and shows the spatial distribution of several variables. Among many possible applications, it is often used for water studies and resource management (Dekker et al., 2002).

At first remote sensing was used for oceans because it is the best technique to cover such far-reaching areas but ocean waters are relatively optically simple, as they are only affected by phytoplankton and therefore already simple systems can assess enough information about these water systems (Dekker et al., 2002). Monitoring inland and coastal waters however have different characteristics, they have high temporal and spatial variations in water quality parameters and are affected by anthropogenic influences (Giardino et al., 2019) and have a greater variability in their optical properties (Dekker et al., 2002), more advanced remote sensing systems, which use imaging spectroscopy, are necessary (Giardino et al., 2019).

6.1 Importance and challenges of in situ radiometric measurements

Imaging spectroscopy data can be measured in space, from airborne platforms and in situ. Satellites and airborne systems can measure large areas with single images, but the measurements are influenced by signals coming from the land surrounding the water body and often the spatial resolution is not high enough for small water bodies (Hommersom et al., 2012). Whereas hand-held autonomous instruments are used for close-range in situ measurements and have the advantage that data is available almost instantly and small water bodies can be assessed more accurately (Hommersom et al., 2012). In situ measurements are used to monitor water systems, assess water quality parameters, to compare reflectance spectra with satellite data (Dev and Shanmugam, 2014; Hueni et al., 2009), validate satellite products and to calibrate satellites (Dev and Shanmugam, 2014; Zibordi and Talone, 2020). This requires knowledge about radiometric quantities, optical properties of water and radiometric measurement basics. This will be further explained in the Background chapter. Instruments basically measure the light that is reflected by the water body (Hommersom et al., 2012). The main desired parameter from water measurements is the water-leaving radiance, respectively the remote sensing reflectance, which shows the spectral reflectance signature of a water body (Groetsch et al., 2017). The remote sensing reflectance is also used for the interpretation of ocean-color data (Mobley, 1999). It can be measured with satellite data as the top of atmosphere radiance or in situ with either in water or above-water optical measurement systems (OMS) on ships, fixed platforms or buoys (Tilstone et al., 2017). These measurements can be done with different sensors and measurement protocols and processed with different methods and both above and underwater measurements come with uncertainties (Tilstone et al., 2017). Possible error sources are for example the instrument or ship self-shading, that in turbid waters light gets attenuated quickly with increasing depth, or the separation of surface-reflectance and water-reflectance for above-water measurements (Gould,

R.W., Arnone, R.A., Sydor, 2001). The removal of the surface-reflectance to get the water-leaving radiance is difficult, as it varies spectrally and depends on wind (leads to waves), foam on the water surface, cloud cover and instrument orientation (Gould, R.W., Arnone, R.A., Sydor, 2001). Spectroradiometric measurements can additionally be unreliable because of the multidimensionality of the measurements, the instability of the measuring instruments and the uncertainty of the calibration factors for the instruments, the different methods to remove errors and the variations in the hemispherical distribution of incoming radiance in the field (Milton et al., 2009). Also, a lot of approaches exist to determine the surface-reflectance correctly. The amount of different systems, which have different calibrations and methods used and the different processing schemes, lead to introduced uncertainties, and the accuracy and comparison of data is affected (Tilstone et al., 2017). Additionally, with the advances in technology, more improved instruments, and higher numbers of different field-portable spectroradiometric devices exist on the market (Milton et al., 2009).

All these factors lead to a high diversity in the processing chain (measurement protocol – processing – instrument) and a high uncertainty which makes it difficult to compare data.

6.2 Research Gap

Right now, a lot of different approaches exist to conduct above-water measurements and the community does not always agree on the same practices. These different approaches compromise the comparability of in situ measurements when obtained across research groups by different operators with different instrumentation and measurement protocols. Therefore, this thesis aims to investigate available in situ approaches, including measurement protocols, processing schemes and instruments and to show what the differences are and how they influence the output data. The thesis additionally aims to provide strategies to minimize the diversity in the processing chain, e.g. by using a data exploitation platform to handle the data. For now already a lot of databases for satellite data and spectral libraries for spectral measurements of land surfaces exist, but none of them focus specifically on in situ radiometric measurements of water systems, or if they do they are not sophisticated enough to handle the whole processing chain. Therefore, also a requirement analysis will be conducted to develop a possible data exploitation platform which will work with data from spectral water measurements. This leads to the following research questions and hypothesis.

6.3 Research question and hypothesis

Differences in the processing chain (measurement protocols – processing - instruments) lead to uncertainties and errors in the generated output. It is hypothesized that a harmonization of the processing chain enables a higher comparability and robustness of in situ measurements. Such a harmonization can be facilitated with a data exploitation platform, as it will help with importing

large datasets of spectra and retrieval of the required data. To proof this hypothesis, the following questions need to be addressed.

- 1) What are the currently used instruments, measurement protocols and processing schemes regarding above-water radiometric measurements?
- 2) What are the differences between the instruments, measurement protocols and processing schemes for above-water radiometric measurements?
- 3) What is a possible requirement analysis for spectral measurements of water systems?
- 4) How does a data exploitation help with the data handling?

7 Background

7.1 Optical properties of water

Measuring the spectral signature of above or below a water surface can reveal information about the optically active components in the water body (Dekker et al., 2002). They can be measured with multi- or hyperspectral sensors (Heege and Fischer, 2004). Additionally, to the radiometric quantities, two types of spectral signatures are defined. Apparent optical properties (AOPs) such as reflectance depend on the ambient light field, measurement geometry, and water composition. While the inherent optical properties (IOPs), absorption and scattering, are insensitive to environmental conditions but depend on the water's composition only (Mobley, 1994) (see Figure 1).

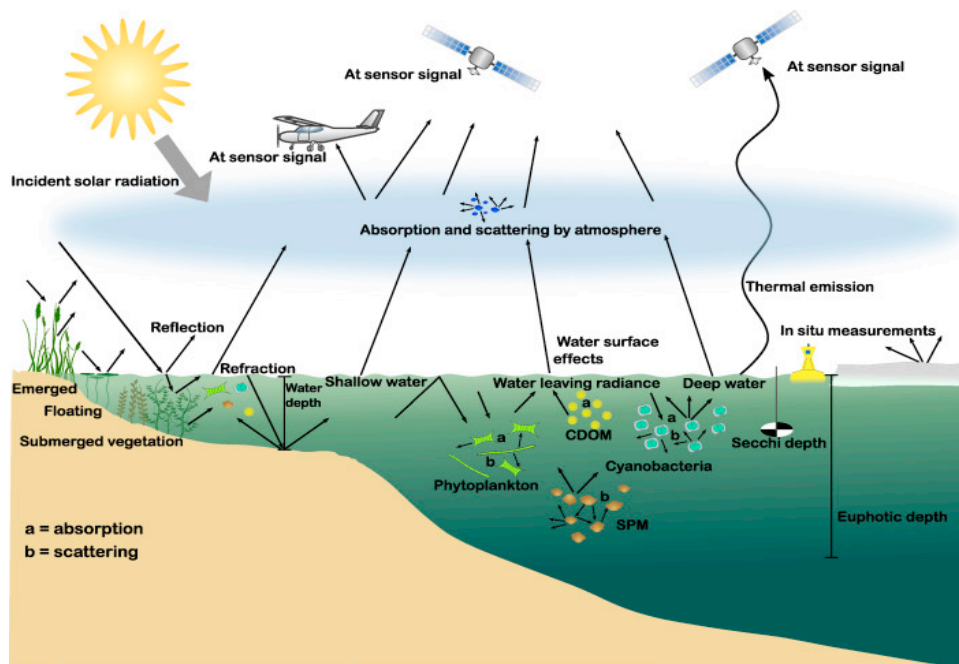


Figure 1: A schematic diagram of the interaction between radiation, the atmosphere, water body and the sensor. Important here is the incident solar radiation which gets either reflected at the water surface or refracted at the bottom of the lake. In the water body itself it can get absorbed or scattered at particles like phytoplankton, cyanobacteria, colored dissolved organic matter (CDOM) or suspended matter (SPM). The remaining signal gets absorbed or scattered in the atmosphere and then reaches the sensor (Modified after Dörnhöfer & Oppelt (2016)).

7.1.1 Definitions radiometric quantities

Determining the spectral signature of a water body requires the measurement of radiometric quantities. The radiance, which is the flux density of radiance energy per unit solid angle and per unit projected area of the radiating surface and the irradiance, which is the flux of radiant power per unit area (Mobley, 1994). The planar irradiance is the irradiance that gets produced when a collimated beam of photons intercepts a plane surface (e.g. sensor surface) and is proportional to the cosine of the angle between the photon directions and the collector surface (Mobley, 1994). The scalar irradiance refers to the irradiance that gets measured if the sensor is equally sensitive to all downwelling light (Mobley, 1994). The radiative transfer for above-water measurements therefore happens as followed (Ruddick et al., 2019a) (see Figure 2). The radiance which travels through the air and eventually hits the water body is called the downwelling sky radiance (L_d/L_{sky}). There it gets either scattered at the surface and is called reflected radiance (L_r) or travels through the water body until it gets either absorbed or scattered at particles in the water itself or at the ground. The part of the scattered irradiance in the water body which travels back to the surface is called upwelling radiance L_u^{0-} and as soon it leaves the water body it is called the water-leaving radiance L_w . The reflected radiance L_r and water-leaving radiance L_w together are the upwelling radiance L_u^{0+} .

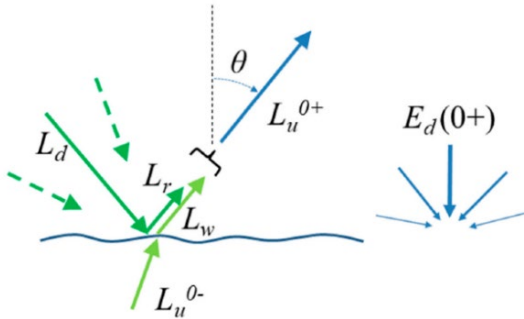


Figure 2: Illustration of definitions of water-leaving radiance, L_w , above and below water upwelling radiances, L_u^{0+} and L_u^{0-} , above-water downwelling (sky) radiance, L_d , above-water upwelling radiance from reflection at the air-water interface ('skylight'), L_r , and downwelling irradiance, E_d^{0+} . With θ_v as the viewing zenith angle. (Modified after Ruddick et al. (2019a))

The measurement protocols to measure L_w , are grouped into four categories: Underwater radiometry either using fixed-depth measurements or vertical profiles, above-water radiometry with sky radiance measurement and skylight removal or on-water radiometry with skylight blocked (Ruddick et al., 2019a). The sensors that are used are either downward or upward pointing or both (Ruddick et al., 2019a). Above-water spectrometers for example measure $E_d^{0+}(\lambda)$ in $\text{Wm}^{-2} \text{nm}^{-1}$ and $L_{sky}(0^+, 180^\circ - \theta_v, \Delta\varphi)$ in $\text{Wm}^{-2} \text{sr}^{-1} \text{nm}^{-1}$ with an upward pointing sensor and $L_u(0^+, \theta_v, \Delta\varphi)$ in $\text{Wm}^{-2} \text{sr}^{-1} \text{nm}^{-1}$ with a downward pointing sensor and where θ and φ define the

viewing direction in zenith and azimuth and λ the wavelength (see Figure 3). More details about the measurement protocols follow in 7.3.1 Above-water measurements and 7.3.2 Below water measurements.

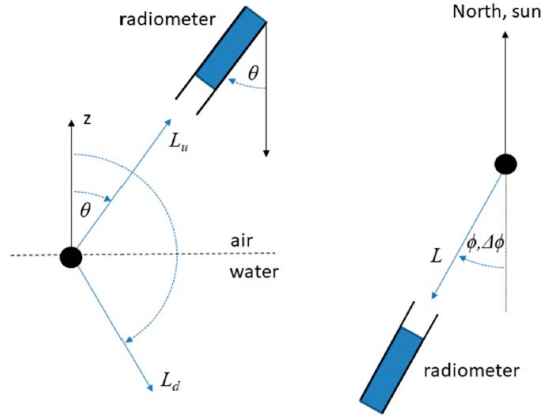


Figure 3: Viewing nadir angle θ measured from downward vertical axis (left) and azimuth viewing angle ϕ and relative azimuth angle $\Delta\phi$ measured clockwise from North and sun (right) (Modified after Ruddick et al. (2019a))

Proposed measurement concepts for these protocols are: calibrated radiance and irradiance measurements, uncalibrated radiance and reflectance plaque measurements or calibrated polarized surface radiance measurements with modeled irradiance and sky radiance (Mueller et al., 2003).

7.1.2 Apparent optical properties

The AOPs depend on the medium (the IOPs), the ambient light field and they need to display enough regular features and stability to describe the water body (Mobley, 1994). The water-leaving radiance L_w ($\text{Wm}^{-2} \text{sr}^{-1} \text{nm}^{-1}$) and the remote sensing reflectance R_{rs} (sr^{-1}) are considered AOPs as they are dependent on the incident radiance distribution at the sea surface (Mueller et al., 2003). The water-leaving radiance is defined as the ‘above-water directional upwelling radiance that has been transmitted across the water-air interface’. It cannot be directly measured, as it is a combination of L_u and L_r . But it can be derived from the following formula:

$$L_w(\theta_v, \Delta\phi) = L_u(0^+, \theta_v, \Delta\phi) - L_r(\theta_v, \Delta\phi) \quad \text{Eq. (1)}$$

Where L_u^{0+} is the upwelling radiance above the air-water interface and L_r is the air-water interface reflection radiance, also described as ‘skylint’.

Ruddick et al. (2019a) further explain, that the skylight, L_r from Eq. (1), can also not be measured directly, it has to be estimated by multiplying the downwelling sky radiance L_{sky} with a reflectance coefficient ρ_F , which is also called ρ_{sky} :

$$L_r(\theta_v, \Delta\varphi) = \rho_{sky} * L_{sky}(0^+, 180^\circ - \theta_v, \Delta\varphi) \quad \text{Eq. (2)}$$

The coefficient ρ_F / ρ_{sky} here describes the ‘fraction of incident skylight that is reflected back towards the water-viewing sensor at the air-water interface and is the Fresnel reflectance coefficient for a flat water surface’.

This leads to the equation:

$$L_w(\lambda; \theta) = L_u(\lambda; \theta) - \rho_{sky} * L_{sky}(\lambda; \theta) \quad \text{Eq. (3)}$$

The water-leaving radiance in the visible and near-infrared region (400 up to 900nm) is used to obtain information about the signal that reaches the sensor (Dörnhöfer and Oppelt, 2016). This signal is influenced by processes like absorption and scattering in the atmosphere, by air-water interface effects and the water body itself and its inherent optical properties (see Figure 1). As the water-leaving radiance is being concealed by the light that is reflected at the water surface, it again depends on the absorption and scattering of the light in the atmosphere (Dekker et al., 2002). Through the calculation of the water-leaving radiance, it is then possible to derive the remote sensing reflectance R_{rs} (in sr^{-1}), which is the ratio of the water-leaving radiance and the downwelling irradiance just above the water surface:

$$R_{rs}(\lambda, \theta, \varphi) = \frac{L_w(\lambda, \theta, \varphi)}{E_d^{0+}(\lambda)} \quad \text{Eq. (4)}$$

R_{rs} measures how much of the downwelling radiance, which is incident onto the water surface, is returned through the water surface in direction (θ, φ) (Mobley, 1994). There is also the spectral irradiance reflectance R , which is just the spectral upwelling over the downwelling plane irradiance. It measures how much of the downward radiance is reflected upward into any direction (Mobley, 1994). For spectral measurements of water however, the spectral remote-sensing reflectance R_{rs} is more of interest.

All the used formulas Eq. (1) – Eq. (4) and corresponding explanations above were taken from Ruddick et al. (2019a). The different ways to calculate the coefficients are discussed in 8.2.

7.1.3 Inherent optical properties

The IOPs are the spectral properties of the medium itself, with two predominant optical processes, absorption, and scattering (Mobley, 1994) (see Figure 1). Absorption (a) is expressed by the absorption coefficient and refers to the removal of photons from the light field resulting from interactions with the water and its constituents; whereas bulk absorption refers to the sum of absorption by all constituents and pure water (Mobley, 1994). Scattering (b) is expressed by the volume scattering function and refers to the part of the incident light which gets redirected with a certain angular distribution; whereas bulk scattering refers to the sum of scattering by all constituents and pure water (Mobley, 1994). The remaining light is transmitted through the water body. Through the measurement of the optical processes of the IOPs, it is possible to do an alternative investigation of the water constituents, if the AOPs cannot be measured directly (Mobley, 1994).

Also, water constituents like phytoplankton and corresponding pigment concentrations, total suspended matter (TSM) or colored dissolved organic matter (CDOM) can be measured through the received spectral signature (Mobley et al., 2004). The watercolor is basically affected by the water constituents which scatter and absorb the radiation which go through the water surface (Dekker et al., 2002). If the color of water depends on several independently varying constituents, it is considered complex, opposed to open ocean water whose optical properties in a first approximation depend solely on phytoplankton concentrations (Mobley et al., 2004).

7.2 Field spectroscopy vs. imaging spectroscopy

Spectroscopy describes the measurement and investigation of spectra which are produced if electromagnetic radiation interacts with materials. This produces a spectral ‘fingerprint’ of the observed material and through analyses of the spectral absorption it is possible to retrieve information about the target (Rast and Painter, 2019). Commercial infrared spectrometers were first used in the 1950s for the pharmaceutical and chemical industry (van der Meer, 2018). 20 to 30 years later, spectrometers found their way into the mineralogy and vegetation sciences, where optical properties of minerals and leaves, and later also water constituents of water bodies were measured (van der Meer, 2018). After the field spectroscopy, imaging spectroscopy was developed (Milton et al., 2009). It is used in the visible-to-shortwave infrared wavelength range (VSWIR) and is also known as ‘hyperspectral imaging’ for terrestrial Earth Observation remote sensing and was developed around the 1980s, with mainly airborne demonstrations (Rast and Painter, 2019). In remote sensing it is one of the fastest growing research areas today and is used in domains like agriculture, soils, biodiversity, environmental issues and inland and coastal waters (Rast and Painter, 2019). Both field and imaging spectroscopy are used to collect spectral data of the Earth’s surface from a remote location, but the instruments are used on different scales. Field spectrometers sample smaller areas for a longer time and with a smaller path length. Instruments

for imaging spectroscopy are either airborne or spaceborne, which measure bigger areas of the Earth's surface with a larger path length. In situ field measurements support the vicarious calibration of airborne and satellite sensors, the upscaling from smaller to larger scenes and contribute to global measurement and monitoring systems (Milton et al., 2009).

7.3 Terrestrial and aquatic reflectance measurements

Terrestrial field spectroscopy is based on relative measurements between the radiance of the target and the radiance of a reference panel (Milton et al., 2009). According to Schaepman-Strub et al. (2006), the reflectance is calculated by the ratio between the radiant exitance (M [$W m^{-2}$]) and the irradiance (E [$W m^{-2}$]), where the radiant exitance is equal to the radiance (L [$W m^{-2} sr^{-1}$]) by a ratio of π .

$$R = \frac{M [W m^{-2}]}{E [W m^{-2}]} \quad \text{Eq. (5)}$$

The resulting reflectance factor between 0 and 1 is the ratio between the radiant flux reflected by a surface and the flux reflected into the identical beam geometry, assuming an ideal diffuse surface, which is simulated by a reflectance panel (Schaepman-Strub et al., 2006). Aquatic measurements however require a different measurement setup.

7.3.1 Above-water measurements

Measurements above the water surface are '*Above-water radiometry with sky radiance measurement and skylight removal*' or '*On-water radiometry with skylight blocked*' (Ruddick et al., 2019a).

7.3.1.1 Above-water radiometry with sky radiance measurement and skylight removal

The first option measures the total upwelling radiance (L_u / L_t), downwelling sky radiance (L_{sky} / L_d) and downwelling irradiance $E_d(0^+)$ (see Figure 4). Through L_u and L_{sky} and a coefficient the water-leaving radiance L_w can be determined (see Eq. (3)), which is then used to calculate the remote-sensing reflectance R_{rs} (see Eq. (4)). Challenges here are feasible constructions which hold the sensor, or the sensor needs to be hand-held, the different approaches to the skylight correction and the influence of the cloud cover and wave activity. Advantages are that the sensor does not have to be cleaned as often as below-water sensors and that the viewing geometry can be chosen.

7.3.1.2 On-water radiometry with skylight blocked

The skylight-blocked approach (Ruddick et al., 2019a) measures with one upward pointing sensor $E_d(0^+)$ and with one vertically deployed downward pointing sensor L_u (see Figure 5). The

downward pointing sensor gets extended with a cone/cylinder so that the tip lies beneath the air-water interface. With this approach, the reflected skylight gets blocked, which means that L_u is simply equal to $L_w(0^+)$ and R_{rs} can be calculated (see Eq. (4)). Challenges here are the waves, which can cause the L_u sensor to be in the air instead of the water, instrument self-shading and the sensor has to be cleaned. The advantage here to the first method is the skylight-blocking.

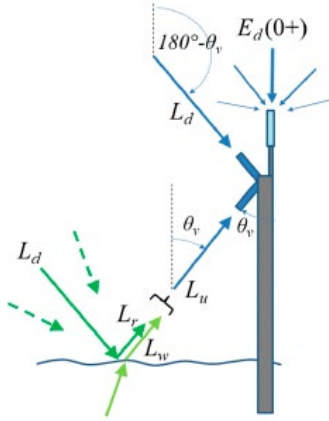


Figure 4: Schematic of ‘Above-water radiometry with sky radiance measurement and skylight removal’ (Modified after Ruddick et al. (2019a))

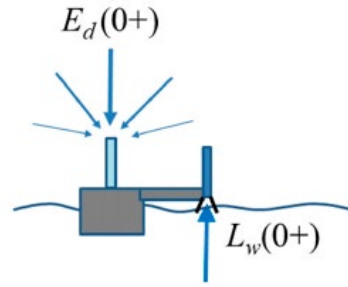


Figure 5: Schematic of ‘On-water radiometry with skylight blocked’ (Modified after Ruddick et al. (Ruddick et al., 2019a))

7.3.2 Below water measurements

Below-water measurements also have two possible setups, ‘Underwater radiometry using fixed-depth measurements’ or ‘Underwater radiometry using vertical profile’ (Ruddick et al., 2019a).

7.3.2.1 Underwater radiometry using fixed-depth measurements

Fixed-depth measurements (Ruddick et al., 2019a) use radiometers which are attached to permanent underwater floating structures (see Figure 6 or Figure 8 (top illustration)). These radiometers measure the upwelling radiance $L_{un}(z)$ at the given depths ($z = z_1, z_2 \dots$). A second sensor measures the downwelling irradiance $E_d(0^+)$. The water-leaving radiance L_{wn} is then estimated by the $L_{un}(z)$ measurements, which makes it possible to determine the R_{rs} :

$$L_{wn} = \frac{T_F}{n_w^2} L_{un}(0^-) \quad \text{Eq. (6)}$$

where T_F is the Fresnel transmittance of radiance from water to air and n_w is the refractive index of water.

With:

$$L_{un}(0^-) = L_{un}(z_1, t_1) \exp[K_{Lu}z_1] \quad \text{Eq. (7)}$$

where K_{Lu} is the constant diffuse attenuation coefficient for upwelling radiance.

And:

$$K_{Lu} = \frac{1}{z_2 - z_1} \ln \left[\frac{L_{un}(z_1)}{L_{un}(z_2)} \right] \quad \text{Eq. (8)}$$

7.3.2.2 Underwater radiometry using vertical profile

The vertical profile method (Ruddick et al., 2019a) measures the same parameters as the first method but with one sensor measuring continuously, starting at the highest depth and then being pulled to the water surface (see Figure 7).

Here $L_{un}(z)$ is derived as followed:

$$L_{un}(z, t_0) = L_{un}(z, t) \frac{E_d^{0+}(t_0)}{E_d^{0+}(t)} \quad \text{Eq. (9)}$$

The water-leaving radiance L_{wn} is then derived equally as in Eq. (6).

7.3.2.3 Underwater radiometry with three sensors

Dev & Shanmugam (2014) suggest a third underwater measurement setup with three sensors just below the water surface. One measures the downwelling irradiance $E_d(0^-)$, one the upwelling radiance $L_u(0^-)$ and another one the upwelling irradiance $E_u(0^-)$ (see Figure 6). $L_u(0^-)$ again, is used to determine L_w , which then is used to calculate R_{rs} (see Eq. (4)).

The water-leaving radiance below water is calculated as followed:

$$L_w^b = \frac{1 - \rho}{n^2} L_u(0^-) \quad \text{Eq. (10)}$$

with $L_u(0^-)$ derived from Eq. (7) and Eq. (8).

Challenges for the below-water measurements are high water movement, shallow waters and high absorption of the signal. The sensors and equipment have to be waterproof and should be cleaned after each use. Also, for the first two methods more equipment is needed for the underwater depth and profiling measurements. The advantage is that the measurements are not influenced by skylint.

To standardize the notations of the radiometric quantities, I will be using L_u for the total upwelling radiance, L_{sky} for the downwelling sky radiance and E_d will stand for $E_d(0^+)$. I will mainly focus on above-water measurements with skylight removal because of the sensors at hand for field measurements.

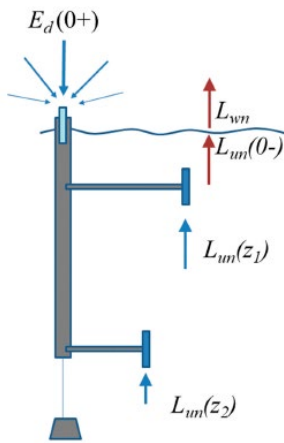


Figure 6: Schematic of 'Underwater radiometry using fixed-depth measurements' (Modified after Ruddick et al. (2019a))

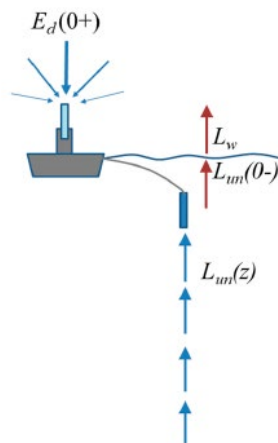


Figure 7: Schematic of 'Underwater radiometry using vertical profile' (Modified after Ruddick et al. (2019a))

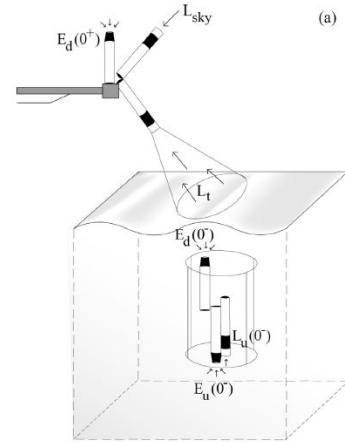


Figure 8: Schematic (lower illustration) of 'Underwater radiometry with three sensors' (Modified after Dev & Shanmugam (2014))

7.4 Spectral libraries and databases / data exploitation platforms

Data can be stored in a spectral library or in spectral database / data exploitation platform. They are necessary to collect, organize and store huge amounts of spectral data and accompanying metadata (Hueni and Tuohy, 2010). The data sampling with spectrometers is done quickly and rather easily, but the data handling, analysis and interpretation is more difficult.

Hueni et al. (2009) explain, that data exploitation platforms for example help with the problem of collecting, organizing, and storing the acquired data of spectra and metadata. These platforms provide efficient and automated methods for data input and queries and can manage large amounts of output data. They also make the comparison of data and the corresponding methods easier by providing enough metadata to assess the quality of the data. Storing additional metadata, makes sure that spectral measurements are combined with descriptive data about the state of the observed object, the sampling environment and setup, and the time of the sampling. This helps with the interpretation, long-term usability and sharing of the data among scientists.

7.4.1 Spectral libraries

Spectral libraries hold data collections of reference spectra for different procedures. Existing libraries for example are the USGS spectral library (Kokaly et al., 2017) or the SPECMIN package (SPECMIN, 2005). They only provide first order statistical information, for example one spectrum per target, without additional second order information. Bojinski et al. (2003) point out

that additional information would be necessary that a spectral library could be more efficient for comparing measured spectra with the library spectra. They further indicate that spectral libraries are usually only available as static files and lack information of the spatiotemporal variability of objects, which leads to a low flexibility and low query performance.

7.4.2 Spectral databases / data exploitation platforms

Spectral databases use a Database Management System (DBMS) for storing spectra and metadata and they offer more functions for data manipulation but there are still some issues with data integrity and redundancy (Hueni et al., 2009). For remote sensing some spectral database systems exist. Many of them are used to store and compare in situ measurements to satellite sensor products, for example the SeaWiFS bio-optical archive and storage system (SeaBASS) (Hooker and Firestone, 1994), the Envisat MERis Matchup In situ Database (MERMAID) (Barker et al., 2008), the Copernicus Ocean Colour In situ Database (OCDB) (EUMETSAT Copernicus, n.d.) or the Lake Bio-optical Measurements and Matchup Data (from lakes and coastal waters) for Remote Sensing (LIMNADES) (University of Stirling, n.d.). Other spectral databases are SPECCHIO (Bojinski et al., 2003) or SpectraProc (Hueni and Tuohy, 2006). For the purpose of this thesis, I will focus on libraries / databases which do not involve satellite data, as we will not work with such data.

7.4.2.1 USGS Spectral Library

The USGS Spectral library (Kokaly et al., 2017) consists of spectra from thousands of materials measured at the United States Geological Survey (USGS) Spectroscopy Laboratory, in the field or with airborne spectrometers. This library was designed to identify and map minerals, vegetation, and manmade materials. Soils, liquids like water and organic compounds or biological materials are also included. The mixtures are physically constructed and mathematically computed. To measure the spectra, four different spectrometers were used, including the Analytical Spectral Devices (ASD) spectroradiometer range (see chapter 8.3.4).

7.4.2.2 SpectraProc

The SpectraProc system by Hueni and Tuohy (2006) is a relational database designed for storing and processing hyperspectral data from the ASD FieldSpec Pro (see chapter 8.3.4). The software also supplies a graphical user interface, organized data storage and easy data retrieval. Spectral data of entire field campaigns can be loaded quickly into the system and therefore helps spectroscopists with a first analysis. The software is also able to synthesize sensors, to do classifications or export files. Only ASD binary files or ENVI Z-Profiles can be loaded as input files. Output files can be generated as three different formats, one of them is CSV, which allows the data to be loaded into 3rd party applications. As the data is loaded raw into the database, some processing steps are needed, for example removal of unwanted bands and data smoothing (see

Figure 9). SpectraProc also supports basic analysis functions, for example separability, discriminant, and principal component analysis. As the system is mostly focused on spectral signature processing and data modelling, it only stores some basic metadata. Still, some of the structures of SpectraProc were used for the latest SPECCHIO design by Hueni et al. (2009).

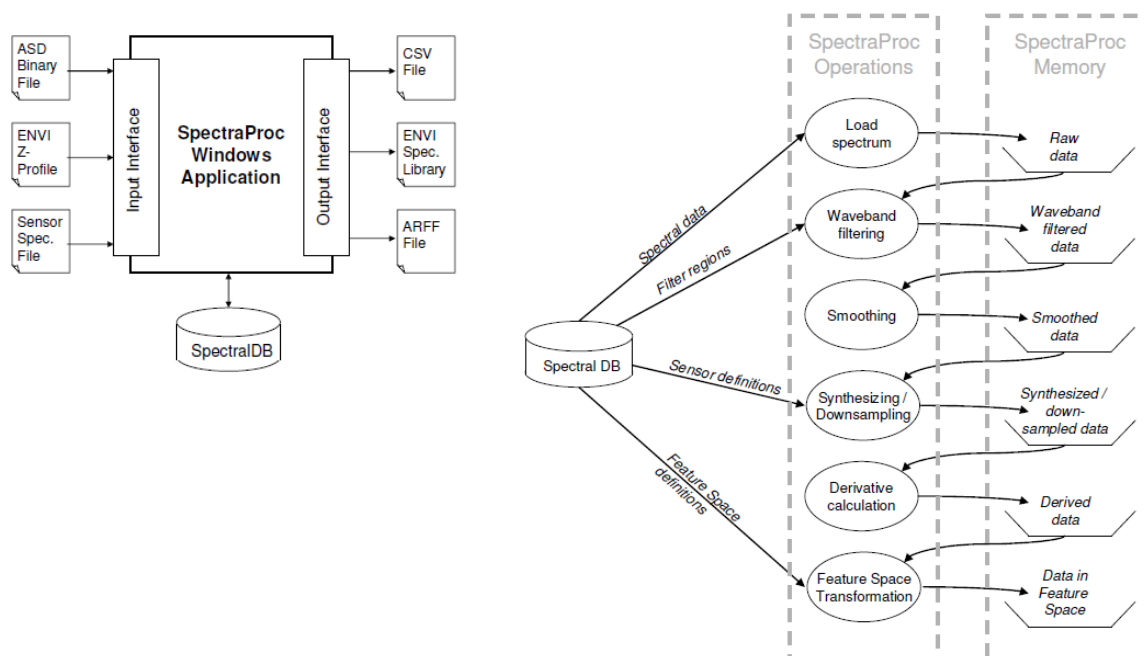


Figure 9: SpectraProc Windows Application with the input interface, spectral database and output interface (left) and the spectral data processing in the database shown by the operations and data stored in the memory (right). (Modified after Hueni & Tuohy (2006))

7.4.2.3 SPECCHIO

Bojinski et al. (2003) and Hueni et al. (2009) describe SPECCHIO as a reference spectrum database that stores spectral campaign data without redundancy which leads to an efficient system for import, storing, editing and retrieval. SPECCHIO also contains laboratory data and spectra from existing spectral collections or modelled spectra. It helps retrieving geophysical and biophysical parameters from the data. The database consists of three components: a web and command line based user interface, an underlying DBMS and a defined data model (see Figure 10). The design principles are logical relations and consistency, intuitive interfaces, flexibility for changes, independence of the file format and scalability of the data.

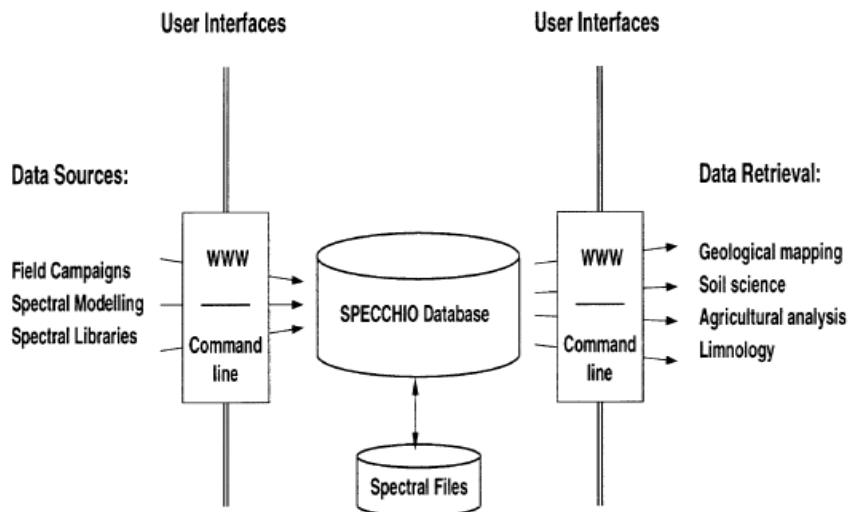


Figure 10: Basic layout of SPECCHIO, showing the data sources and the data retrieval. Spectral files are fed into the SPECCHIO database. (Modified after Bojinski et al. (2003))

In SPECCHIO a wide range of metadata can be stored (Hueni et al., 2009). Metadata variables contained in the data model are general campaign variables, spatial and temporal information (date and time of the sampling), target information (including pictures), sampling geometry (e.g. zenith and azimuth angles), measurement details (instrument, sampling, units), environmental conditions (e.g. cloud cover, wind speed) and file information. The storage of metadata helps with accurately documenting the measurement process and therefore leads to long-term usability of the data between scientists and defining common standards and protocols (Hueni et al., 2017). Data with non-existent metadata or only minimal metadata are not usable for other people who are not familiar with the data set and the data cannot be fully trustworthy and comprehensible (Hueni et al., 2009).

8 Methods

Besides the acquisition of the data and the storing of the data on a data exploitation platform, many steps are required. First of all, the data has to be measured following a measurement protocol, which defines how the data is sampled (e.g. measurement geometry). After that the data will be processed and the desired parameters are derived. To successfully acquire the desired parameters, specific instruments can be used which follow different measurement protocols and come with different software to handle the data. All these steps come with a lot of dissimilarities, a lot of different measurement protocols, processing schemes and instruments exist. Based on what is used, different outcomes and errors will be produced. This section outlines what possibilities exist at the moment to acquire in situ spectral data of aquatic measurements. To show the practical implications of these different possibilities, a case study has been conducted on the lake 'Greifensee' with the instrument RAMSES TriOS.

8.1 Measurement protocols

A lot of measurement protocols exist from different authors, but a lot of them just repeat what already has been demonstrated. The two presented protocols by NASA (National Aeronautics and Space Administration) and ESA (European Space Agency) are well established protocols written by many experts in their field. These protocols are frequently reviewed and updated if new findings arise.

8.1.1 NASA Ocean Optics protocols

Mueller et al. (2003) suggest a measurement protocol in their ‘Ocean Optics Protocols For Satellite Ocean Color Sensor Validation, Revision 4, Volume III’ for above-water measurements for retrieving water-leaving radiance and the corresponding sky radiance for a given zenith and azimuth angle. The protocol does not suggest any of the three measurement concepts, presented in 7.1.1, as best practice, but it recommends for any measurement method the viewing angles of $\theta = 40^\circ$ - 45° and $\varphi = 135^\circ$ (must be between $90^\circ < \varphi < 180^\circ$). These angles are chosen to avoid sun glint contamination, because the viewing zenith angle points away from the ship and the viewing azimuth angle away from the solar azimuth. There is a suggestion for wind speeds over 5 ms^{-1} , to take a 20° field of view (FOV) because with larger viewing angles the uncertainties of the skylight reflection and the upward radiance transmission are larger. This happens because with wind the water surface gets roughened and the variations are spatially and temporally on a smaller scale than the area seen by the field of view and the integration time of the sensor. When radiance measurements are done on a ship, the measuring position should be close to the bow of the ship. From this position it is easy to see where the water is not influenced by the ship's wake or foam. An angle of 180° away from the sun's azimuth, measurements with the sun close overhead and measurements with foam or floating material should be avoided. Measurements should be taken during periods of several seconds or minutes because of the temporal change of the surface reflectance.

8.1.2 ESA FRM4SOC protocols

The fiducial reference measurements for satellite ocean color (FRM4SOC) technical report on protocols of field radiometers (Tilstone et al., 2017), suggest how to use the RAMSES TriOS and the WISP system (see chapter 8.3). In their field measurements, the RAMSES TriOS radiometers were mounted with a steel frame at the prow of the ship, facing forward to avoid ship shadowing. They also suggest mounting the downwelling radiance sensor separately to avoid optical interference. They fixed the sea and sky-viewing angle to $\theta = 40^\circ$ and the azimuth angle $\varphi = 135^\circ$ with respect to the sun. During the measurement wind speed, sea, sun and sky conditions should be noted. Also, the ship position and orientation should be monitored. Underway measurements are also possible if the ship is heading of $\varphi = 135^\circ$ relative to the sun. The data is acquired with

the MSDA_XE software (see chapter 8.3.6.2). With the software the data is calibrated, and dark values are removed. Before processing Tilstone et al. (2017) suggest to remove incomplete spectra and outliers and avoid measurements with temporal fluctuations due to clouds or haze. The water-leaving radiance is calculated with Eq. (3), where the air-sea reflection coefficient is estimated for sunny conditions as a function of wind speed by Mobley (1999):

$$\rho_{sky} = 0.0256 + 0.00039 * W + 0.000034 * W^2 \quad \text{Eq. (11)}$$

After processing the produced spectra should be inspected for errors. Also, measurements outside the range 400-900nm are neglected because of high uncertainty and instrument noise. For the Water Insight's WISP-3 handheld spectrometer, they set 42° for the sky-viewing angles. The same azimuth angle of $\phi = 135^\circ$ relative to the sun was used as for RAMSES TriOS. The instrument was hand-held by a person using the buttons on the instrument, as suggested by Water Insight. Tilstone et al. (2017) also used the WISPweb for data processing, which is controlled by Water Insight. Therefore, no further information about the data processing is available. They also point out that WISP produces a smaller number of measurements in a 10 minute time window and the irradiance measurement can be affected by ship shadowing as it is hand-held.

8.2 Processing

The remote sensing reflectance R_{rs} is used for the interpretation of ocean-color data (Mobley, 1999). As we saw, R_{rs} is a ratio between L_w and E_d , where E_d can be directly measured and L_w has to be derived by L_u and L_r . To get L_r , L_{sky} is being multiplied by an air-water surface reflection coefficient. This coefficient must be determined correctly, because it cannot be measured, and any uncertainty will influence the accuracy of R_{rs} directly (Ruddick et al., 2019a). Other denotations of the coefficient exist, Fresnel reflection coefficient or sea surface reflectance factor. For simplification I will use the terminology air-water surface reflection coefficient or simply reflection coefficient, as the Fresnel reflectance only is used in cases of a flat water surface with uniform sky radiance distribution (Ruddick et al., 2019a).

To determine the value of the reflection coefficient ρ_{sky} , a lot of different approaches are available. The chosen approaches take on different methods, depending on the measurement background. They either focus on turbid waters (Ruddick et al., 2006), coastal waters (Simis & Olsson, 2013), providing an offset correction for sky and sun glint (Groetsch et al., 2017 & Groetsch et al. 2020) or a more general approach (Ruddick et al., 2019a). There also exist standard values, Dev & Shanmugam (2014) for example suggest a value of $\rho = 0.028$, which means that 2.8% of the light is reflected from the sea surface. This constant is used because ρ is complicated to assess as it depends on many factors like wavelength, wind speed, sun zenith angles and

viewing geometry. Mobley (1999) suggests different values for different situations depending on cloud cover, wind speed and different viewing geometries, based on simulations.

8.2.1 Fresnel reflectance factor by Ruddick et al. (2019a)

Ruddick et al. (2019a) uses the Fresnel reflection equation for ρ_F , which depends on the incident angle and the refraction of water:

$$\rho_F(\theta_v) = \frac{1}{2} \left\{ \left[\frac{\sin(\theta_v - \theta_t)}{\sin(\theta_v + \theta_t)} \right]^2 + \left[\frac{\tan(\theta_v - \theta_t)}{\tan(\theta_v + \theta_t)} \right]^2 \right\} \quad \text{Eq. (12)}$$

where

$$\theta_t = 180^\circ - \sin^{-1}(\sin \theta_v / n_w) \quad \text{Eq. (13)}$$

with θ_v as the viewing zenith angle, θ_t as the angle of light transmitted to below water after refraction and n_w as the refraction of water, estimated by a value of 1.34. In the measurement setup in Figure 4, the viewing zenith angle θ_v can be seen. The method does not suggest a ‘best’ zenith or azimuth viewing angle.

This approach assumes a flat water surface, only specular reflection processes, unpolarized downwelling light and a small sensor field of view. In reality, these factors are rarely given, because factors like wind speed or cloud cover can rapidly change during a measurement. Therefore, this method comes with a lot of considerations and protocol-dependent sources of uncertainty, that need to be considered.

8.2.2 Clear / cloudy sky by Ruddick et al. (2006)

Ruddick et al. (2006) investigated the case of moderately turbid to highly turbid waters. Measurements were taken with $\theta = 40^\circ$ as viewing zenith angle and $\varphi = 135^\circ$ as viewing azimuth angle away from the sun. The air-water surface reflection coefficient corresponds to the Fresnel Reflection coefficient for a flat water surface. They differentiated between clear and cloudy skies, because with wind speed the coefficient varies strongly for a clear sky but is independent for a cloudy sky. By looking at the ratio of L_{sky}/E_d at 750nm, it can be determined which case applies. For a clear sky, ρ_{sky} equals to $0.0256 + 0.00039W + 0.000034W^2$ for $L_{sky}/E_d < 0.05$. For a cloudy sky, ρ_{sky} equals to 0.0256 for $L_{sky}/E_d > 0.05$.

8.2.3 Spectral ‘fingerprint’ by Simis & Olsson (2013)

Simis & Olsson (2013) investigated another method deriving ρ_{sky} for calculating the R_{rs} for coastal waters. They used a new automated method for moving platforms, so that the ‘ideal’ measuring angles of $\theta = 40^\circ$ for the viewing zenith angle and angle $\varphi > 90^\circ$ (ideally $\varphi = 135^\circ$) for

the viewing azimuth angle could be maintained. The method by Ruddick et al. (2006) is not applicable for their case, as it is based on turbid waters. Turbid waters have a high variability in the backscatter intensity because of suspended materials coming from rivers and banks, which induces the need for a more detailed method. The proposed method estimates ρ_{sky} for clear and turbid waters of hyperspectral radiometric measurements. It is based on the assumption that the spectral pattern of the downwelling light should not be seen in R_{rs} , because the shape of R_{rs} is dependent of the inherent optical properties. The ρ_{sky} should be optimized so that atmospheric features are as little as possible in R_{rs} . Simis & Olsson (2013) call it the ‘fingerprint’ method. A requirement for this method is that the atmospheric fingerprint needs distinct different spectral signatures from the water-leaving radiance. They suggest that the UV and NIR channels help to differentiate the atmospheric signal from the water-leaving radiance. The ρ_{sky} is optimized in three steps. First the atmospheric absorption features in L_u and L_{sky} are identified by the highest and lowest values, which resemble the sharpest drops and rises in the spectra of the most prominent features. Secondly upper and lower limits for ρ_{sky} are set to detect suspect values. The lower limit is set to 0.024 and the upper limit to the value of ρ_{sky} that yields $R_{rs} = 0$. Thirdly, for a good ρ_{sky} the shape of the downwelling radiance spectrum should not propagate to the shape of R_{rs} . The resulting model of Simis & Olsson (2013) cannot show spectral variations when the cloud cover exceeds 40%, which is why they applied their simulations only to clear sky conditions. Resulting values for ρ_{sky} were between 0.0247, for the case of a cloud covered sky with 5 m s^{-1} wind speed, and 0.0375 for the case of a clear sky with 15 m s^{-1} wind speed. No wind speed and any cloud cover resulted in $\rho_{sky} = 0.0257$.

8.2.4 3C model by Groetsch et al. (2017)

Groetsch et al. (2017) looked into the approaches of Ruddick et al. (2006) and Simis & Olsson (2013); these two assume that ρ_{sky} is spectrally constant, but it should rather be considered as a function with strong wavelength dependency. Groetsch et al. (2017) point out that with these two approaches L_r can only be presented correctly through the product of ρ_{sky} and L_{sky} if the sky radiance is uniformly distributed. They suggest a different method, which focuses on separating the spectrally distinct sunglint from the surface-reflected sky radiance. It divides the irradiance into the direct solar irradiance E_{dd} , the diffuse molecular-scattered irradiance E_{dsr} and the diffuse aerosol-scattered irradiance E_{dsa} , which leads to the name 3C model (three-component model). This model also requires aerosol optical properties as an input, which can be measured or derived through atmospheric correction results or bio-optical modelling. It also generates a spectrally resolved correction factor, which is validated in the end. The model was mainly developed for measurements at high wind speeds with fixed sensors and measurement geometries. Measurements were done again with the ‘ideal’ viewing azimuth and zenith angles ($\theta = 40^\circ$ & $\phi = 135^\circ$), but the method itself was developed to work also with unknown azimuth angles.

The 3C model was revised again only recently by Groetsch et al. (2020), where they explored the limits of this method. They focused on observation geometry and wind speed as the main drivers for sky and sun glint contamination. Their simulations showed that spectral dependencies of the sky light distribution and sky glint contributions should still be considered over wind speeds of 4m s^{-1} and sun-glint minimizing viewing angles between $\varphi = 90$ and 135° . They could also show that the 3C model can derive water reflectance for wind speeds up to 8m s^{-1} and viewing angles greater than 20° .

8.3 Sensors / Measurement instruments

The following introduced instruments in this chapter, are the most common used at Eawag (Swiss Federal Institute of Aquatic Science and Technology) and in the cited literature. Other radiometers are for example TACCS (Tethered Attenuation Coefficient Chain Sensor) (Hommersom et al., 2012), SeaPRISM (Zibordi et al., 2012) or SATLANTIC HyperSAS System (Tilstone et al., 2017).

8.3.1 WISP-3

The water insight spectrometer (WISP-3) has three hyperspectral radiometers, is hand-held (see Figure 11) and the measurements are done automatically, because it works without a connection to a computer or to a power source (Hommersom et al., 2012). WISP-3 was designed to monitor water quality and to validate optical satellites. The three radiometers measure the downwelling irradiance $E_d(\lambda)$, the downwelling radiance from the sky $L_{sky}(\lambda; \theta)$ (with $\theta = 42$ deg from the zenith) and the total upwelling radiance $L_u(\lambda; \theta)$ (with 42 deg from the nadir ($\theta = 138$ deg)) (see Figure 11). WISP-3 has a spectral range of ~ 380 to 800 nm. It takes five measurements by each radiometer, which takes in between 30 to 90 seconds. WISP-3 can also calculate averages of L_{sky} , L_u and E_d , and derive the average reflectance R_{rs} and it also corrects dark readings. For stable measurements without high fluctuations in radiances, it is best to operate the instrument under fully sunny or fully overcast skies. With algorithms, some water quality parameters, like chlorophyll-a (Chl-a) and suspended matter, can be extracted from the reflectance spectra.

The raw data is stored on a SD-card in WISP and uploaded to the WISPweb by the user with the corresponding account to the instrument (see chapter 8.3.6.1).

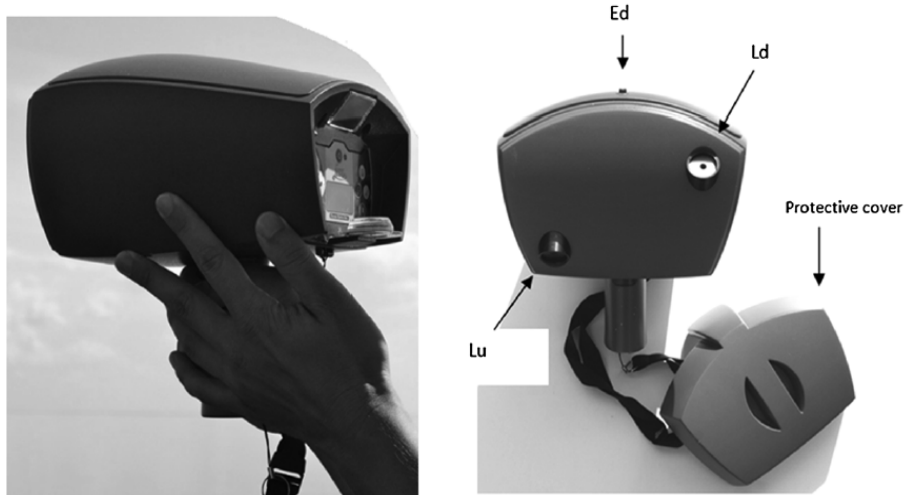


Figure 11: Handling of WISP-3 (left) and an overview of the three radiometers (right) (Modified after Hommersom et al. (2012))

8.3.2 RAMSES TriOS

The RAMSES TriOS system is intended to provide high quality spectra with high accuracy, which are used for aquatic measurement setups (Simon and Shanmugam, 2016). RAMSES TriOS works with three radiometers (see Figure 12), and it can be used below or above water (Hommersom et al., 2012). The system above water measures E_d with an irradiance sensor and two radiance sensors which measure $L_{sky}(\lambda; \theta)$ (with $\theta = 41$ or 40 deg from the zenith) and $L_u(\lambda; \theta)$ (with 41 or 40 deg from the nadir ($\theta = 139$ or 140 deg)). It has a spectral range from 320 to 950 nm, measures light intensities for 255 wavelengths and has an automatic integration time between 4 and 4096 ms (TriOS Mess- und Datentechnik GmbH, 2013). For above-water measurements, RAMSES TriOS can be mounted on a platform, away from the ship to avoid shadowing effects of the ship and instrument self-shading effects. The sensor is operated through an attached field laptop. The software MSDA_XE is used to control the measurements, either single measurements or serial measurements with different measurement intervals. The acquired data is also stored in MSDA_XE (see chapter 8.3.6.2).



Figure 12: Setup of RAMSES TriOS with the three sensor L_u , L_{sky} and E_d (from left to right) (Picture by Alicia Hug)

8.3.3 ASD FieldSpec

ASD FieldSpec (see Figure 13) is a hand-held hyperspectral instrument with one radiometer, that can be used on land or below or above water (Hommersom et al., 2012). E_d is measured with a remote cosine receptor (RCR) mounted on the radiometer fiber. The R_{rs} can again be calculated with the same equation as in Eq. (4). ASD FieldSpec 4 (Malvern Panalytical, 2019) comes in three versions with different spectral resolution options, suited for different user needs. The ASD FieldSpec has a full spectral range from 350 to 2500nm which provides data collection in VIS/NIR/SWIR. It also has a fast integration speed if you are limited in time and a long-range wireless capability to cover large measurement areas.

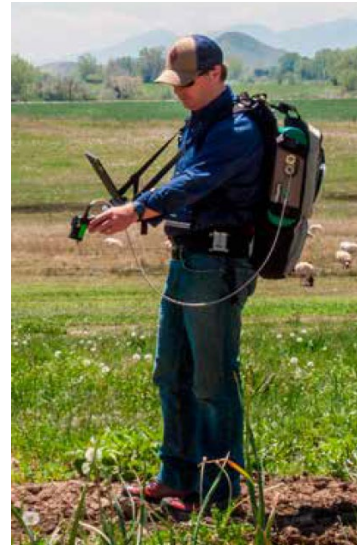


Figure 13: Possible field setup of ASD Fieldspec, for measuring a terrestrial surface. (Modified after Malvern Panalytical (2019))

8.3.4 AC-S

The Spectral Absorption and Attenuation Sensor, AC-S (see Figure 14), is an in situ spectrophotometer (Sea-Bird Scientific, 2013). It measures absorption and beam attenuation and has a spectral range from 400 to 730nm. The sensor is deployed vertically to 45 degrees off-vertical orientation into the water at different depths. It contains two tubes through which water is pumped, the attenuation flow tube is dark with a plastic chamber and it measures the part of the signal which directly goes to the sensor (beam attenuation coefficient 'c'). The absorption tube has a light tube lined with quartz and it measures what is absorbed of the signal in the tube itself (absorption coefficient 'a'). The total scattering 'b' is then derived by subtraction of the total attenuation and absorption coefficients. The output values of the absorption and attenuation are always in comparison to a reference signal of clean water (Dev and Shanmugam, 2014). Corrections for temperature, salinity and scattering need to be applied to the coefficients (Sea-Bird Scientific, 2013).



Figure 14: AC-S Sensor (Modified after Sea-Bird Scientific (2018))

8.3.5 ECO-VSF 3

All the following information about this sensor is taken from the producer's manual WET Labs (2007). The VSF 3 is a three-angle, three-wavelength Volume Scattering Function Meter from WET Labs Inc. (see Figure 15). As the names indicates, it measures the optical scattering in water at three angles (100, 125 and 150 degrees) and three wavelengths (470, 532 and 660nm), through which it is possible to provide the shape of the Volume Scattering Function (VSF). The sensor is built up by three potted monolithic optical flanges and the housing which is responsible for the signal processing and the controller circuitry. Three LED-based transmitters, which are coupled to three receivers are responsible for setting up the 100, 125 and 150 degrees. The three sensor heads each operate at one wavelength, 470 (blue), 532 (green) and 660nm (red). Knowing the angular distribution of the scattered radiation is crucial for the interpretation of measurements and for analysis of particle shapes and models of the visibility of water. ECO-VSF 3 also helps to better understand the relationship between the water-leaving radiance and the backscattering in the same direction. Also, specific angles of backscattering and the total backscattering coefficient can be determined.



Figure 15: Sensor ECO-VSF 3 (Modified after WET Labs (2006))

In the following table (Table 1) an overview can be seen of all five instruments:

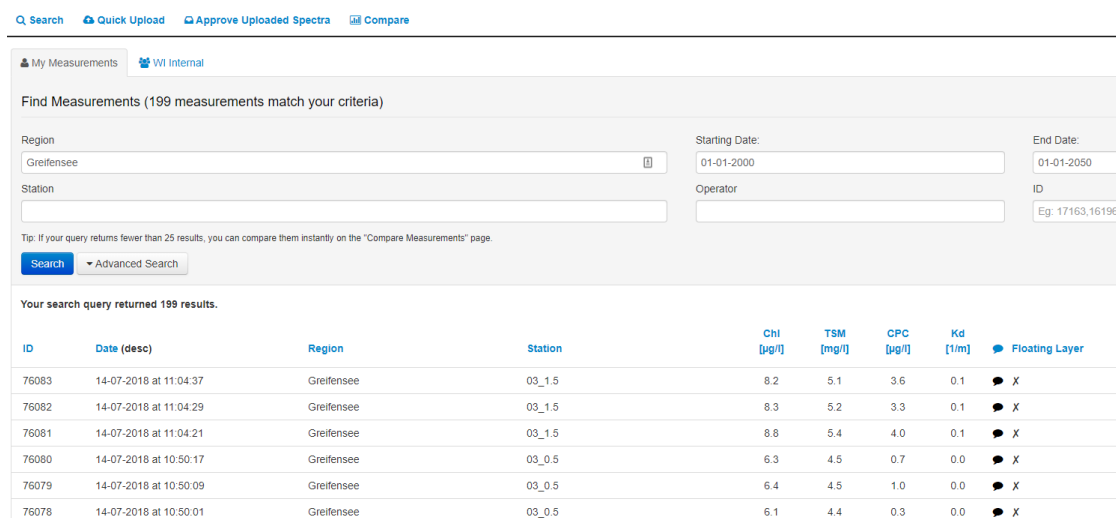
Table 1: Overview of the five introduced sensors with the suggested measurement protocols and parameter estimation (Dev and Shanmugam, 2014; Hommersom et al., 2012; Sea-Bird Scientific, 2013; Simis and Olsson, 2013; Tilstone et al., 2017; TriOS Mess- und Datentechnik GmbH, 2013; WET Labs, 2007).

Sensor	Measurement protocol	Parameter estimation
WISP-3	E_d L_u ($\theta = 42^\circ$, $\varphi = 135^\circ$) L_{sky} ($\theta = 42^\circ$, $\varphi = 135^\circ$)	L_w and R_{rs} →Eq. (3) & Eq. (4)
RAMSES TriOS	E_d L_u ($\theta = 40^\circ$, $\varphi = 135^\circ$) L_{sky} ($\theta = 40^\circ$, $\varphi = 135^\circ$)	L_w and R_{rs} →Eq. (3) and Eq. (4)
ASD FieldSpec	E_d L_u ($\theta = 40^\circ$, $\varphi = 135^\circ$) L_{sky} ($\theta = 40^\circ$, $\varphi = 135^\circ$)	L_w and R_{rs} →Eq. (3)& Eq. (4)
AC-S	absorption & attenuation	-attenuation coefficient $c(\lambda)$ -absorption coefficient $a(\lambda)$
ECO-VSF 3	optical scattering: -3 wavelengths: 470 nm, 532 nm, 660 nm -3 angles: 100°, 125°, 150°	-shape of Volume Scattering Function (VSF) -specific angles of backscattering -total backscattering coefficient b_b

8.3.6 Data Handling

8.3.6.1 WISPweb

The WISP-3 measurement data is stored and analyzed on WISPweb from the SD card which is connected to a computer. The corresponding website provides the following information (Water Insight, n.d.). On the website one can login into their account to see their data, which is only visible if you have access to this account. When uploading the data, there is also the possibility to add metadata, the region and station with the coordinates, the weather conditions and additional comments (see Figure 16). The uploaded data is calibrated, and water quality parameters are derived, for example Chlorophyll-a, and Suspended Particulate Matter (SPM).



The screenshot shows the WISPweb interface with search filters and a table of results. The filters include Region (Greifensee), Starting Date (01-01-2000), End Date (01-01-2050), Station, and Operator. The search results table is as follows:

ID	Date (desc)	Region	Station	Chl [$\mu\text{g/l}$]	TSM [mg/l]	CPC [$\mu\text{g/l}$]	Kd [$1/\text{m}$]	Floating Layer
76083	14-07-2018 at 11:04:37	Greifensee	03_1.5	8.2	5.1	3.6	0.1	X
76082	14-07-2018 at 11:04:29	Greifensee	03_1.5	8.3	5.2	3.3	0.1	X
76081	14-07-2018 at 11:04:21	Greifensee	03_1.5	8.8	5.4	4.0	0.1	X
76080	14-07-2018 at 10:50:17	Greifensee	03_0.5	6.3	4.5	0.7	0.0	X
76079	14-07-2018 at 10:50:09	Greifensee	03_0.5	6.4	4.5	1.0	0.0	X
76078	14-07-2018 at 10:50:01	Greifensee	03_0.5	6.1	4.4	0.3	0.0	X

Figure 16: Screenshot of the user interface of WISPweb from the Eawag account. The measurements are sorted by the region Greifensee and by the starting and end date. Each measurement has an ID, date, region and station name. For each measurement water quality parameters are derived from the optical information (Chlorophyll-a (Chl-a), Total Suspended Particulate Matter (TSM), Phycocyanin (CPC) and a measure for Transparency (Kd)). Comments about the floating layer, GPS coordinates and cloud cover can be added. (Screenshot taken from <https://wisweb.waterinsight.nl/>, 19.07.2020)

The L_w and R_{rs} are automatically calculated according to Eq. (3) and Eq. (4). The air-sea interface reflection coefficient (ρ_{sky}) depends on the wind speed and is set to a standard value of 0.028 in WISP, when no wind speed is measured or for cases with wind $<5\text{ m s}^{-1}$. For cases with wind $>5\text{ m s}^{-1}$, values for ρ_{sky} are taken from Mobley (1999). For each measurement, the irradiance and radiance spectra are shown (see Figure 17) and the remote sensing reflectance (see Figure 18) and with the calculated water quality parameters and metadata. The spectra are presented in a range of 400 to 800nm. WISPweb also lets you compare selected measurements with each other, and you can see the results on a map, if the GPS positions are added in the metadata. The reflectance shows the ratio between downwelling and upwelling light, which how much of the incoming sunlight is getting to the sensor after travelling through the water.

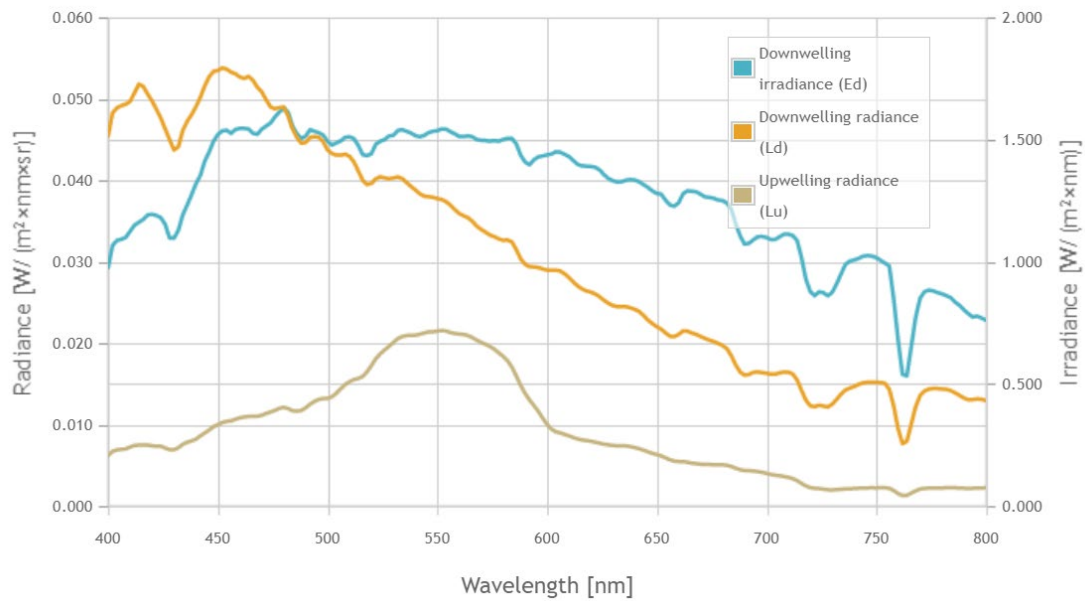


Figure 17: Screenshots of the downwelling irradiance (E_d), downwelling radiance (L_d) and upwelling radiance (L_u) from the first measurement from Figure 16. The irradiance reads on the right y-axis and both radiance read on the left y-axis. (Screenshot taken from <https://wispweb.waterinsight.nl/>, 19.07.2020)

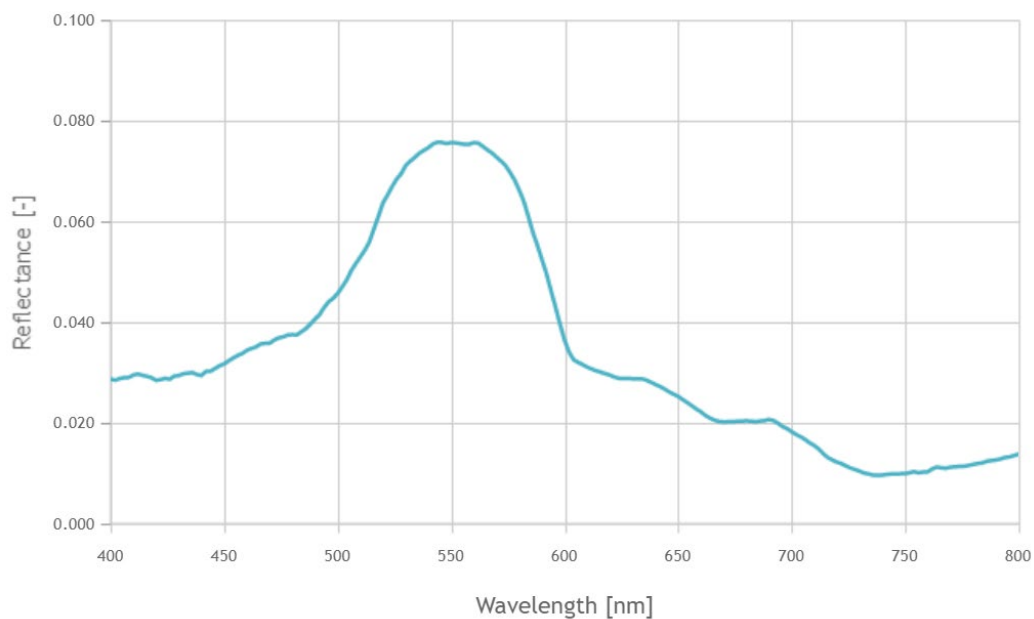


Figure 18: Screenshot of the Subsurface Irradiance Reflectance (R_0 -) from the first measurement from Figure 16. (Screenshot taken from <https://wispweb.waterinsight.nl/>, 19.07.2020)

The color of the water can be determined, depending on how much light is measured. The water is bright if the reflectance is high (closer to 1) and dark if the reflectance is low (closer to 0). If the reflectance is highest between 400 and 500nm, the water has a blue-ish color, if it is highest between 500 and 600nm, the water is more green, which indicates the presence of algae, and if it is highest between 600 and 700nm, the water is more brown-red-ish, which indicates a high sediment load. The calculated reflectance is a ratio and should therefore have values between 0 and 1. Values out of this range should be removed. Unfortunately, Water Insight does not provide

enough information about the used method to calculate the reflectance and if they use an air-water surface reflection coefficient for the calculation of the skylint.

8.3.6.2 TriOS MSDA_XE

The data handling software which is used for RAMSES TriOS is the Multi Sensor Data Acquisition System – Extended Edition (MSDA_XE) (see Figure 18). It controls all sensor types by TriOS, including RAMSES. The sensor is connected to the field laptop, through which the measurements can be controlled. It is possible to do single measurements or multiple measurements with individual measurement intervals.

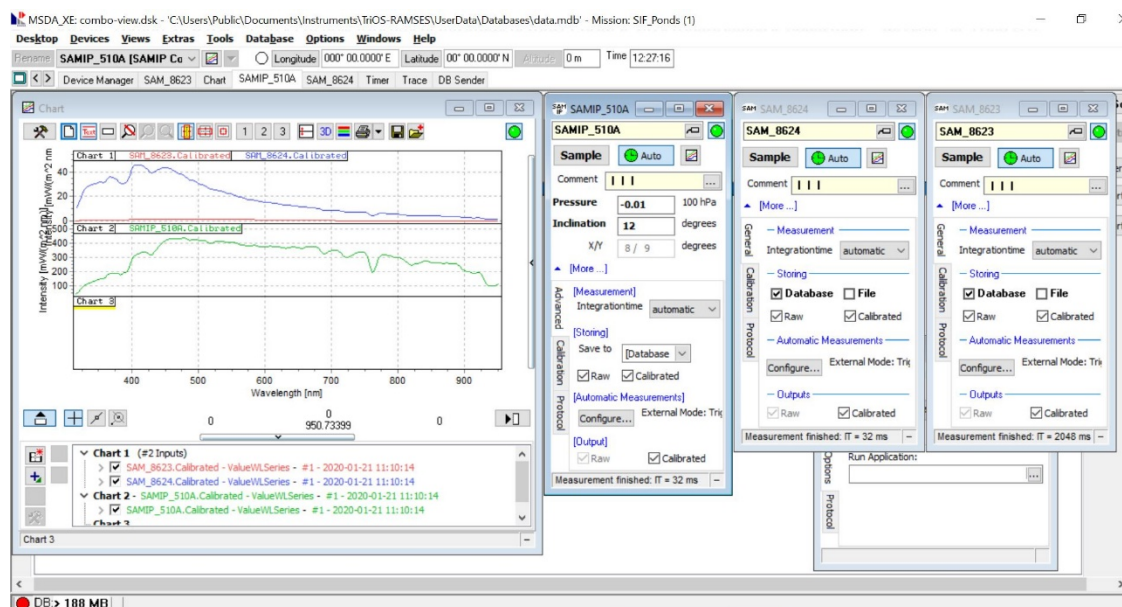


Figure 19: Screenshot of the software MSDA_XE, with the charts for the three sensors on the left side window and the control panels on the three window on the right side. The sampling can be executed over any of the three ‘Sample’ buttons. Pressure and inclination can be seen in the SAMIP_510A window and also the integrationtime can be set in this window. (Screenshot by Alicia Hug)

The measurements are saved by the date and time of the measurement to tell them apart. Additional comments and position data also help with the data handling. To export the desired data, the database can be filtered, and different export formats are available. This allows the further processing of the hyperspectral data with a third party software. The available export files are TriOS Format, MatLab Code, MatLab Serial Data or raw data. The configuration of the file naming and number of files is possible with single files, key files, number files or through a mask. When the data shall be reimported into MSDA-XE, it is necessary to use the TriOS Format. All the above information and more instructions can be found in the manual (TriOS Mess- und Datentechnik GmbH, 2013).

8.4 Case Study

8.4.1 Study Site

Field data were acquired on ‘Greifensee’ in the Canton of Zurich, with a research boat of Eawag, which is equipped to monitor the lake.

Greifensee is about 30m deep and gets mixed from the top to the ground almost every winter. The catchment area of the lake is 156 km² and it is strongly affected by human emissions. It also has a high proportion of agricultural and settlement areas compared to other large Swiss lakes.

The phosphorus level dropped since the 1970s but around 2010 it was increasing again, due to bad mixing of the water layers and climate change. In 2018 the lake was at a phosphorus level of 0.08 mgP/l (AWEL, 2018). The phosphorus concentration is thus still above the cantonal target of 0.025 mgP/l and the natural value of around 0.02 mgP /l (BAFU, 2016).

8.4.2 Instrument and Methods

Four sets of measurements were collected with RAMSES TriOS, taken on the 21.01.2020 in the morning around 11am. The sky was clear with a little bit of haze, and the air temperature was about 4 degrees Celsius. In total 16 measurements were taken at two different points on the lake. For each point, eight measurements were taken at different unknown azimuth angles (see Figure 19). The zenith angle was fixed to $\theta = 40^\circ$ and measurements were made over the spectral range of 320 to 950nm. On the left side of the boat the sky was clear, and on the right side of the boat the sky was hazy. The three sensors were mounted on a steel frame at 45° zenith and nadir angles. The instrument was held by Daniel Odermatt on the roof of the boat because the planned construction to mount the instrument at the bow of the ship, was still being built. This construction should additionally help to balance out the ships movements and to avoid shadowing effects. Additionally, the GPS position was recorded during the measurements.

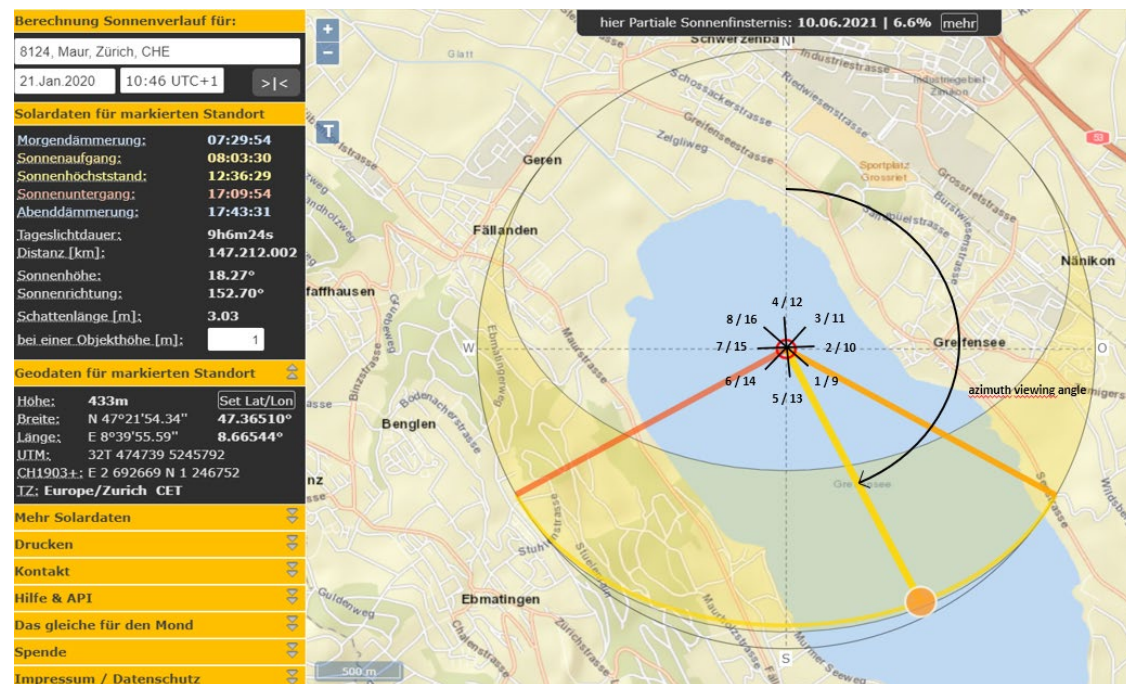


Figure 20: Measurement setup of the first position with the approximate positions of the eight measurement points (azimuth angles unknown). The dark orange line resembles the sunset, the yellow line the sunbeam for the current time, and the light orange line the sunrise. For the second position the setup was the same, where 1 = 9, 2 = 10, 3 = 11, 4 = 12, 5 = 13, 6 = 14, 7 = 15 and 8 = 16. (Screenshot taken from <https://www.sonnenverlauf.de/#/47.3651,8.6654,14/2020.01.21/10:46/1/3, 13.06.2020>)

8.4.3 Data

RAMSES TriOS generates for each measurement pressure data, the inclination, E_d raw and calibrated, L_u raw and calibrated and L_{sky} raw and calibrated. The raw spectra are not calibrated, these are only the raw counts from the spectrometer. The calibration is used for measurements in the air. This data is stored by date and time on the field laptop on TriOS MSDA_XE sorted by the corresponding sensors, 8622 (E_d), 8623 (L_u) and 8624 (L_{sky}).

8.4.4 Processing

The data was first sorted by filters in TriOS MSDA_XE itself, so that in the end the 16 needed measurements were separated from the false or not needed measurements. Only the calibrated spectra from E_d , L_u and L_{sky} were used as the measurements were done in the air. In the end each sensor had data for 16 measurements in text file format. The data from the inclination sensor was not used because at the time of the measurements it did not work properly.

The first test was to see if the prevailing measurement conditions influenced the measurement data. The differences were on one hand the two different measuring spots and on the other hand the different sky conditions, as the sky to the east was sunny with little clouds and the sky to the west had some haze (see Figure 20).



Figure 21: A 360° view (left) of the second measurement position, where the haze is not visible (photo by Daniel Odermatt) and a picture from the first measurement position (right), where the haze can be seen (photo by Alicia Hug)

The second set of tests was to see if the different processing schemes influenced the measurement data. This was done by comparing the four different methods to calculate the air-water surface reflectance coefficient and the remote sensing reflectance (see chapter 8.2). Measurements 1-4, 5-8, 9-12 and 13-16 were compared with each other (see Figure 19), so for both measuring positions both sides were tested.

The third set of tests was to see if the different measurement protocols influence the measurement data. As for each measurement the same three parameters E_d , L_u and L_{sky} were measured, only the differences in the viewing zenith and azimuth angles were tested. Because the inclination sensor was broken, the exact viewing zenith angle was unknown. However, RAMSES TriOS should be fixed at $\theta = 40^\circ$, which means that, if the instrument is held vertically, the measurements were done with $\theta = 40^\circ$. To test if this was true, seven different angles were tested for four chosen measurements. The angles were $\theta = 35^\circ, 38^\circ, 39^\circ, 40^\circ, 41^\circ, 42^\circ$ and 45° . A deviation of more than 5° is unlikely, which is why a range from 35° to 45° was chosen, with narrower steps around 40° . To test the difference in the viewing azimuth angles, also measurements 1-4, 5-8, 9-12 and 13-16 were compared with each other (see Figure 19).

The data processing was done in Python 3.8 and in Microsoft Excel.

8.4.5 Data evaluation

8.4.5.1 Outlier determination

To spot and eliminate outliers, they were firstly characterized by reflectance values too high or too low compared to the other measurements. And secondly by two factors which eliminate possible error sources. One source is if the E_d sensor is not measuring vertically, so it measures too much dark values from the horizon, which leads to an underestimation of the E_d values and therefore to an overestimated reflectance over the whole spectra. The other source is if the L_u sensor is not pointed correctly to the desired spot, so therefore it measures more surface reflection

in all wavelengths. This overestimation is compensated in the NIR region and the used reflectance coefficient is proportionally transferred to the shorter wavelengths. As the surface reflection is higher in smaller wavelengths, the compensated error from the coefficient also rises, which leads to negative reflectance values. We selected measurements with a reflectance of around 0 at 400nm but positive reflectance values at least after 410 nm – because reflectance should not be negative and reflectance starts in the visible range of the electromagnetic spectrum starting at 400 nm – and by a relatively low but still positive NIR reflectance.

8.4.5.2 Mean average error (MAE)

The MAE will be used to determine the error values between two selected measurements with the same scale to show the accuracy of the measurements (Seegers et al., 2018).

The MAE is calculated as followed:

$$MAE = \frac{\sum_{i=1}^n |M_i - O_i|}{n} \quad \text{Eq. (14)}$$

where M stands for modeled values, O for observed values and n for the sample size.

The MAE was chosen because it does not amplify outliers (less sensitive to outliers) and accurately reflects the error magnitude (Seegers et al., 2018).

9 Results

This chapter shows the results of the different tests regarding measurement conditions, measurement protocols, processing schemes and sensors. After that, a requirement analysis was conducted to show what needs to be considered when doing spectral measurements of water bodies and what the different steps are if a data exploitation platform is going to be used to handle the data. In the end, the gaps between the state of the art now and what would be the desired processing chain are examined.

9.1 Measurements Greifensee

9.1.1 Outliers

The outlier measurements were number 4, 8, 12 and 16, which are the measurements with the biggest azimuth angle away from the sun (see Figure 19).

Measurement number 4 (see Figure 21) is considered an outlier, as it starts already at 0.001 at 400 nm and the reflectance in NIR is way too high, also compared to the other measurements. Number 2 seems to be the best measurement, as it has no values below 0 and at 400nm the R_{rs} starts at around 0 and has a rather low NIR reflectance. Measurement number 1 and 3 were not chosen as

for all four methods, except for Simis & Olsson (2013), they either had reflectance values too high or below 0 at 400 nm.

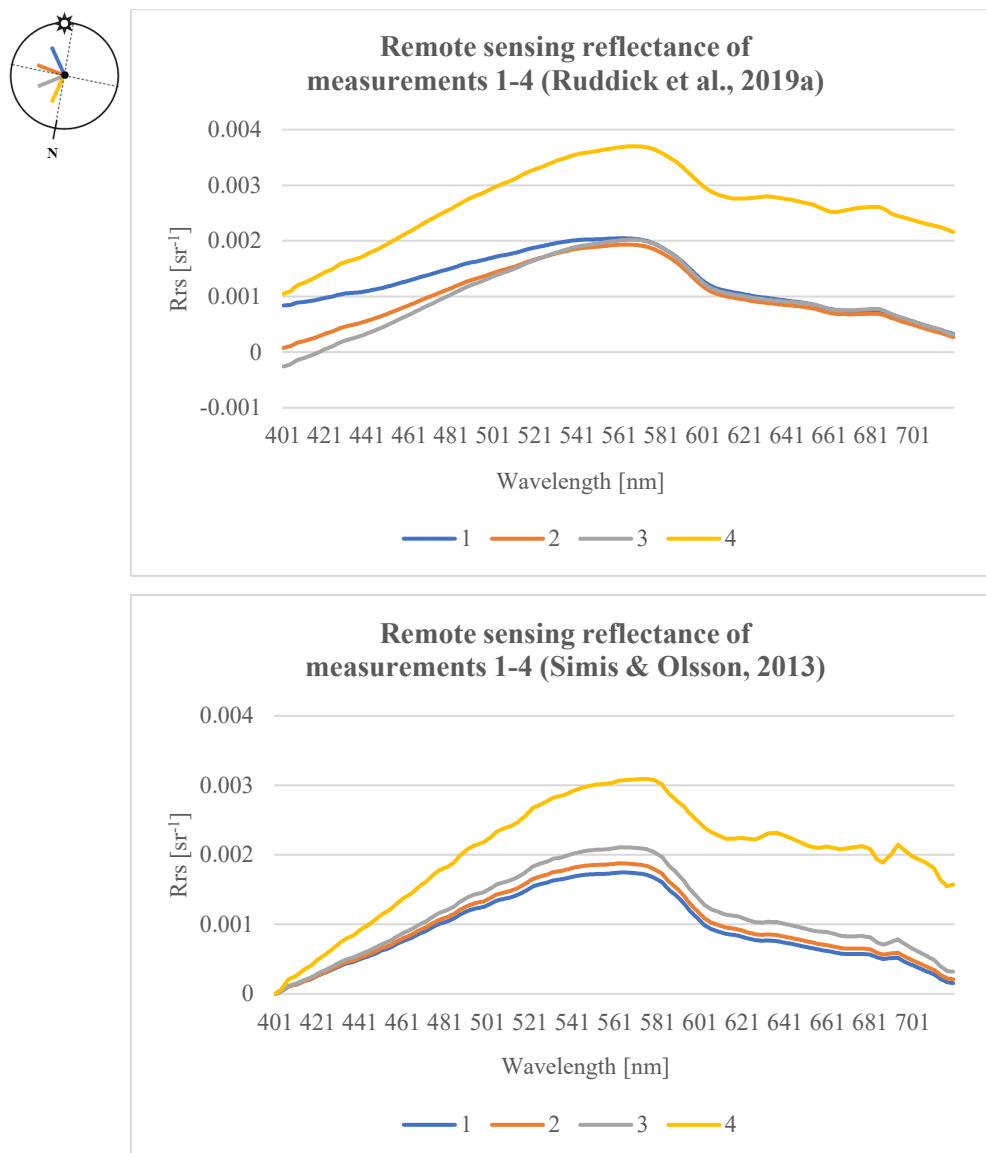


Figure 22: Remote sensing reflectance [sr^{-1}] from measurements 1-4 per wavelength [nm], with the outlier measurement number 4 in yellow. Shown are the results from the processing schemes from Ruddick et al. (2019a) and from Simis & Olsson (2013) (all graphs from the other methods can be found in the Appendix 13.1).

For measurement number 8 (see Figure 22) the curve of the spectrum looks about the same as for measurement number 4, where the reflectance for number 8 is too high compared to the other measurements, but the offset is not as big. Here measurement number 6 seems to be the best as it has positive values shortly after 400 nm and has a relatively low NIR reflectance. Measurement number 7 was not chosen as the best measurement, although it has a lower NIR reflectance, but the reflectance values only get positive after around 450 nm. And number 5 has too high reflectance values around 400nm and in the NIR region.

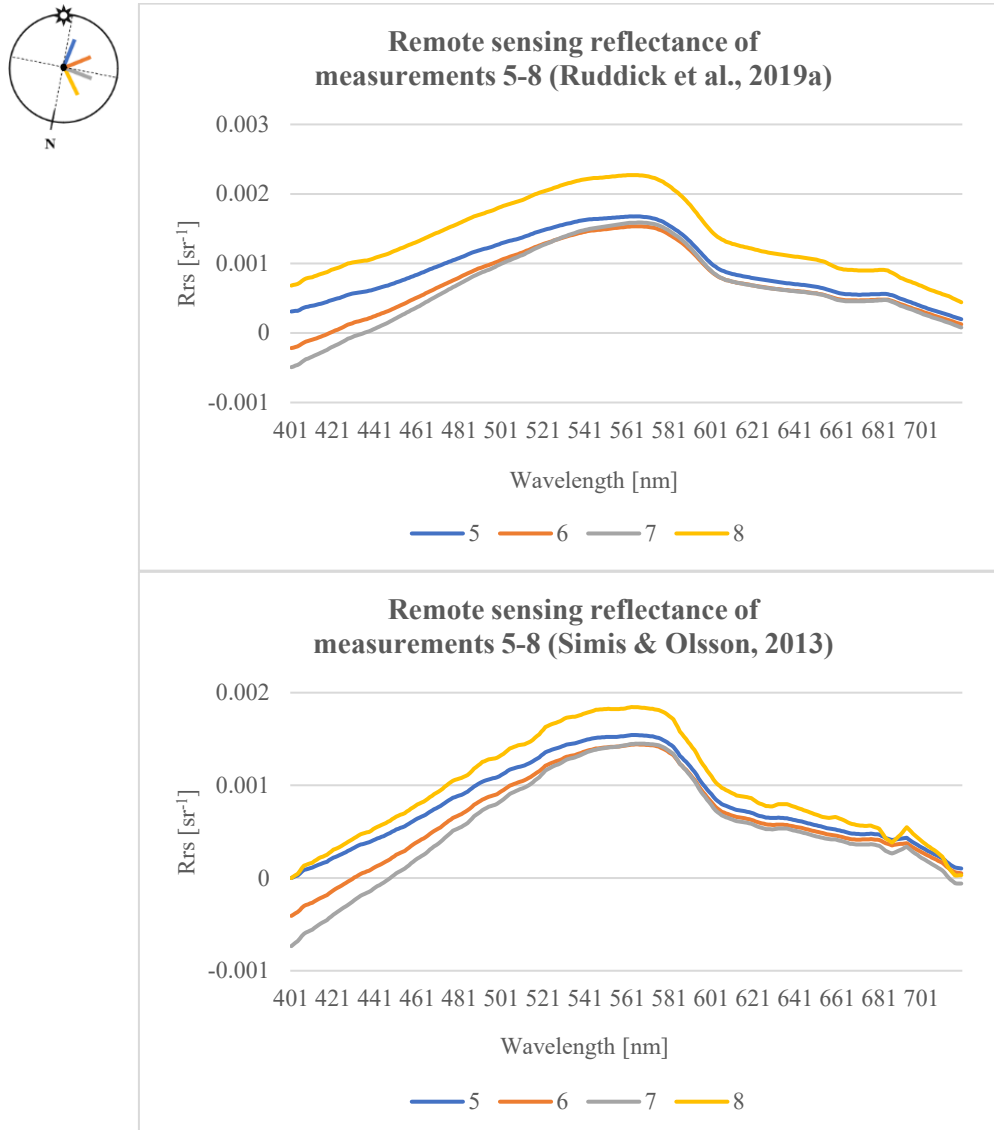


Figure 23: Remote sensing reflectance [sr⁻¹] from measurements 5-8 per wavelength [nm], with the outlier measurement number 8 in yellow. Shown are the results from the processing schemes from Ruddick et al. (2019a) and from Simis & Olsson (2013) (all graphs from the other methods can be found in the Appendix 13.1).

The outlier measurement number 12 (see Figure 23) is characterized by a reflectance too low below the measurements 9-11. Also compared to the other measurements in general, the maximum of the curve at around 0.001 is low. Measurement number 6 seems to be the best here, as it starts with positive values at 400 nm and has a rather low reflectance in near. Measurement 9 has again values too high at 400 nm and in NIR, and measurement 11 only starts with positive values after 440 nm and has a rather low reflectance in general.

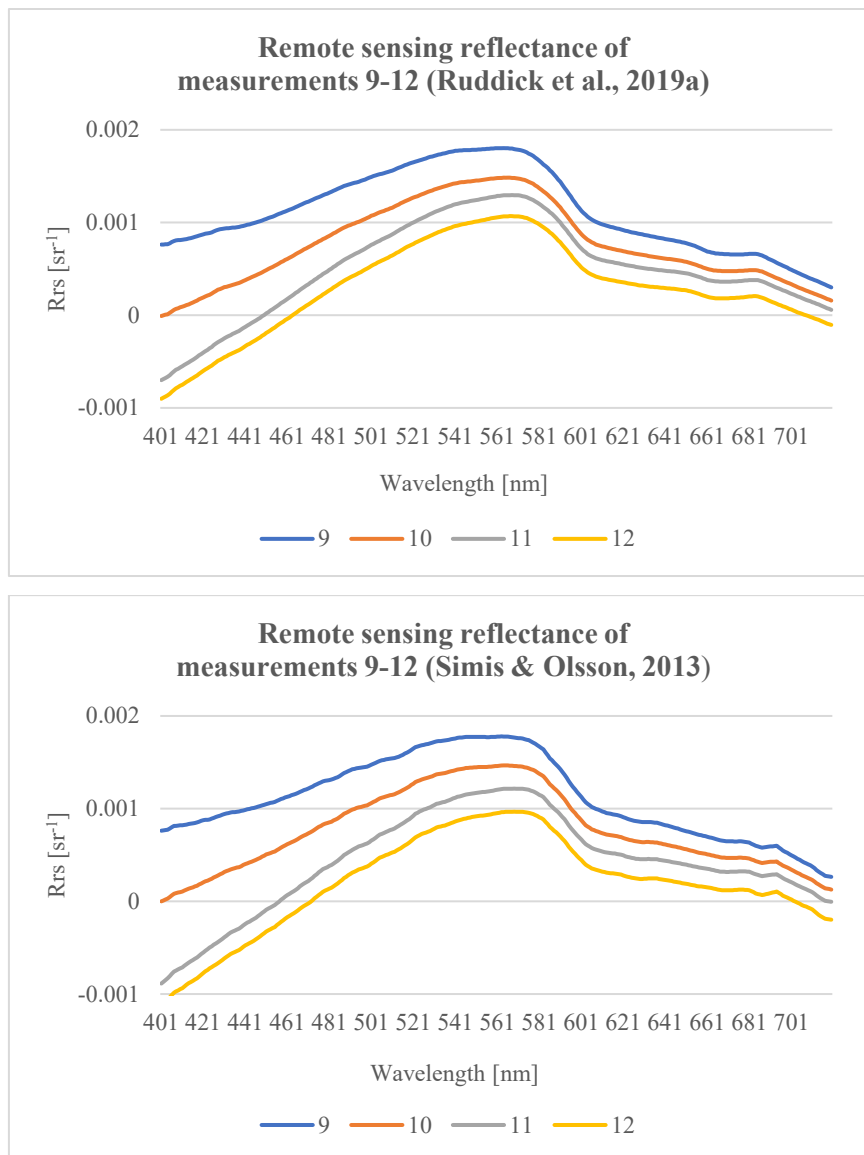
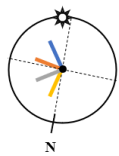


Figure 24: Remote sensing reflectance [sr^{-1}] from measurements 9-12 per wavelength [nm], with the outlier measurement number 12 in yellow. Shown are the results from the processing schemes from Ruddick et al. (2019a) and from Simis & Olsson (2013) (all graphs from the other methods can be found in the Appendix 13.1).

Measurement number 16 (see Figure 24) again has overestimated reflectance values compared to measurements 9-11. Here measurement number 14 looks the best, as it again starts around 0 at 400nm and has a low reflectance in NIR. Measurements number 13 again has reflectance values too high at 400 nm and in the NIR region and measurement number 15 has reflectance values below 0 until around 450 nm.

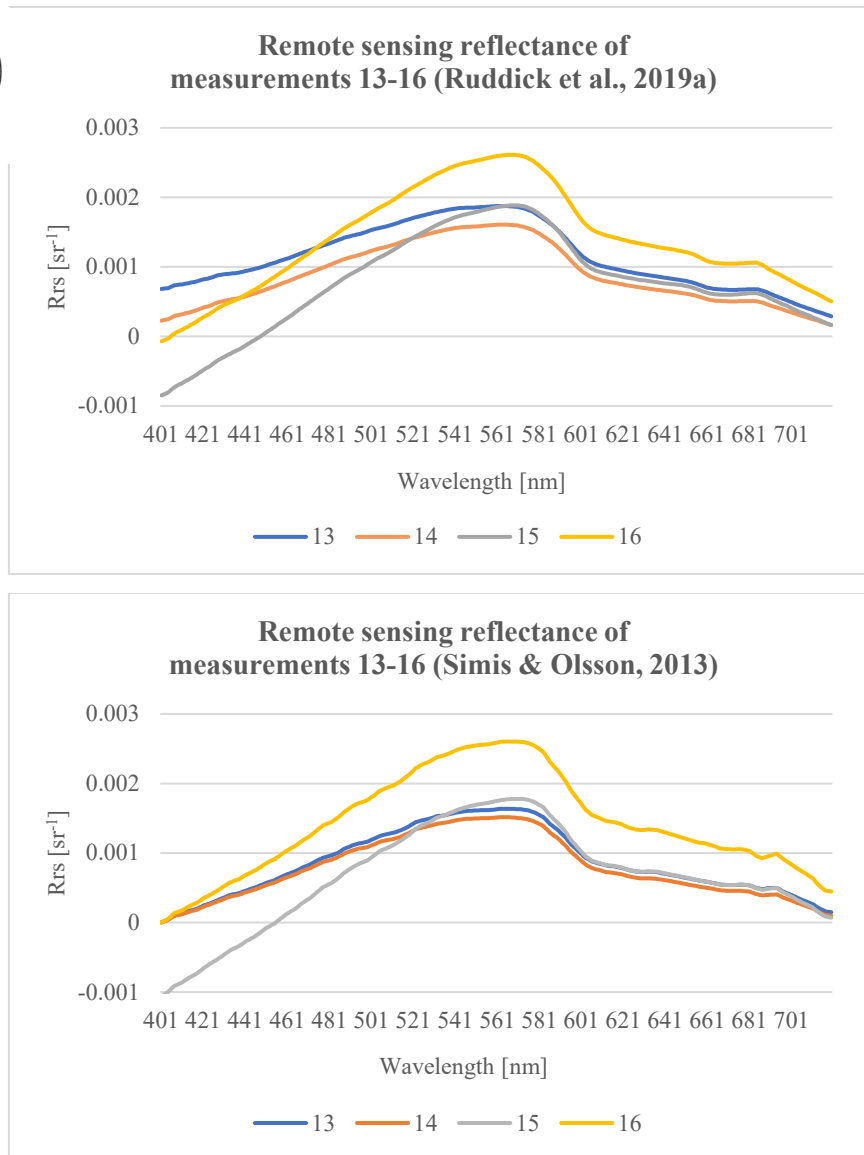
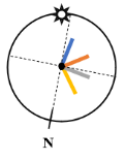


Figure 25: Remote sensing reflectance [sr^{-1}] from measurements 13-16 per wavelength [nm], with the outlier measurement number 16 in yellow. Shown are the results from the processing schemes from Ruddick et al. (2019a) and from Simis & Olsson (2013) (all graphs from the other methods can be found in the Appendix 13.1).

After determining the ‘best’ measurements 2, 6, 10 and 14, the Mean Average Error (MAE) (see Eq. (14)) was used to determine the error between the ‘best’ measurements and the other measurements and outliers. Here the best measurements were used as the modeled values and the other measurements and outliers as observed values and the number of measurements from 400 to 720 nm as sample size. In the following table (Table 2), the values for each method can be seen, where the higher the value, the higher the error. The numbers in red are the highest error values, which are also the measurements categorized as outliers.

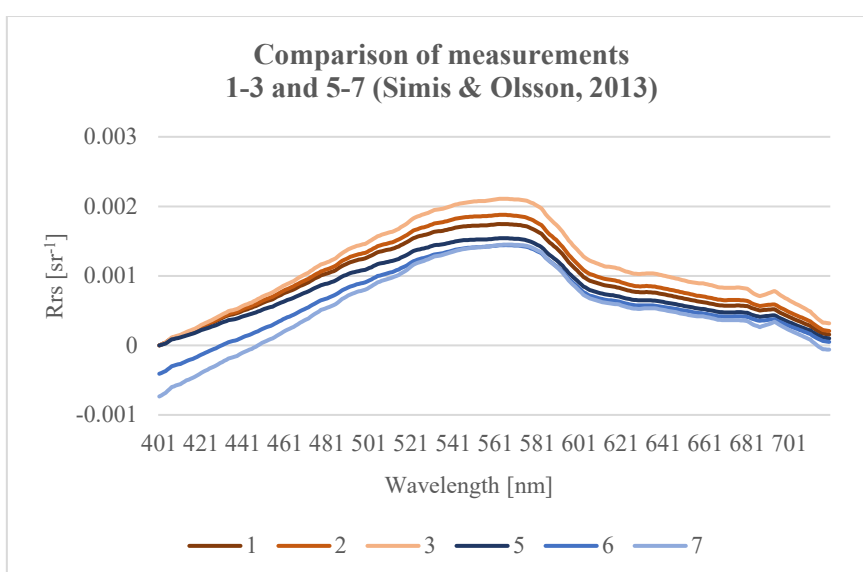
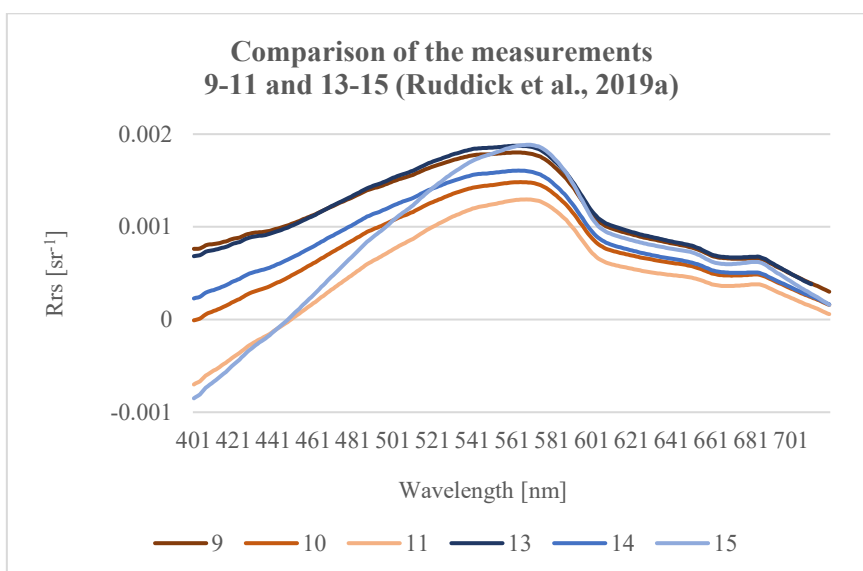
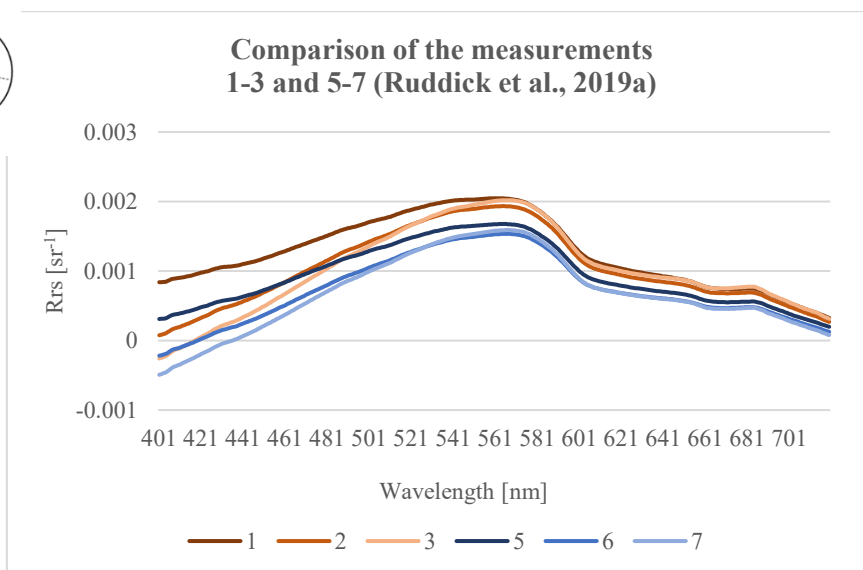
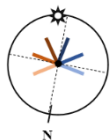
Table 2: Mean average error [± 1000] of the observed values of all four processing schemes (between 0 and 1). The modeled values are the chosen ‘best’ measurements 2, 6, 10 and 14. Values in red symbolize the highest values.

Modeled	2			6			10			14		
Observed	1	3	4	5	7	8	9	11	12	13	15	16
Ruddick et al., 2006	0.24	0.1	1.64	0.2	0.05	0.66	0.36	0.27	0.49	0.26	0.28	0.53
Ruddick et al., 2019a	0.23	0.1	1.63	0.2	0.07	0.66	0.36	0.26	0.47	0.26	0.28	0.55
Simis & Olsson, 2013	0.08	0.15	1.03	0.15	0.09	0.31	0.35	0.34	0.57	0.08	0.28	0.63
Groetsch et al., 2017	0.14	0.1	0.43	0.2	0.07	0.63	0.17	0.27	0.48	0.12	0.28	0.53

9.1.2 Measurement conditions

The first test to see if the prevailing measurement conditions had any influence on the data, showed that between the two different measuring positions (measurements 1-7 vs. 9-15), no clear difference could be seen (see Figure 25). Between the two measurement positions the weather and lake conditions did not change a lot and were stable (unproductive part of the year, sunny, only little clouds, no wind), although the two positions were 20 to 25 minutes and about 2 km apart. So, for both positions the spectra have similar shapes, the highest reflectance values lay in the green spectrum at around 560nm and the range of the values have about the same extent.

Between the clear and the hazy side there seems to be a difference but there was no clear evidence that for example the hazy side had a lower R_{rs} than the sunny side or the other way around. For both methods, Ruddick et al. (2019a) and Simis & Olsson (2013), for measurements 1-3 and 5-7 (see Figure 25, first two graphs), it seems that the ‘sunny’ side (1-3, red-ish colors) has a higher reflectance in general than the ‘hazy’ side (5-7, blue-ish colors). Looking at measurements 9-11 and 13-15 (see Figure 25, last two graphs) this assumption can be neglected, because there is no clear difference between the two sets of measurements.



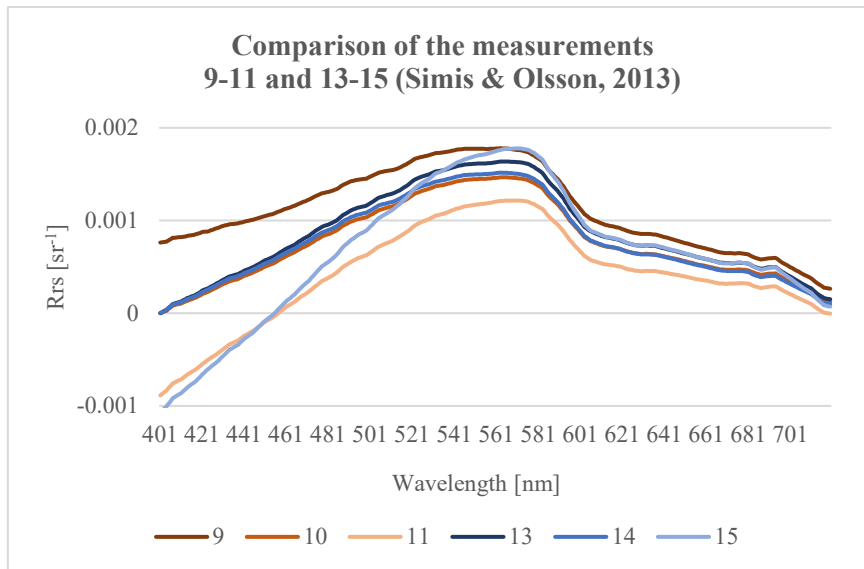
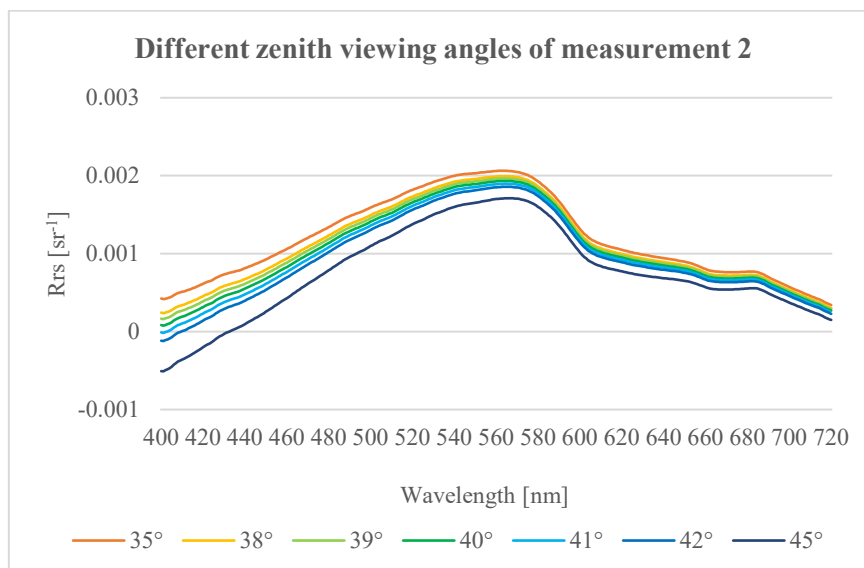
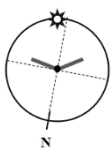


Figure 26: Comparison of two measuring positions (two top graphs vs. two bottom graphs) and of the ‘sunny’ (measurements 1-3 & 9-11) and the ‘hazy’ side (measurements 5-7 & 13-15) (all graphs from the other methods can be found in the Appendix 13.2).

9.1.3 Measurement protocols

The third test showed that different zenith viewing angles have an influence on the remote sensing reflectance. The test was done with the method by Ruddick et al. (2019a), because one of the main inputs is the zenith viewing angle θ_v (= nadir angle), see Eq. (7). The four good measurements 2, 6, 10 and 14 were tested with the angles $\theta = 35^\circ, 38^\circ, 39^\circ, 40^\circ, 41^\circ, 42^\circ$ and 45° . Viewing angles above 45° or under 35° were not tested as these are rather unlikely if the instrument should have been fixed to $\theta = 40^\circ$. For all four measurements, the shape of the spectra stays the same but the higher the angle the lower the R_{rs} value and the lower the angle the higher R_{rs} value (see Figure 26).



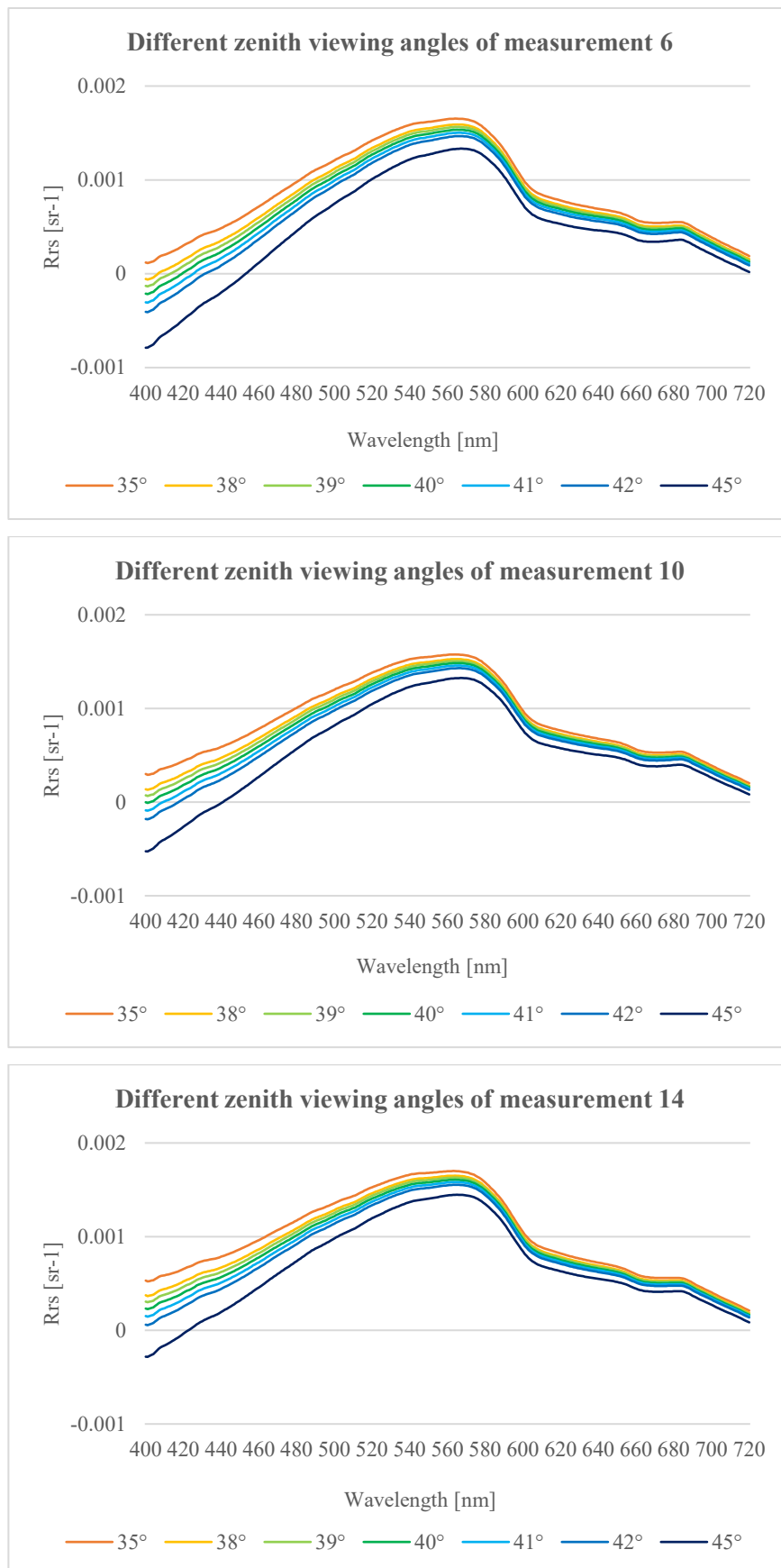


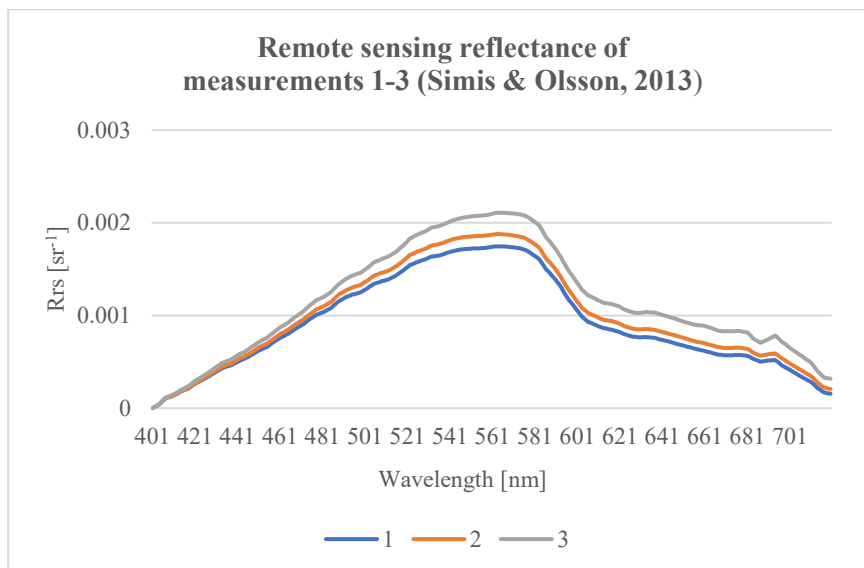
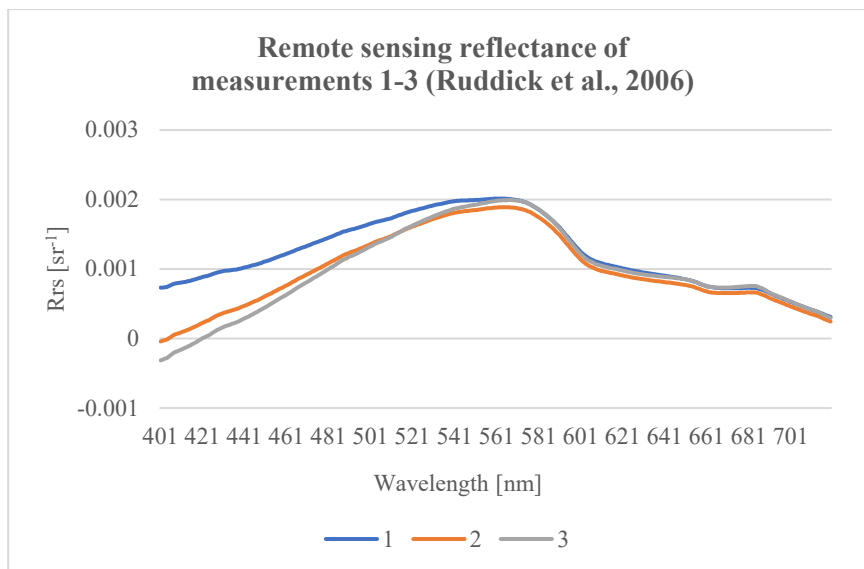
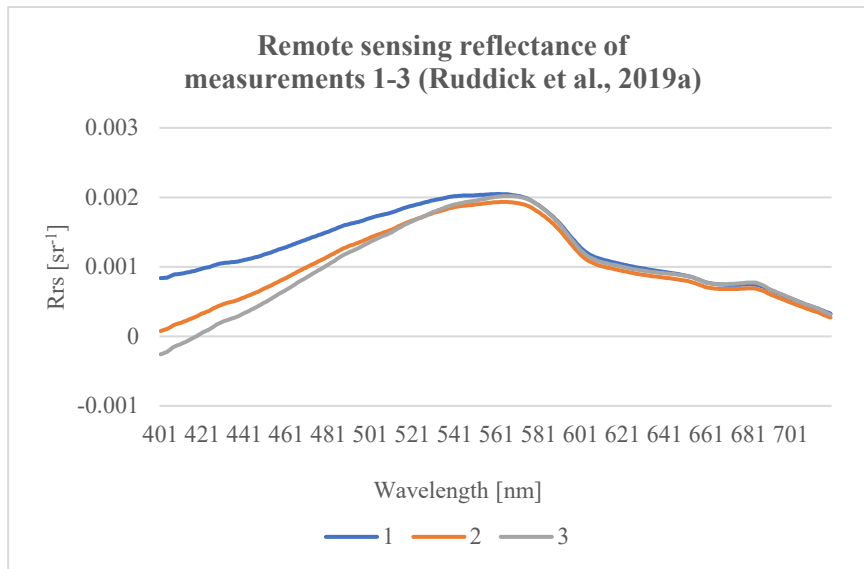
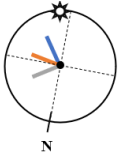
Figure 27: Remote sensing reflectance of measurements 2, 6, 10 and 14 with different zenith viewing angles, 35°, 38°, 39°, 40°, 41°, 42° and 45°, processed with the method by Ruddick et al. (2019a).

For testing the dissimilarity between the viewing zenith angles, also the MAE was applied. Differences between 38° and 42° with one degree and 1 nm steps (400-720 nm) were tested. The resulting MAE was between 0.0003 and 0.0004, which got slightly larger the higher the viewing zenith angle. The smallest difference between two angles was 0.0001 and the highest was 0.0009. As for the difference between the wavelengths, it showed that for all zenith viewing angles, shorter wavelengths had a slightly higher difference than the longer wavelengths. This observation supports the before mentioned error source in 8.4.5.1, which affects the shorter wavelengths, if the L_u sensor is not pointed correctly and causes an overestimation of the reflectance.

For the different viewing azimuth angles, the assumption that the higher the azimuth angle, the higher the remote sensing reflectance, was tested. It only was true for measurements 9-12 (see Figure 23), but for all other measurements it was not always the case (see Figure 21, Figure 22, Figure 24). The diversity between the measurements was too random, even without the outliers, to do further data analysis towards this assumption. Without further data testing, this assumption can be dismissed. Also, because the azimuth angles are unknown, it was not possible to test if the ‘ideal’ azimuth angle of $\varphi = 135^\circ$ results in better data than other angles.

9.1.4 Processing schemes

The second set of tests showed that the different processing schemes influenced the data output. The methods of Ruddick et al. (2019a) and Ruddick et al. (2006) showed similar results as the processing resulted in similar ρ_{sky} values, which led to similar reflectance values (see Figure 27). The fingerprint method by Simis & Olsson (2013) and the 3C model by Groetsch et al. (2017) resulted in slightly different outcomes, as they took a lot more factors into account to calculate the R_{rs} . They both calculate a different ρ_{sky} for each given wavelength by the sensor, whereas Ruddick et al. (2019a) just calculate one ρ_{sky} for all the measurements and Ruddick et al. (2006) either takes the given value for a cloudy sky or a clear sky. Taking a different ρ_{sky} for each wavelength leads to a more exact estimation of the R_{rs} , which is visible in the produced spectra, as they do not seem as ‘smooth’. Here also the interpolation of the wavelengths should be considered. RAMSES TriOS only produces values every 3 nm, therefore the values had to be interpolated to a spectral resolution of 1 nm.



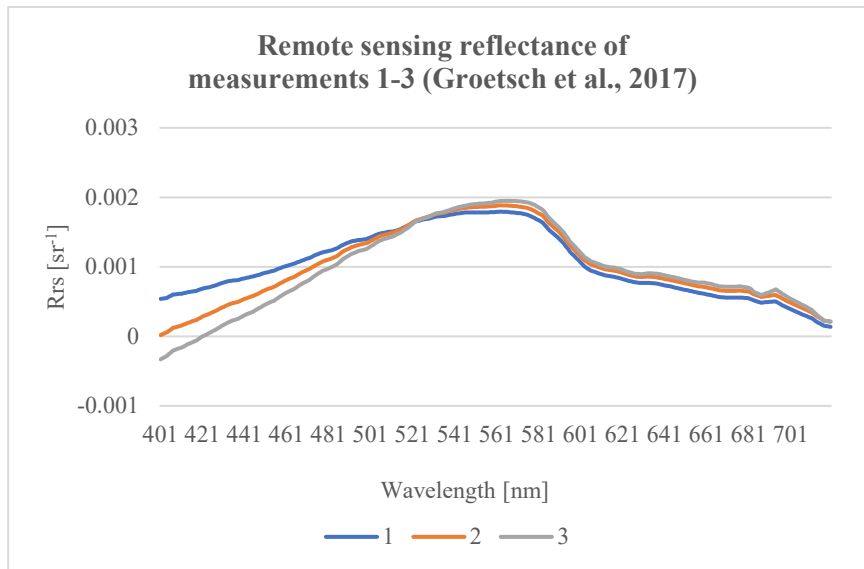


Figure 28: Comparison of the four processing schemes of measurements 1-3 (all graphs from the other methods can be found in the Appendix 13.3).

The mean average error was also applied to the four best measurements between the four processing schemes (see Table 3). The resulting MAE ranges between 0.00002 and 0.0001. Here no clear statement can be made that for example two processing schemes have more similar results than the other two. As the values of the measurements range approximately from 0 to 0.002, a MAE of 0.00002 to 0.0001 is rather small, which means that the processing schemes produce pretty similar results, with only some discrepancies.

Table 3: Mean average error [$\div 1000$] between all four methods for the best measurements 2, 6, 10 and 14. Red values symbolize the highest and green the lowest values.

Measurement	2				6			
	Ruddick et al., 2006	Ruddick et al., 2019a	Simis & Olsson, 2013	Groetsch et al., 2017	Ruddick et al., 2006	Ruddick et al., 2019a	Simis & Olsson, 2013	Groetsch et al., 2017
Ruddick et al., 2006		0.05	0.02	0.03		0.05	0.04	0.02
Ruddick et al., 2019a	0.05		0.04	0.04	0.05		0.09	0.03
Simis & Olsson, 2013	0.02	0.04		0.01	0.04	0.09		0.06
Groetsch et al., 2017	0.03	0.04	0.01		0.02	0.03	0.06	

Measurement	10				14			
Method	Ruddick et al., 2006	Ruddick et al., 2019a	Simis & Olsson, 2013	Groetsch et al., 2017	Ruddick et al., 2006	Ruddick et al., 2019a	Simis & Olsson, 2013	Groetsch et al., 2017
Ruddick et al., 2006		0.04	0.04	0.02		0.04	0.05	0.02
Ruddick et al., 2019a	0.04		0.01	0.03	0.04		0.1	0.03
Simis & Olsson, 2013	0.02	0.01		0.02	0.05	0.1		0.07
Groetsch et al., 2017	0.02	0.03	0.02		0.02	0.03	0.07	

9.2 Similarities and differences of the sensors

As the measurements were only done with one sensor, RAMSES TriOS, the differences of the instruments could not be tested in the field. Therefore this chapter will be based on literature from chapter 7.4 and the findings regarding sensor accuracy of Hommersom et al. (2012).

The three instruments, WISP-3, RAMSES TriOS and ASD FieldSpec are all hyperspectral radiometers which measure E_d , L_u and L_{sky} . The AC-S and the ECO-VSF 3 are pretty unique sensors in their specific setup and application. These sensors can for example be used in addition to one of the radiometers. At a first look, the three radiometers may seem very similar, as the basic measurement principles are the same. But the setups and measurement protocols differ. All three radiometers measure the same three parameters and they can all be used for above-water measurements. For the calculation of the remote sensing reflectance, all three use Eq. (3) and Eq. (4) (see Table 4).

WISP-3 is operated only by hand, and during the time of the measurement the person holding it must maintain the exact position, with a stretched out arm at 90 degrees, which can be challenging. The viewing angles in nadir and zenith are fixed to $\theta = 42^\circ$ by Water Insight, and the azimuth angle relative to the sun is recommended to be at $\phi = 135^\circ$. Even though the raw data is provided, the data processing takes place on WISPweb. Unfortunately, it is not fully disclosed by Water Insight how the calculation is done to get from the raw data to the remote sensing reflectance.

RAMSES TriOS is mounted on a steel frame and can then be mounted on the ship, ideally with a construction which balances out the ships movements and maintains the desired zenith viewing angle. Such a construction was not available yet during the measurement on Greifensee, which made it harder to acquire the data. The viewing geometry of RAMSES TriOS is not fixed, it can be chosen by any measurement protocol, for example by Mueller et al. (2003), Tilstone et al.

(2017), Simis (2013), Dev & Shanmugam (2014), Dekker et al. (2002) or Kutser et al. (2013). Also, the measurement intervals can be altered.

ASD FieldSpec is also hand-held but the instrument itself is carried as a backpack. This instrument was not particularly designed for only water measurements, it can also be used on land. The viewing geometry is also not fixed, but also here the suggested zenith viewing angle is $\theta = 40^\circ$ and the azimuth viewing angle $\phi = 135^\circ$. ASD FieldSpec has only one radiometer to measure all three parameters, whereas WISP-3 and RAMSES TriOS have three radiometers. Also, the spectral ranges of the three instruments differ, but all of them are adequate to cover the spectral signature of water.

Table 4: Intercomparison of WISP-3, RAMSES TriOS and ASD FieldSpec (Modified after Hommersom et al. (2012)).

Instrument	WISP-3	RAMSES TriOS	ASD FieldSpec
Deployment	Above water	Above water	Above water
Radiometers	E_d, L_u, L_{sky} Hyperspectral	E_d, L_u, L_{sky} Hyperspectral	E_d, L_u, L_{sky} Hyperspectral
Method	Three radiometers	Three radiometers	One radiometer, E_d with RCR
FOV (radiances)	3 deg	7 deg	6 deg
Angle relative to zenith and nadir	$\theta = 42$ deg	$\theta = 41 / 40$ deg	$\theta = 40$ deg
Equations for R_{rs}	Eq. (3) & Eq. (4)	Eq. (3) & Eq. (4)	Eq. (3) & Eq. (4)

9.2.1 Sensor accuracy

In the year 2012, WISP-3 recently came out, which led Hommersom et al. (2012) to this study, where they compared WISP-3 to TriOS RAMSES, ASD FieldSpec and TACCS. The focus of the comparison was laid on the quality of the obtained reflectance spectra because they affect the accuracy of the used algorithms to derive water quality parameters. They tested the performance of these radiometers on field campaigns on lakes with different water constituents and under changing cloud cover and with waves. These ‘unperfect’ measuring conditions were intentionally chosen, because they are thought to be more representative of the conditions you usually face on the field. After the measurements, Hommersom et al. (2012) compared, the spectra of E_d , L_{sky} , L_u and the R_{rs} from the different instruments with each other. They concluded that how accurate measurements are, depends on mainly three factors, the sensitivity of the spectrometer, the calibration of the spectrometer and the correct deployment. The biggest errors in their study were caused by wave action, not using the same calibration sources for the instruments and not measuring at the exact same moment and not pointing the instrument at the same spot. However,

the largest effect between the instruments was caused by L_u because not all instruments have the same accuracy in the 480 to 680nm region and because of the included unknown proportion of direct sky reflection.

9.3 Requirement analysis

This requirement analysis sums up which factors have to be considered and which steps have to be taken before conducting spectral measurement on a lake. It also implements the necessary steps when handling the data with the data exploitation platform SPECCHIO. This requirement analysis is based on literature, the interview with Bastian Buman, the IT specialist of the Remote Sensing of Water Systems (RSWS) of the Department of Geography, regarding SPECCHIO and my own experiences while conducting measurements on Greifensee and processing the data.

9.3.1 Measurement setup

Before the actual data acquisition, the measurement setup has to be chosen. For aquatic measurements there are several possibilities (Banks et al., 2020; Ruddick et al., 2019a, 2019b). Either measuring from a platform is possible, with the sensors fixed right at the water level or at a certain height, or underwater. Measuring from a boat is the other option, also either above water at certain heights or underwater. Here the defining factors are on the one hand the sensor that will be used, if it is suited for underwater measurements or only above-water measurements, and also the equipment, that is accessible, if you have access to boats or platforms. On the other hand it is important what parameters (Giardino et al., 2019; Mobley et al., 2004) are going to be measured and what you want to get from the data in the end, and if the data can be required by underwater or above water and if additional measurements need to be taken (Tilstone et al., 2017). Additional to the measurement setup, the time and weather need to be considered, as they influence the data quality. Optimal conditions would be: clear sky, no to little wind and a high position of the sun (Ruddick et al., 2019a).

9.3.2 Sensors

Additional to the measurement setup, a sensor must be chosen. Here it is important to know what the sensor is capable of measuring, what additional equipment is needed, e.g. field laptop or mounting frame, and how you can access the produced data (Alikas et al., 2020; Hommersom et al., 2012; Ruddick et al., 2019a; Tilstone et al., 2020). Another factor also will be, which sensors already are available, for example at your workplace or research institute, and if it is affordable if you need to acquire a new sensor. Training people or providing staff that knows how to operate the sensors is also necessary (Banks et al., 2020).

9.3.3 Data

For in situ measurements of aquatic systems, three parameters are needed, E_d , L_u and L_{sky} (above-water) or E_d , L_u and E_u (underwater) (Ruddick et al., 2019a). These are especially needed if the L_w and then the R_{rs} want to be determined (Mobley, 1999). This is why spectrometers, which are used for these measurements, usually have three sensors, one for each parameter, like for example RAMSES TriOS and WISP (Hommersom et al., 2012). But this three parameter themselves are not sufficient for a further data analysis and interpretation. Metadata and even additional measurements are helpful (Banks et al., 2020; Hueni et al., 2009). First, the measurement setup has to be described by the metadata. Date, time and GPS coordinates are essential information for reproducibility (Banks et al., 2020) and to determine the position of the sun. Weather conditions, for example the state of the sky (clear / partly cloudy / cloudy) or the wind velocity, which also influences the movement of the water, will help with the interpretation of the data (Banks et al., 2020). Pictures of the setup and 360° pictures of the surroundings are helpful. Additional measurements of the viewing zenith and azimuth angles are beneficial for determining if the measurement was good or maybe influenced by errors (Ruddick et al., 2019a). If the sensor has an inclination sensor, for example RAMSES TriOS, it is important to test it beforehand, to see if it works correctly, because it will show if your sensor was deployed correctly at the desired angle (TriOS Mess- und Datentechnik GmbH, 2013). Other additional measurements can also be done underwater, for example with the AC-S (Sea-Bird Scientific, 2013), absorption and attenuation could be measured, or water samples could be taken if you want to know more about the quality of the water.

9.3.4 Measurement protocols

Before starting to measure, a measurement protocol needs to be chosen based on either experiences from previous measurement campaigns or from literature. For example, if you measure above water, you need to know at which viewing zenith and azimuth angles you will measure the three parameters E_d , L_u and L_{sky} (Ruddick et al., 2019a). For example, $\theta = 40^\circ$ for the viewing zenith angle and $\varphi = 135^\circ$ for the viewing azimuth angle (Mueller et al., 2003; Tilstone et al., 2017). Furthermore, you need to know if you want a continuous measurement period stationary (Giardino et al., 2019) or during a boat ride (Simis and Olsson, 2013) or only singular measurements at only one position or multiple positions. For continuous measurements, the measurement intervals need to be defined and should be the same for all instruments (Banks et al., 2020).

9.3.5 Processing schemes

As there exist several processing schemes, which can lead to different outcomes (Groetsch et al., 2017; Ruddick et al., 2019a, 2006; Simis and Olsson, 2013), it is necessary to know which

processing scheme will fit the best for the measurements taken. Either the processing is done automatically, for example data of WISP will be processed in the WISPweb directly (Water Insight, n.d.), or it is done manually, for example with data of RAMSES TriOS. But also, the automatic systems use a defined processing scheme, which should be known if you choose this method. As for the manual processing schemes, the calculation of L_w and R_{rs} mainly relies on the correct determination of ρ_{sky} (Mobley, 1999), it is important to know how the processing scheme determines this factor. ρ_{sky} is a function of many factors, like the incident angle of the radiance, the water surface roughness (including wind velocity), atmospheric influences, the state of the sky (clear vs. cloudy sky) and the type of water body (clear vs. turbid water) (Groetsch et al., 2017; Mobley, 1999; Ruddick et al., 2006; Simis and Olsson, 2013). Therefore, it is important to know the measurement conditions and on what type of water body the data was acquired, so that a fitting processing scheme can be chosen.

9.3.6 Data exploitation platform

The processing of the data by hand, how I have done it, with multiple programs, e.g. Python for the processing and Excel for the data clean up and data analysis, is really time consuming. It also makes it difficult to store data and metadata and does not provide accessibility to other scientists. As mentioned before, data exploitation platforms will help with these problems and will make the whole processing chain more efficient. A fitting option would be SPECCHIO, as it allows storing spectra and metadata without redundancy, retrieving geophysical and biophysical parameters, testing different processing schemes and helps with uncertainty propagation because the whole processing chain happens in one system (Hueni et al., 2009).

According to Bastian Buman the following points in SPECCHIO need to be considered. SPECCHIO has no limits of how much spectra can be uploaded, it just needs to be clear which spectra is which and the file format should be defined. For example, RAMSES TriOS and WISP have generic data files (‘.dat’) or text files (‘.txt’). Not every file format is supported by SPECCHIO, so this needs to be checked before uploading the data into the system. The data can be raw or already calibrated. Raw data needs the corresponding formula and calibration file to convert it to calibrated data. For the collection of the metadata, almost everything is possible, from uploading pictures, to add additional measurements, information about the environmental conditions, the target information, and the viewing geometry. The processing of the data in SPECCHIO happens through Java or Matlab scripts, or it is possible to use another program, e.g. Python, which will access the data from the SPECCHIO database and then feeds the output back to the database. Like this any new method can be applied to the data. When the data is processed, several output options are available, for example display either each measurement for itself or in a time series, downloading the values of L_w and R_{rs} or plotting the data for comparison. Analytical comparison (e.g. correlation) is not possible in SPECCHIO. Either the output data can

be downloaded and processed further, or the analysis can be done in other programs, e.g. Python, which will access the input data from the SPECCHIO database.

Based on these facts by Bastian Buman and my data processing of the Greifensee data, the following processing chain in SPECCHIO based on RAMSES TriOS data is illustrated:

1. Input: The input data from RAMSES TriOS is obtained from the software MSDA_XE. Here the data can already be sorted and filtered, so that in the end only the desired data will be downloaded. The software also acts as data storage, as it saves all uploaded data. When downloading the data, it is important to choose the file format .dat. These files are all structured in the same way for each sensor, first the information about the sensor, data type and date and time and second the values per wavelength (for calibrated data) or counts from the sensor serially numbered (raw data). Only the calibrated data are of interest, which will also be loaded into SPECCHIO.
2. SPECCHIO: The calibrated data will be loaded into SPECCHIO as .dat files and stored without redundancy. Additional metadata can be added. Also, the inclination file should be added, as it provides the inclination angle of the sensor of every measurement, which corresponds to the viewing zenith angle. If the inclination sensor did not work properly, the viewing zenith angle should be added as metadata.
3. Processing: The processing can be done with any programming language. If you use an already existing script, use it in the format it is provided, to eliminate errors, which could arise when transferring the code to another programming language. Important here is that the input code of the script will access the input data from the SPECCHIO database. The input code needs to know the name and the type of the data files. The data then will be downloaded and processed. It is also important to interpolate the data, if the processed data does not have the same units, e.g. 1 nm wavelengths steps. This will make a comparison easier. The output will be uploaded to the SPECCHIO database again, for example the values for R_{rs} .
4. Analysis: The analysis can also be done in any programming language, e.g. again with Python. For the analysis the script should again access the data from the SPECCHIO database, do the analysis, and upload the resulting data to the database again.
5. Output: The processed and analyzed data can then in the end be downloaded from the SPECCHIO database in any data format.

9.3.7 Standardization

A processing chain like this would require some standardization. One would be that the data file format should for example be in the .dat format, no matter from which instrument the data is coming. The files themselves then should always have the same type of name so that the script

does not have to be rewritten each time and to make processing easier. If possible, already calibrated files should be used to minimize calculation errors. If only raw data is available, the instrument needs to be calibrated regularly, to remove errors based on old calibration files. In general instruments should be calibrated regularly to avoid errors (Banks et al., 2020; Hommersom et al., 2012). The registration of the metadata should also be as thoroughly as possible, as it will help other users understanding the data and makes reproducibility of measurements easier (Hueni et al., 2009). During the processing and analysis, it should be documented what was done and which method was used. Output data should always be uploaded again to the SPECCHIO database and not just stored locally.

9.3.8 Data quality

The data quality can be determined by preprocessing and postprocessing data checks and by the quality assurance of the instrument (Tilstone et al., 2017). It can also be determined if there is a reference spectrum available, for example by previous measurement campaigns or spectra produced in the lab or by satellites (Tilstone et al., 2020). Measures of errors or deviation of the data values can also help assessing the data quality (Seegers et al., 2018; Tilstone et al., 2020). It can also be determined relatively, if beforehand a desired outcome was defined, which can be described by the data sufficiently or not and if additional measurements are needed. Possible errors and uncertainties of the used methods should be known (Ruddick et al., 2019a), to be able to follow the error through the whole processing chain and to handle any error or uncertainty propagation.

9.4 Gaps

Between the state of the art and the desired processing chain, only some gaps exist. One concerns the coding of the scripts, as the line regarding the input data must be adapted to getting the data from SPECCHIO and the interpolation of the wavelengths needs to be implemented as a standard step during processing. Another factor is the data analysis, which was done in Excel for the Greifensee data. As Excel files are unfavorable files for SPECCHIO, the data analysis would need to be transferred for example also to a Python script like the different processing methods. The biggest gap would be if an instrument is used which for example has unfitting data files or lacks information about the calibration for the raw data. This was the case for the WISP instrument, as it only delivers raw data and the processing is done in WISPweb itself. How the raw data gets calibrated, is not fully transparent by the manufacturer and how the data is then processed is not displayed in WISPweb (Water Insight, n.d.). So, if you want to process WISP data yourself, some more information would be needed.

10 Discussion

10.1 Processing chain components and their impact on reflectance retrievals

The first two research questions looked at the currently used measurement protocols, processing schemes and instruments and their differences as these steps matter in the processing chain. This was investigated by a literature review and the case study conducted on Greifensee.

10.1.1 Measurement protocols

A lot of different measurement protocols exist, but the one that is still getting referred to a lot today, is the one from Mobley (1999). He concluded after numerical simulations that viewing directions of $\theta = 40^\circ$ in zenith and $\varphi = 135^\circ$ in azimuth are the best compromise between all requirements. Also both protocols from Mueller et al. (2003) and Tilstone et al. (2017) refer to Mobley (1999). The recent studies from Ruddick et al. (2019a) and (2019b), which did a review of the water measurement protocols, point out the viewing angles by Mobley (1999), but comment that the possibility of using other angles exist. For example, for using a reflectance plaque or if measuring on a mirror-flat lake with a high sun zenith, the viewing angles should be adapted.

As this suggested protocol has been tested a lot, the focus of this thesis was not to prove if these angles were ‘the best’. The goal was to show the difference in the data if different angles are used. For the test of the different azimuth viewing angles, only random unknown angles were tested. Although differences could be shown between the angles, they could not be quantified. It would also have been interesting to measure at the ‘ideal’ azimuth angle and compare it to the rest of the measurements.

The MAE was used for a measure of error between the different zenith viewing angles. It showed that for shorter wavelengths the differences were higher, which could have been looked further into, but too little data was available. Here it would also have been interesting to test different zenith viewing angles during the measurements to see how it would have influenced the data.

Unfortunately, only after the conducted measurements it became clear that measuring the exact zenith and azimuth angles would have been helpful to make more clear statements and to avoid errors induced by the wrong viewing geometry. For example zenith viewing angles below $\theta = 40^\circ$ and $\varphi = 135^\circ$ lead to higher sunglint effects (Mueller et al., 2003), and angles above $\theta = 40^\circ$ make the reflectance coefficient more sensitive to small changes of the viewing angles (Ruddick et al., 2019a).

10.1.2 Instruments

There already exist some studies that compared above-water radiometer measurements with each other. The already mentioned study from Hommersom et al. (2012) compared WISP-3, RAMSES

TriOS, ASD FieldSpec and TACCS on the Wadden Sea. Other more recent studies also compared radiometers on the ocean, for example Tilstone et al. (2020) compared RAMSES TriOS, SeaBird HyperSAS, SeaPRISM and PANTHYR with each other on the Adriatic Sea. Alikas et al. (2020) conducted a comparison between RAMSES TriOS and SeaBird HyperSAS on the 27th Atlantic Meridional Transect (AMT27) cruise. As these studies conduct their experiments on the ocean and not on lakes, there is still a need for studies conducted on complex waters, like lakes, to test and compare above-water radiometers with each other. One good recent example are the studies by Vabson et al. (2019a) & (2019b), who did a lab intercomparison and a field intercomparison on a lake in Estonia of RAMSES TriOS, WISP-3, HyperOCR, SR-3500 and SeaPRISM. They followed the suggested measurement protocols for above-water measurements. But as this study was done on a platform with the sensors mounted at 7.5m, it would also be of interest to conduct such a study on a boat/ship. The most recent and detailed review however was done by Ruddick et al. (2018) who reviewed the most common used ocean color radiometers used for satellite validation. They tested above and underwater sensors like RAMSES TriOS, WISP-3 or SeaPRISM on ocean waters. This study summarizes all characteristics of the instruments and to a level of detail which is necessary to do an uncertainty budget regarding the instruments (Banks et al., 2020).

This thesis only includes some chosen instruments, not all which are currently available. They were chosen based on what is currently used at the institute Eawag and well known in the aquatic community. The case study itself was only conducted with one instrument, RAMSES TriOS, on a lake because initially more measurement campaigns were planned but could not be executed. Therefore, I had to base the analysis of the instruments on the available literature. The focus was laid on the spectroradiometers which can be used for above-water measurements. But to fully show the accuracy of each sensor and the uncertainty budget, the literature itself will not be enough. The instruments should be compared with each other by above-water measurements on lakes to see which will work best with which measurement setup and causes the least errors. For example, a study like the one from Ruddick et al. (2018) but which tests the instruments on inland lakes.

10.1.3 Processing schemes

Regarding the processing of the data, scientists do not agree as much when it comes to the determination of the water-leaving radiance and the remote sensing reflectance. The formula how to derive L_w and R_{rs} is given by Mobley (1999) but how to calculate ρ_{sky} appropriately is still uncertain because it is influenced by many factors. Here a lot of approaches exist, depending on the factors that are considered important and what kind of water body will be measured, as becomes obvious from the comparison of four processing schemes. Here surely a need exists to

test these approaches and to come to a collective use of selected approaches among the water community.

Both processing schemes from Ruddick (2019a) and (2006) are rather simple and quick methods. Both just calculate one ρ_{sky} for the whole dataset. Ruddick et al. (2006) only distinguishes between a clear and a cloudy sky, which can lead to errors in the data if other factors, for example wind, influenced the data. Ruddick et al. (2019a) has a more general approach but it comes with correction factors which have to be applied to the processed data. This was not done with the data from Greifensee. Both processing schemes from Simis & Olsson (2013) and Groetsch et al. (2017) calculate a value for ρ_{sky} for each wavelength, which can lead to more accurate results. Simis & Olsson (2013) laid their focus on the spectral optimization through minimizing the influence of atmospheric absorption features in the resulting R_{rs} and on waters with varying spectral signatures like coastal waters. They concluded that their method worked best with a clear sky. However, they tested their method on the high-absorbing and low-scattering Baltic Sea with a construction that held the desired ‘optimal’ azimuth viewing angle. Therefore, it is uncertain how well this method works for measurements on lakes with different viewing azimuth angles. Groetsch et al. (2017) focused more on measurements with highly variable sky glint contribution, high wind speeds and unknown viewing angles. Their method was also tested on the Baltic Sea and adapted to the conditions on sea. Also, with this method it is uncertain how well it worked with the Greifensee measurements. The MAE between the best measurements and the four methods did not show any clear tendency to one ‘best’ method. Here more tests and analysis would be necessary to test the methods and their utilization for measurements on lakes.

The data processing was conducted with Python, which is quicker than processing by hand, but it requires some programming skills. Not as complex approaches as the two from Ruddick et al. (2006) and Ruddick et al. (2019a) can be implemented as simple scripts. But if using processing schemes from other scientists with more complex methods, it is best if they share their code openly, to prevent misunderstandings of the method itself and therefore error in the data. Implementing it in a data exploitation platform would also prevent that the limited programming capability by the user would influence the data quality. The data analysis was done in Excel, which was really time consuming although not a lot of data was processed. This step should be also be executed with data programming if larger datasets are handled. It could also be implemented in a Python script to save time and produce graphs more easily. The MAE was a good measure of error for the data which was available. If a reference spectrum existed or if a second measurement was done with more sensors, other measurements of error could have been applied.

10.2 Reliability of case study

The case study itself has to be assessed to make conclusions about the reliability. First, the measurement setup and used sensors can lead to introduced uncertainties in the data, if the measurement was not done correctly. Also, the used measurement protocols and processing schemes can lead to errors. And eventually the requirement analysis should be looked at critically.

10.2.1 Measurement setup and sensor

The measurement setup could have led to some errors in my data. First of all, the measurement took place in the end of January in the morning, when the position of the sun is not as high as in the summer. This leads to a lower at which radiation hits the water surface, which could introduce errors in the measurement of the irradiance and radiance.

Secondly, the bow of the ship was pointing to the sun during the measurement, but waves sometimes altered the position of the boat, which could lead to errors regarding the viewing azimuth angle.

And lastly, the pointing of the construction which held the three sensors was done by hand and not by an additional construction, which is able to maintain the exact viewing angles. This could also lead to errors in the viewing azimuth and zenith angle.

Regarding the sensors only the handling of RAMSES TriOS can be assessed because it was the only used instrument. This instrument requires the two irradiance sensors and the radiance sensor, the construction which holds the sensors and the field laptop. The construction which holds the sensors also should be mounted on a construction which can balance out the movements of the ships and can hold the desired viewing angles. For the Greifensee measurements such a construction would have been helpful, because holding it by hand is laborious. The data acquisition however was done quickly and easy and everything could be controlled over the field laptop. The only problem was the inclination sensor, which did not work for unknown reasons. This should be tested before hand for next measurements. All in all, I would say that if you have the suitable setup for this sensor, it will be a good sensor with various possibilities of how to measure, e.g. underwater or above-water and with different viewing angles.

10.2.2 Measurement protocols and processing

The used protocol could introduce errors because the exact azimuth and zenith viewing angles are not known. The azimuth angles were completely unknown, and the viewing zenith angle was estimated to $\theta = 40^\circ$ because the instrument was fixed to this angle, but this could have changed during the measurements if the instrument was not held horizontally. This usually can be corrected with the help of the inclination sensor but because it did not measure correctly, it was not possible for this case. Therefore, comparing the measurements with each other was difficult and also

comparing the two measuring sides and the measuring positions did show any clear results because not the same angles were used for all measurements.

The processing schemes themselves could also lead to errors because they were fit for a specific case of water / measurement conditions or do not consider all factors which influence the reflectance coefficient. Which method in the end worked best, could not be assessed because there was no reference of how it should have looked like.

For the purpose of this thesis the measurements were sufficient, as they were only needed to show differences in the processing chain and not to exactly measure the water-leaving radiance and the remote sensing reflectance. But for a more detailed data analysis, a more accurate execution of the measurements would have been necessary.

10.2.3 Requirement analysis for spectral measurements on lakes

For the third research question, a possible requirement analysis was established. Some studies already show some guidelines and suggestions for radiometric measurement of water bodies. For example, Ruddick et al. (2019a) who reviewed the measurement protocols for water-leaving radiance and for the downwelling irradiance for the validation of satellite data and suggested guidelines to follow when conducting such measurements. Or Banks et al. (2020) who reviewed the FRM4SOC projects including the suggested methodology and came up with recommended actions when conducting these fiducial reference measurements.

My requirement analysis shows what needs to be considered when taking spectral measurements on a lake. It includes a concrete example of what to do if spectral data, for example data from RAMSES TriOS, is handled with a data exploitation platform, like SPECCHIO. This requirement analysis is also applicable to data of other instruments with similar data types and also to data exploitation platforms with a similar structure like SPECCHIO. As the requirement analysis is only developed in theory, it still needs to be applied in practice and the necessary steps need to be implemented in SPECCHIO.

10.3 Towards harmonized in situ measurements using a data exploitation platform

The fourth research question of how a data exploitation platform could help with the data handling was again conducted by a literature review and the discussion with Bastian Buman, The literature review showed that there exist a lot of spectral libraries and databases but none of them are exactly tailored to spectral measurements of water. Therefore the existing SPECCHIO was looked closer at, because it already works very well for spectral measurements of terrestrial surfaces and only needs to be adapted to work for water measurements. It is also suited to help with the harmonization of the processing chain, because it coordinates the data storage and handling, stores all kinds of metadata to help with comparing and reproducing the measurements, enables data

sharing between scientists and minimizes error propagation. What still is required to implement such a system is the consolidation of the measurement protocols and the integration of the processing schemes. It would also be beneficial if different data formats of different sensors can be read. The steps how to load the data, process and analyze them also needs to be harmonized. Additionally, more analysis options need to be implemented into SPECCHIO.

In the end I would suggest an add-on explicitly for water measurements to the already existing SPECCHIO, which for example could be called 'AQUASPECCHIO'.

11 Conclusion

In this thesis, the different methods of conducting in situ aquatic measurements were shown and some of them were tested in a case study. It was shown that a lot of differences exist in the steps of the processing chain (measurement protocols – processing schemes – instruments). The goal was to lower this diversity. As a solution, a requirement analysis was established what should be considered when performing water measurements. It implies the usage of a data exploitation platform which would lead to a consolidated harmonized processing chain. Such a platform helps with combining and coordinating the separate steps of the processing chain among each other. This means that the different approaches to conduct water measurements are saved, assessed, and summarized to create an ordered structure. This leads to a higher comparability of the data and a defined standard on how to conduct water measurements.

A best instrument, measurement protocol or processing scheme cannot be named, because there is no definition of what is the 'best' method to conduct water measurements. In general, it remains a challenge to assess the accuracy of these methods. It is only possible to show how the different approaches and methods work, what their advantages and disadvantages are and where possible error sources are.

The asked research questions in the beginning could be answered and the hypothesis could be confirmed. However, as this thesis focused more on a theoretical approach for a solution, a follow up on the practical implementation is necessary. This also implies more testing and comparing different instruments on different water bodies with different setups and test and compare the different measurement protocols and processing schemes on their accuracy and maybe develop updated or more accurate methods. The requirement analysis can be used as a guideline when doing spectral (above) water measurements. With experience it can be expanded and specified. It should also keep updated with the recent advances in the scientific community. Also, a platform like the suggested 'AQUASPECCHIO' needs to be implemented first.

Generally, the knowledge of the processes happening during water measurements need to be deepened in the community. Also, an active exchange between scientists and transparency of used methods and data are necessary to improve the practice of water measurements.

12 References

- Alikas, K., Vabson, V., Ansko, I., Tilstone, G.H., Dall’Olmo, G., Nencioli, F., Vendt, R., Donlon, C., Casal, T., 2020. Comparison of above-water seabird and TriOS radiometers along an atlantic meridional transect. *Remote Sens.* 12. <https://doi.org/10.3390/rs12101669>
- AWEL, 2018. Wasser und Gewässer 2018.
- BAFU, 2016. Faktenblatt: Der Greifensee, Zustand bezüglich Wasserqualität.
- Banks, A.C., Vendt, R., Alikas, K., Bialek, A., Kuusk, J., Lerebourg, C., Ruddick, K., Tilstone, G., Vabson, V., Donlon, C., Casal, T., 2020. Fiducial reference measurements for satellite ocean colour (FRM4SOC). *Remote Sens.* 12, 1–37. <https://doi.org/10.3390/RS12081322>
- Barker, K., Mazeran, C., Lerebourg, C., Bouvet, M., Antoine, D., Ondrusek, M., Zibordi, G., Lavender, S., 2008. MERMAID: the MERIS matchup in-situ database. *Proc. 2nd MERIS/(A)ATSR User Work.* 1–6.
- Bojinski, S., Schaepman, M., Schläpfer, D., Itten, K., 2003. SPECCHIO: A spectrum database for remote sensing applications. *Comput. Geosci.* 29, 27–38. [https://doi.org/10.1016/S0098-3004\(02\)00107-3](https://doi.org/10.1016/S0098-3004(02)00107-3)
- Dekker, A.G., Brando, V.E., Anstee, J.M., Pinnel, N., Kutser, T., Hoogenboom, E.J., Peters, S., Pasterkamp, R., Vos, R., Olbert, C., Malthus, T.J.M., 2002. Imaging spectroscopy of water, in: *Imaging Spectrometry: Basic Principles and Prospective Applications.* pp. 307–359.
- Dev, P.J., Shanmugam, P., 2014. A new theory and its application to remove the effect of surface-reflected light in above-surface radiance data from clear and turbid waters. *J. Quant. Spectrosc. Radiat. Transf.* 142, 75–92. <https://doi.org/10.1016/j.jqsrt.2014.03.021>
- Dörnhöfer, K., Opelet, N., 2016. Remote sensing for lake research and monitoring - Recent advances. *Ecol. Indic.* 64, 105–122. <https://doi.org/10.1016/j.ecolind.2015.12.009>
- Giardino, C., Brando, V.E., Gege, P., Pinnel, N., Hochberg, E., Knaeps, E., Reusen, I., Doerffer, R., Bresciani, M., Braga, F., Foerster, S., Champollion, N., Dekker, A., 2019. Imaging Spectrometry of Inland and Coastal Waters: State of the Art, Achievements and Perspectives. *Surv. Geophys.* 40, 401–429. <https://doi.org/10.1007/s10712-018-9476-0>
- Gould, R.W., Arnone, R.A., Sydor, M., 2001. Absorption, Scattering, and Remote-Sensing Reflectance Relationships in Coastal Waters: Testing aNew Inversion Algorithm. *J. Coast. Res.* 17, 328–341.
- Groetsch, P., Foster, R., Gilson, A., 2020. Exploring the limits for sky and sun glint correction of hyperspectral above-surface reflectance observations. *Appl. Opt.* 59, 2942–2954. <https://doi.org/10.1364/ao.385853>
- Groetsch, P.M.M., Gege, P., Simis, S.G.H., Eleveld, M.A., Peters, S.W.M., 2017. Validation of a spectral correction procedure for sun and sky reflections in above-water reflectance measurements. *Opt. Express* 25, 1–20. <https://doi.org/10.1364/oe.25.00a742>
- Heege, T., Fischer, J., 2004. Mapping of water constituents in Lake Constance using multispectral airborne scanner data and a physically based processing scheme. *Can. J. Remote Sens.* 30, 77–86. <https://doi.org/10.5589/m03-056>
- Hommersom, A., Kratzer, S., Laanen, M., Ansko, I., Ligi, M., Bresciani, M., Giardino, C., Beltrán-Abaunza, J.M., Moore, G., Wernand, M., Peters, S., 2012. Intercomparison in the field between the new WISP-3 and other radiometers (TriOS Ramses, ASD FieldSpec, and TACCS). *J. Appl. Remote Sens.* 6, 1–21. <https://doi.org/10.1117/1.jrs.6.063615>
- Hooker, B., Firestone, R., 1994. The SeaWiFS and Storage System (SeaBASS), Part 1. NASA Tech. Memo. - SeaWiFS Tech. Rep. Ser. 20, 1–37.
- Hueni, A., Damm, A., Kneubuehler, M., Schlapfer, D., Schaepman, M.E., 2017. Field and airborne spectroscopy cross validation - some considerations. *IEEE J. Sel. Top. Appl. Earth Obs. Remote Sens.* 1–19. <https://doi.org/10.1109/JSTARS.2016.2593984>
- Hueni, A., Nieke, J., Schopfer, J., Kneubühler, M., Itten, K.I., 2009. The spectral database SPECCHIO for improved long-term usability and data sharing. *Comput. Geosci.* 35, 557–565. <https://doi.org/10.1016/j.cageo.2008.03.015>
- Hueni, A., Tuohy, M., 2010. Spectroradiometer data structuring, pre-processing and analysis – an IT based approach. *J. Spat. Sci.* 51, 93–102.
- Hueni, A., Tuohy, M., 2006. Spectroradiometer data structuring, pre-processing and analysis—an IT based approach. *J. Spat. Sci.* 51, 93–102.

- <https://doi.org/10.1080/14498596.2006.9635084>
- Kokaly, R.F., Clark, R.N., Swayze, G.A., Livo, K.E., Hoefen, T.M., Pearson, N.C., Wise, R.A., Benzal, W.M., Lowers, H.A., Driscoll, R.L., Klein, A.J., 2017. USGS Spectral Library Version 7, U.S. Geological Survey Data Series 1035. <https://doi.org/10.1111/j.1467-9310.1980.tb01113.x>
- Kutser, T., Vahtmäe, E., Paavel, B., Kauer, T., 2013. Removing glint effects from field radiometry data measured in optically complex coastal and inland waters. *Remote Sens. Environ.* 133, 85–89. <https://doi.org/10.1016/j.rse.2013.02.011>
- Malvern Panalytical, 2019. ASD FieldSpec® 4: The industry-leading portable device for field spectroscopy. Malvern Panalytical.
- Milton, E.J., Schaepman, M.E., Anderson, K., Kneubühler, M., Fox, N., 2009. Progress in field spectroscopy. *Remote Sens. Environ.* 113, 92–109. <https://doi.org/10.1016/j.rse.2007.08.001>
- Mobley, C., 1994. *Light and Water: Radiative Transfer in Natural Waters*. Acad. Press.
- Mobley, C.D., 1999. Estimation of the remote-sensing reflectance from above-surface measurements. *Appl. Opt.* 38, 7442. <https://doi.org/10.1364/ao.38.007442>
- Mobley, C.D., Stramski, D., Bissett, W.P., Boss, E., 2004. Optical modeling of ocean waters: Is the case 1 - case 2 classification still useful? *Oceanography* 17, 60–67. <https://doi.org/http://dx.doi.org/10.5670/oceanog.2004.48>
- Mueller, J.L., Morel, A., Frouin, R., Davis, C., Arnone, R., Carder, K., Lee, Z.P., Steward, R.G., Hooker, S., Mobley, C.D., McLean, S., Holben, B., Miller, M., Pietras, C., Knobelspiesse, K.D., Fargion, G.S., Porter, J., Voss, K., 2003. Ocean optics protocols for satellite ocean color sensor validation, Revision 4, Volume III: Radiometric measurements and data analysis protocols. NASA Tech. Memo. 21621 3, 1–78.
- Rast, M., Painter, T.H., 2019. Earth Observation Imaging Spectroscopy for Terrestrial Systems: An Overview of Its History, Techniques, and Applications of Its Missions. *Surv. Geophys.* 40, 303–331. <https://doi.org/10.1007/s10712-019-09517-z>
- Ruddick, K.G., Banks, A.C., Donlob, C., Kuusk, J., Tilstone, G.H., Vabson, V., Vendt, R., 2018. FRM4SOC D-70: Technical Report TR-2, A Review of Commonly Used Fiducial Reference Measurement (FRM) Ocean Colour Radiometers (OCR) used for Satellite Validation. esa fiducial Ref. Meas. Satell. Ocean Color.
- Ruddick, K.G., De Cauwer, V., Park, Y.J., Moore, G., 2006. Seaborne measurements of near infrared water-leaving reflectance: The similarity spectrum for turbid waters. *Limnol. Oceanogr.* 51, 1167–1179. <https://doi.org/10.4319/lo.2006.51.2.1167>
- Ruddick, K.G., Voss, K., Boss, E., Castagna, A., Frouin, R., Gilerson, A., Hieronymi, M., Carol Johnson, B., Kuusk, J., Lee, Z., Ondrusek, M., Vabson, V., Vendt, R., 2019a. A review of protocols for fiducial reference measurements of water-leaving radiance for validation of satellite remote-sensing data over water. *Remote Sens.* 11, 1–27. <https://doi.org/10.3390/rs11192198>
- Ruddick, K.G., Voss, K., Boss, E., Castagna, A., Frouin, R., Gilerson, A., Hieronymi, M., Carol Johnson, B., Kuusk, J., Lee, Z., Ondrusek, M., Vabson, V., Vendt, R., 2019b. A review of protocols for fiducial reference measurements of water-leaving radiance for the validation of satellite remote sensing data over water. *Remote Sens.* 11, 1–38. <https://doi.org/10.3390/rs11192198>
- Ruddick, K.G., Voss, K., Boss, E., Castagna, A., Frouin, R., Gilerson, A., Hieronymi, M., Carol Johnson, B., Kuusk, J., Lee, Z., Ondrusek, M., Vabson, V., Vendt, R., 2019c. A review of protocols for fiducial reference measurements of downwelling irradiance for the validation of satellite remote sensing data over water. *Remote Sens.* 11, 1–27. <https://doi.org/10.3390/rs11192198>
- Schaepman-Strub, G., Schaepman, M.E., Painter, T.H., Dangel, S., Martonchik, J. V., 2006. Reflectance quantities in optical remote sensing—definitions and case studies. *Remote Sens. Environ.* 103, 27–42. <https://doi.org/10.1016/j.rse.2006.03.002>
- Sea-Bird Scientific, 2018. ac-s In-situ spectrophotometer datasheet. Sea-Bird Sci.
- Sea-Bird Scientific, 2013. Spectral Absorption and Attenuation Sensor, ac-s User’s Guide. Sea-Bird Sci. 1–26.
- Seegers, B.N., Stumpf, R.P., Schaeffer, B.A., Loftin, K.A., Werdell, P.J., 2018. Performance

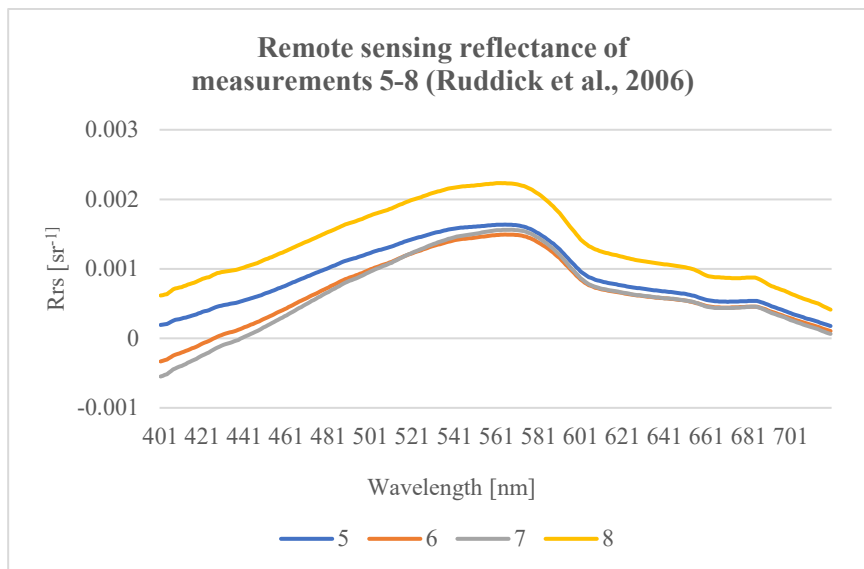
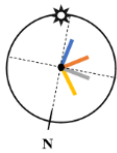
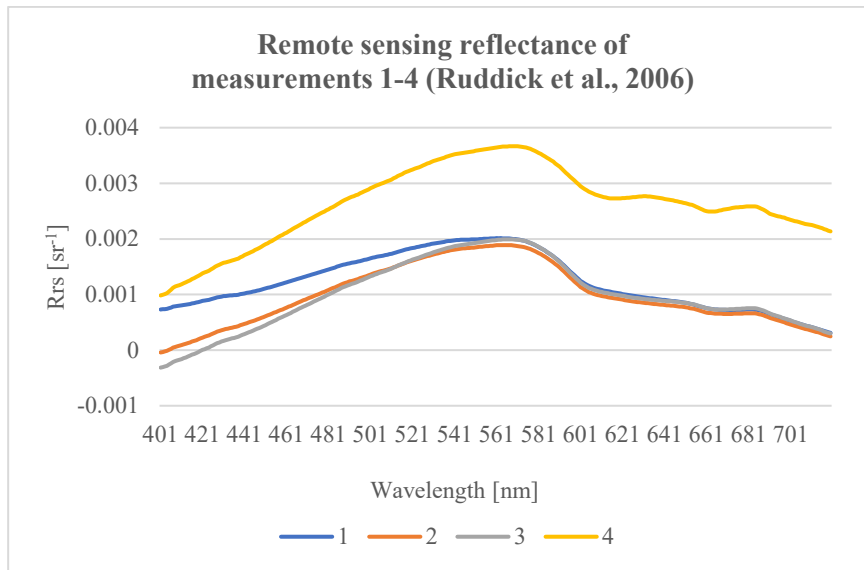
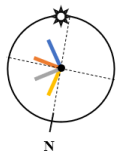
- metrics for the assessment of satellite data products: an ocean color case study. *Opt. Express* 26, 1–19. <https://doi.org/10.1364/oe.26.007404>
- Simis, S.G.H., Olsson, J., 2013. Unattended processing of shipborne hyperspectral reflectance measurements. *Remote Sens. Environ.* 135, 202–212. <https://doi.org/10.1016/j.rse.2013.04.001>
- Simon, A., Shanmugam, P., 2016. Estimation of the spectral diffuse attenuation coefficient of downwelling irradiance in inland and coastal waters from hyperspectral remote sensing data: Validation with experimental data. *Int. J. Appl. Earth Obs. Geoinf.* 49, 117–125. <https://doi.org/10.1016/j.jag.2016.02.003>
- Tilstone, G., Dall’Olmo, G., Brewin, R., Ruddick, K., Vanhellemont, Q., Alikas, K., Vendt, R., Ligi, M., Ansko, I., Kuusk, J., Vabson, V., 2017. FRM4SOC TECHNICAL REPORT (TR-8) ON “PROTOCOLS AND PROCEDURES FOR FIELD INTER-COMPARISONS OF FIDUCIAL REFERENCE MEASUREMENT (FRM) FIELD OCEAN COLOUR RADIOMETERS (OCR) USED FOR SATELLITE VALIDATION ON ATLANTIC MERIDIONAL TRANSECT 27”. esa fiducial Ref. Meas. Satell. Ocean Color 1–28.
- Tilstone, G., Dall’Olmo, G., Hieronymi, M., Ruddick, K., Beck, M., Ligi, M., Costa, M., D’Alimonte, D., Vellucci, V., Vansteenwegen, D., Bracher, A., Wiegmann, S., Kuusk, J., Vabson, V., Ansko, I., Vendt, R., Donlon, C., Casal, T., 2020. Field intercomparison of radiometer measurements for ocean colour validation. *Remote Sens.* 12. <https://doi.org/10.3390/rs12101587>
- TriOS Mess- und Datentechnik GmbH, 2013. MSDA_XE Manual. TriOS Opt. Sensors.
- Vabson, V., Kuusk, J., Ansko, I., Vendt, R., Alikas, K., Ruddick, K., Ansper, A., Bresciani, M., Burmester, H., Costa, M., D’Alimonte, D., Dall’Olmo, G., Damiri, B., Dinter, T., Giardino, C., Kangro, K., Ligi, M., Paavel, B., Tilstone, G., Van Dommelen, R., Wiegmann, S., Bracher, A., Donlon, C., Casal, T., 2019a. Laboratory intercomparison of radiometers used for satellite validation in the 400-900 nm range. *Remote Sens.* 11. <https://doi.org/10.3390/rs11091129>
- Vabson, V., Kuusk, J., Ansko, I., Vendt, R., Alikas, K., Ruddick, K., Ansper, A., Bresciani, M., Burmester, H., Costa, M., D’Alimonte, D., Dall’Olmo, G., Damiri, B., Dinter, T., Giardino, C., Kangro, K., Ligi, M., Paavel, B., Tilstone, G., Van Dommelen, R., Wiegmann, S., Bracher, A., Donlon, C., Casal, T., 2019b. Field intercomparison of radiometers used for satellite validation in the 400-900 nm range. *Remote Sens.* 11. <https://doi.org/10.3390/rs11091129>
- van der Meer, F., 2018. Near-infrared laboratory spectroscopy of mineral chemistry: A review. *Int. J. Appl. Earth Obs. Geoinf.* 65, 71–78. <https://doi.org/10.1016/j.jag.2017.10.004>
- WET Labs, 2007. ECO-VSF 3, Three-angle, Three-wavelength Volume Scattering Function Meter, User’s Guide. WET Labs 1–15.
- WET Labs, 2006. VSF3 Specifications Sheet. WET Labs.
- Zibordi, G., Ruddick, K., Ansko, I., Moore, G., Kratzer, S., Icely, J., Reinart, A., 2012. In situ determination of the remote sensing reflectance: An inter-comparison. *Ocean Sci.* 8, 567–586. <https://doi.org/10.5194/os-8-567-2012>
- Zibordi, G., Talone, M., 2020. On the equivalence of near-surface methods to determine the water-leaving radiance. *Opt. Express* 28, 3200. <https://doi.org/10.1364/oe.28.003200>

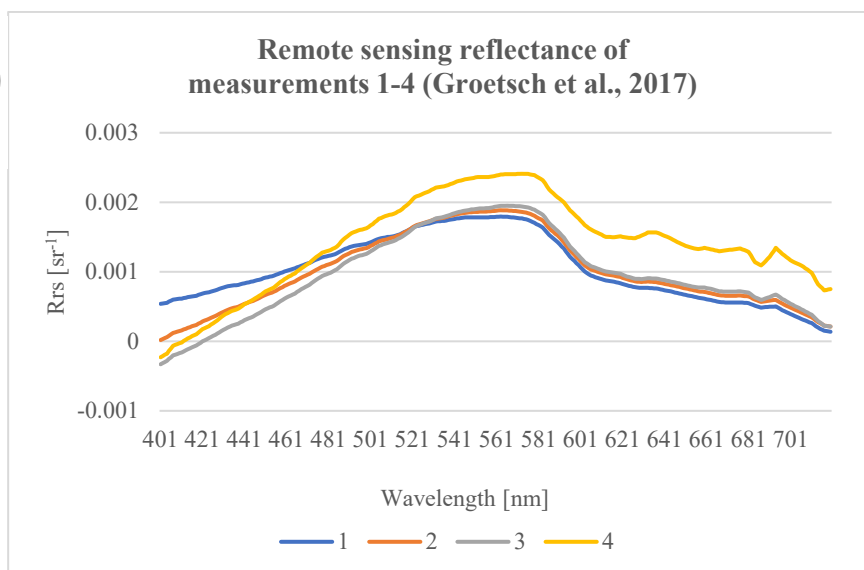
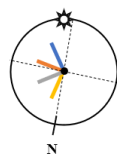
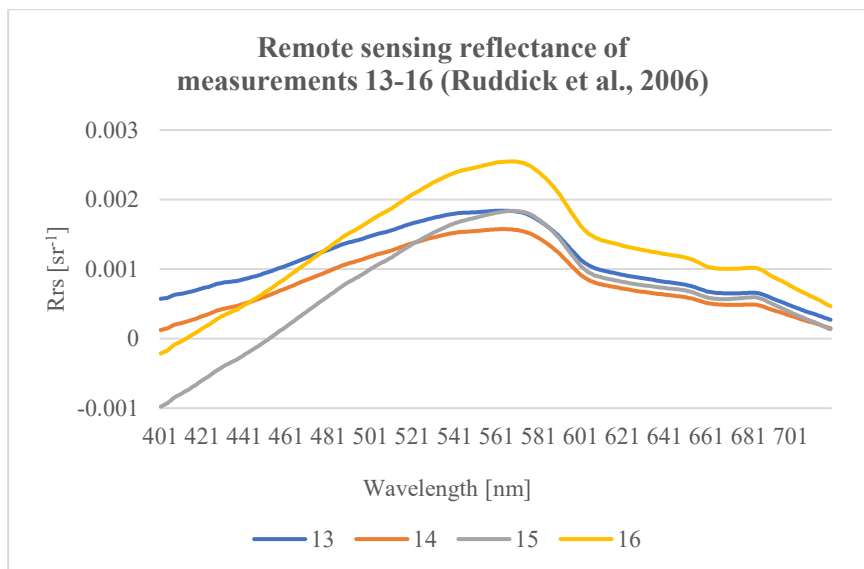
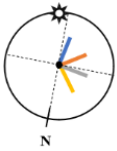
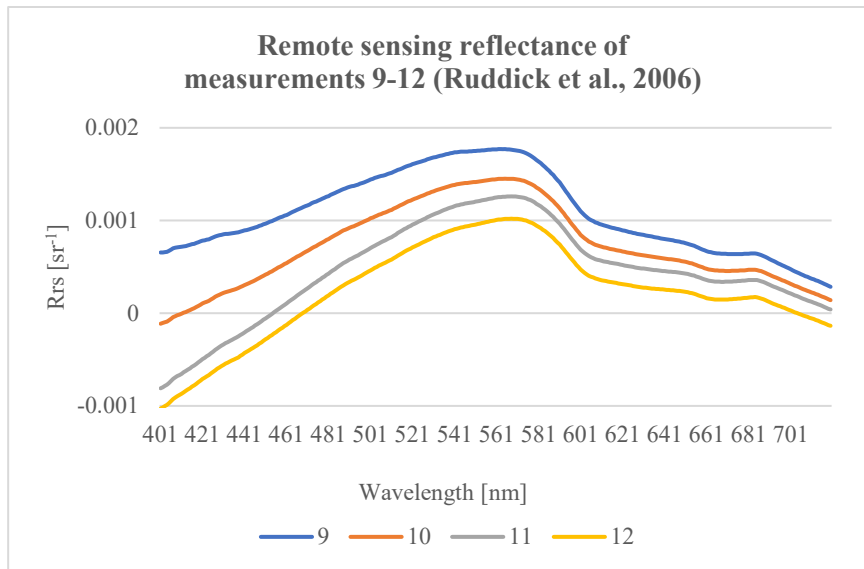
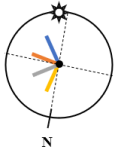
Websites:

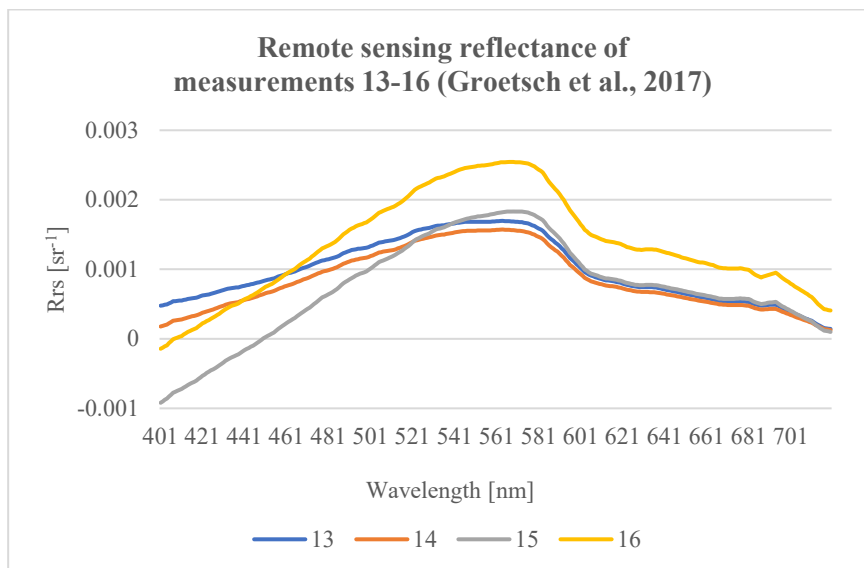
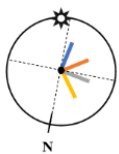
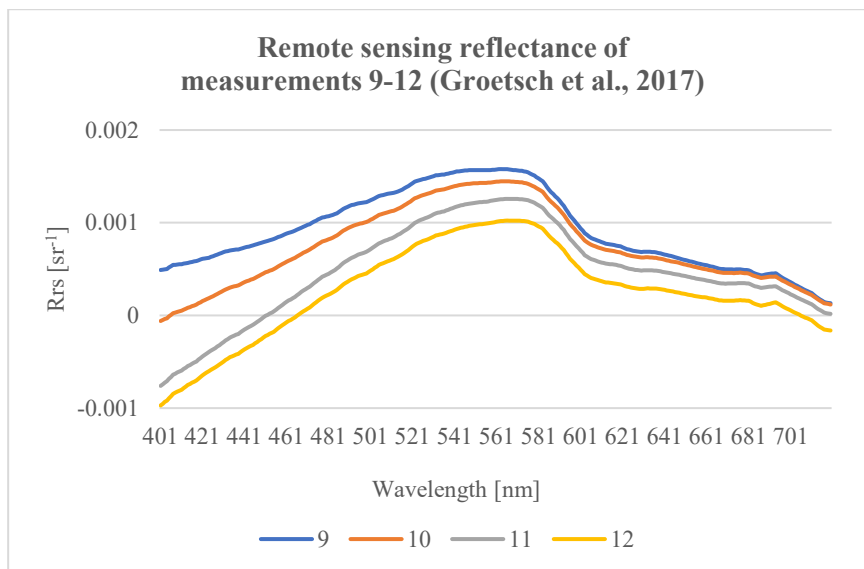
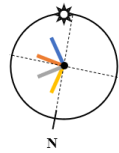
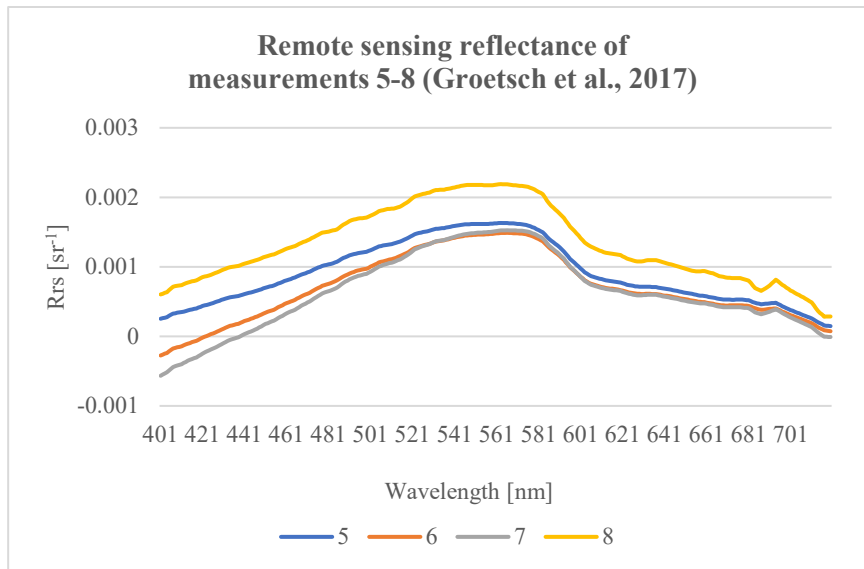
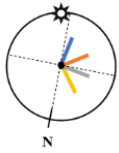
- EUMETSAT Copernicus, n.d. Ocean Colour In situ Database. Available online: <https://ocdb.eumetsat.int> (Accessed on 23 September 2020).
- University of Stirling, n.d. LIMNADES. Available online: https://limnades.stir.ac.uk/Limnades_login/index.php (Accessed on 23 September 2020).
- Water Insight, n.d. WISPweb. Available Online: <https://wispweb.waterinsight.nl> (Accessed on 24 March 2020).

13 Appendix

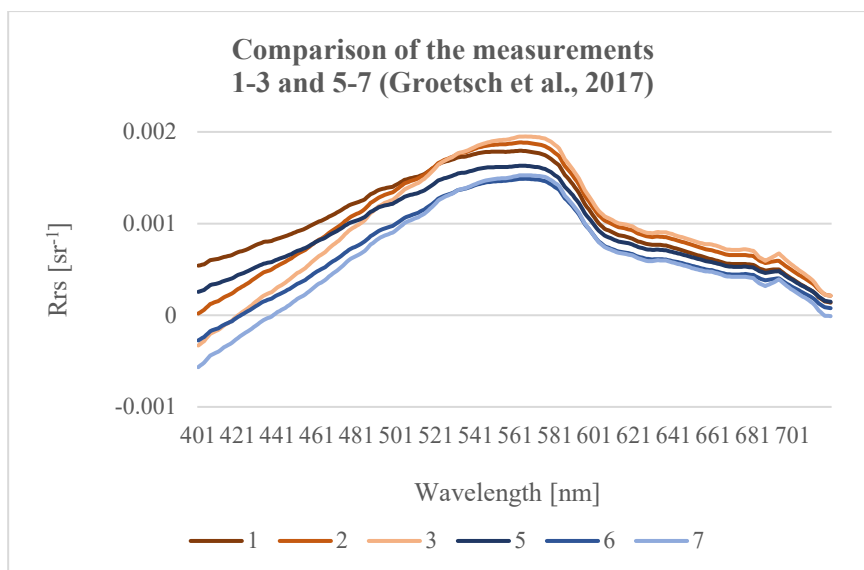
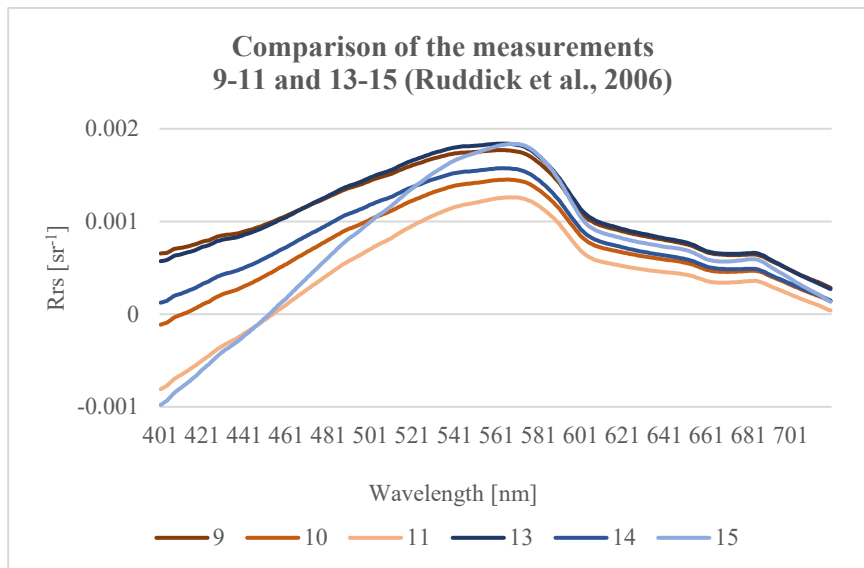
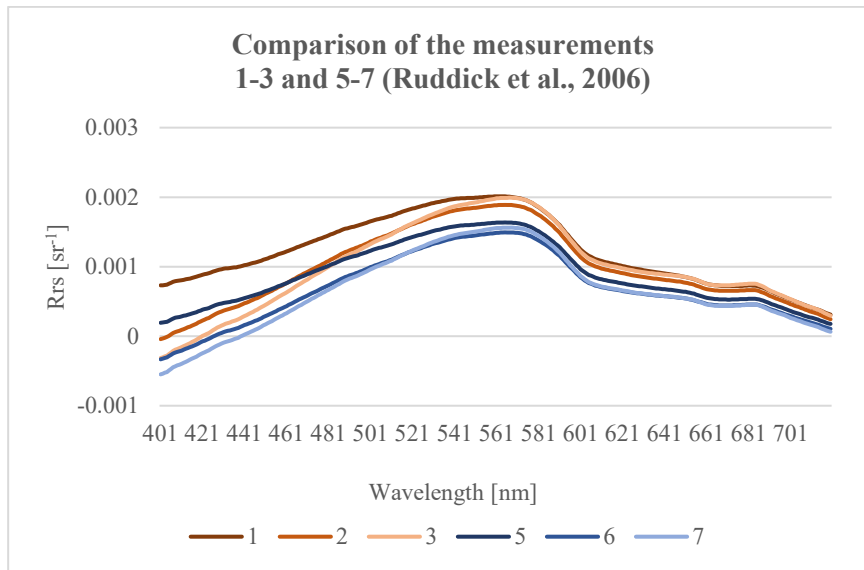
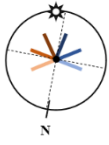
13.1 Outliers

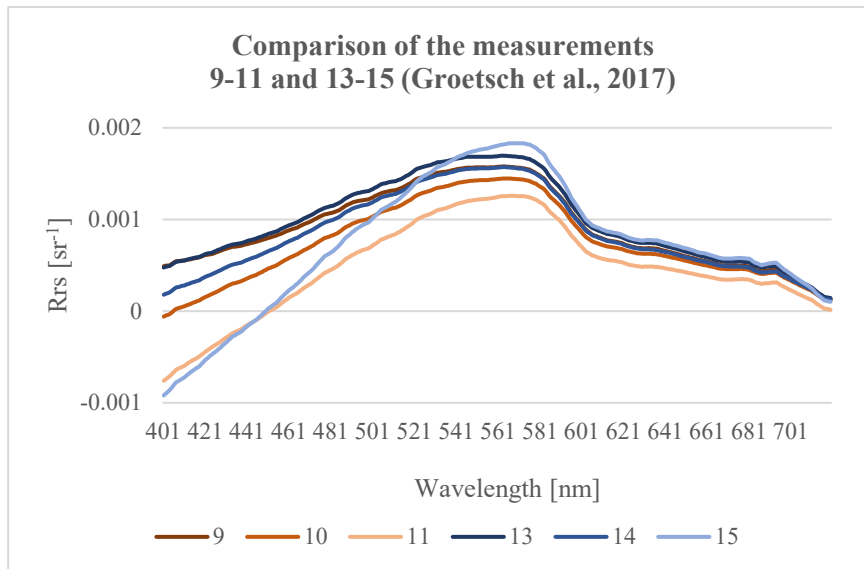




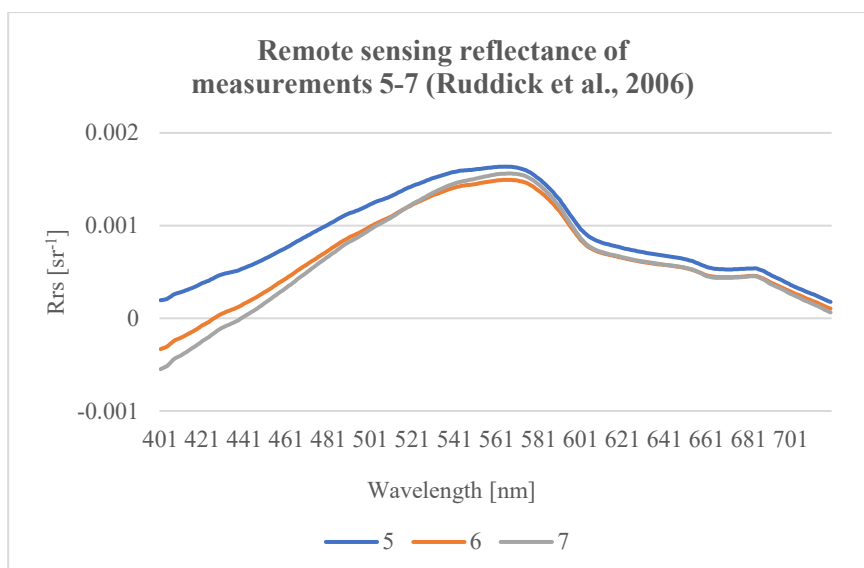
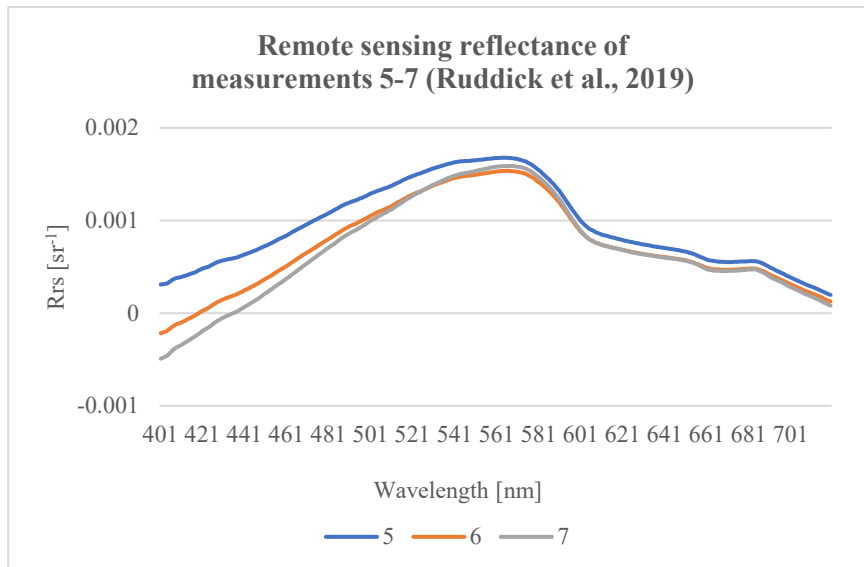
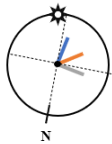


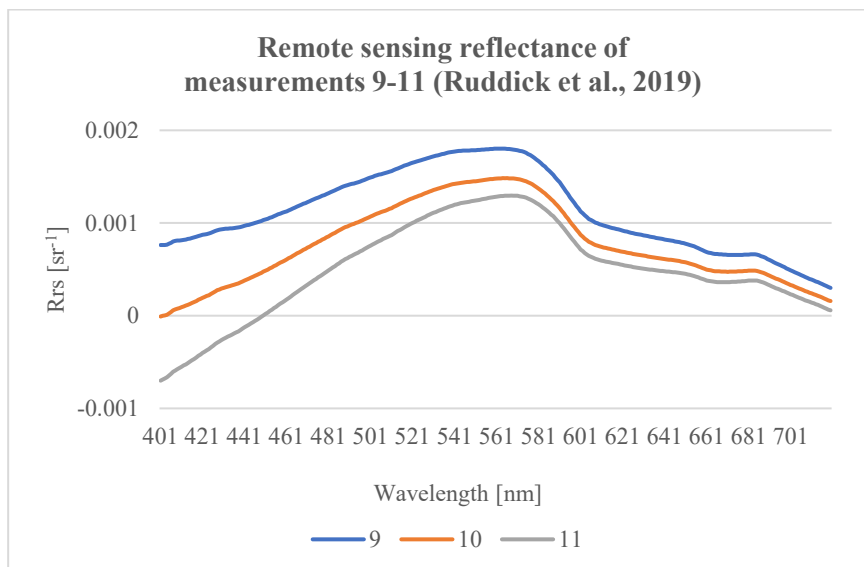
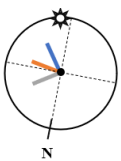
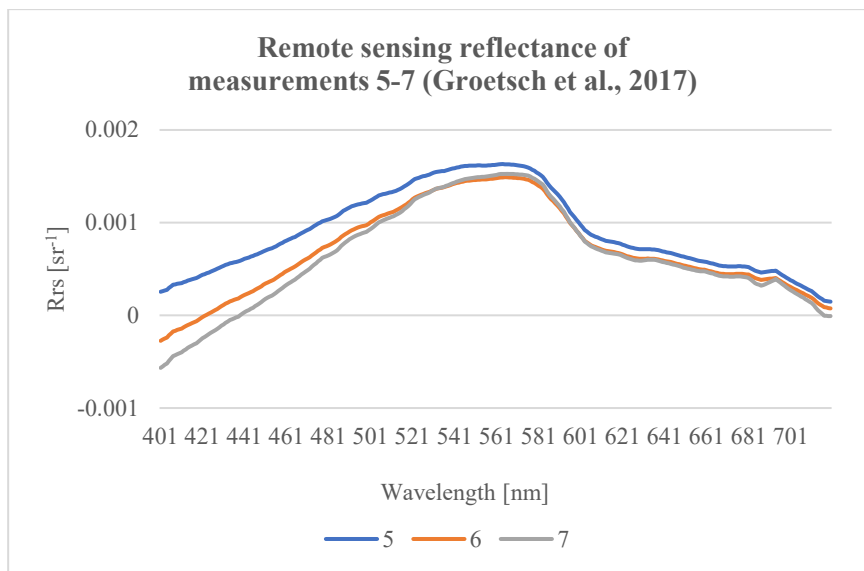
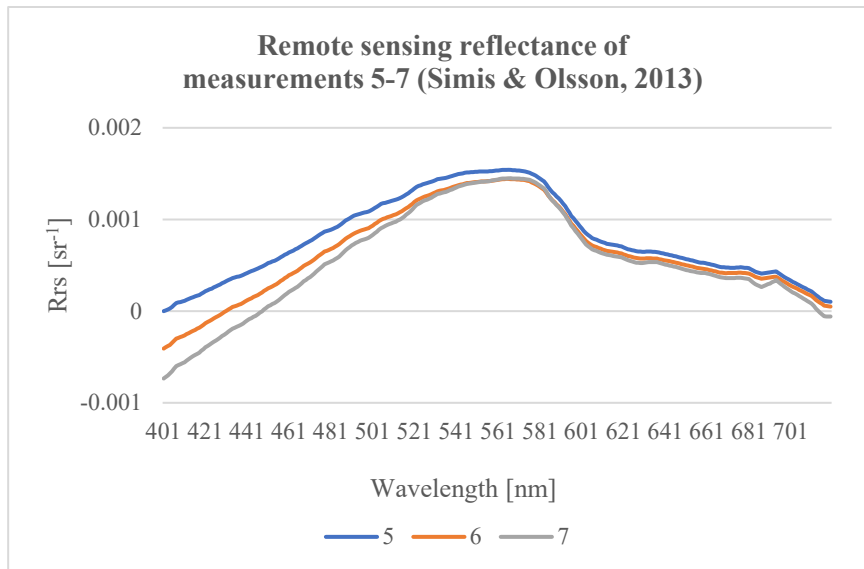
13.2 Measurement conditions

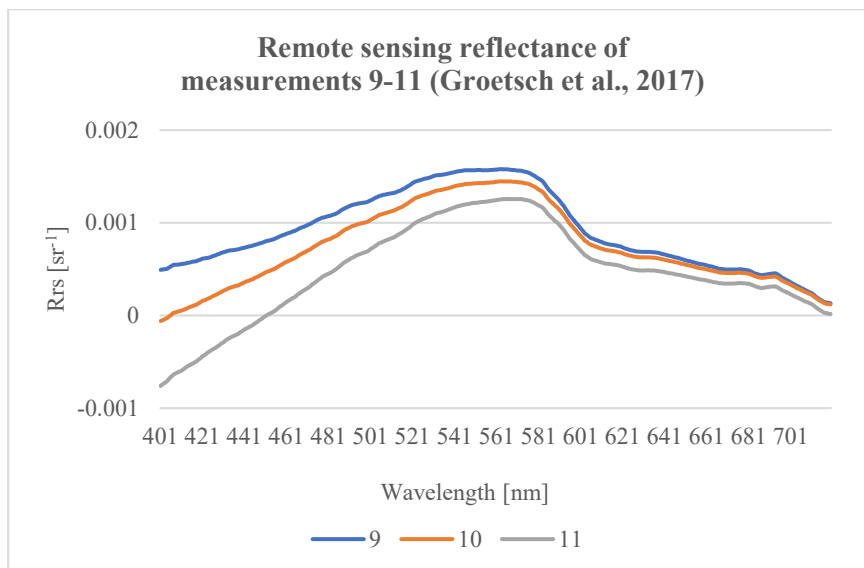
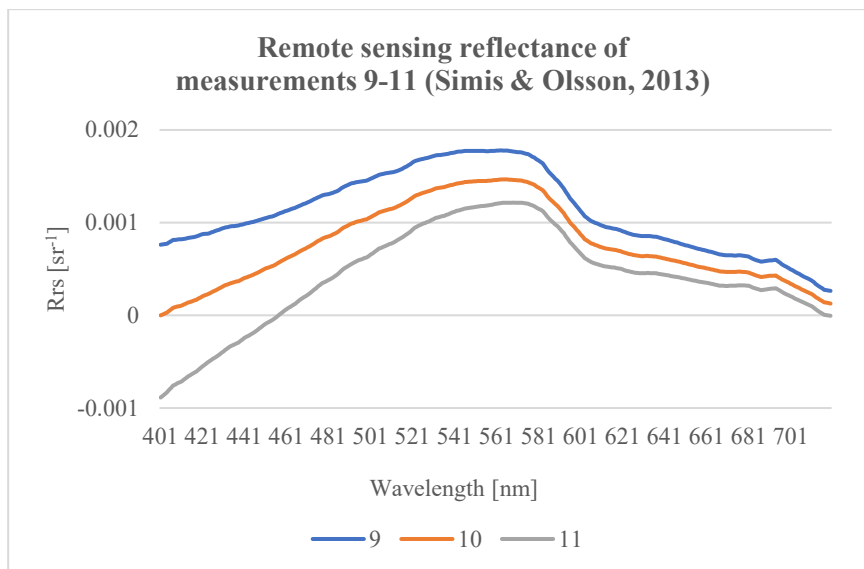
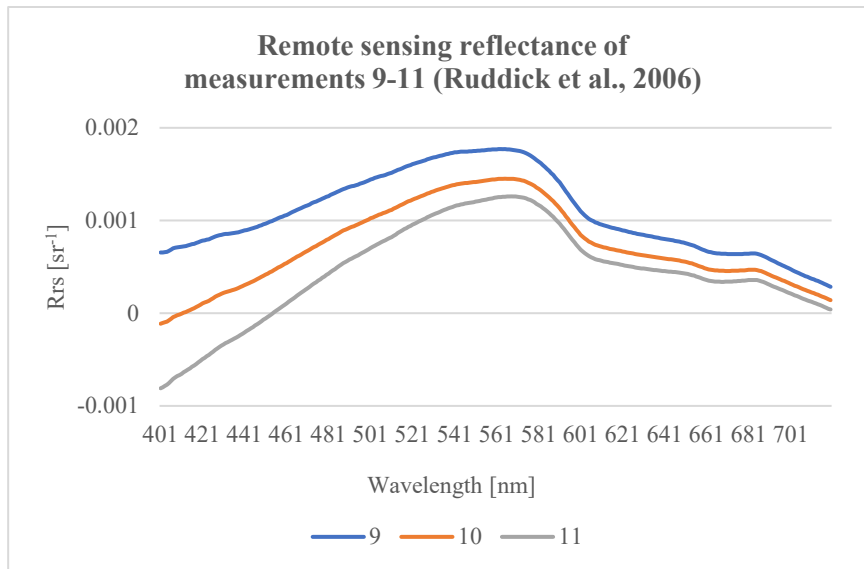


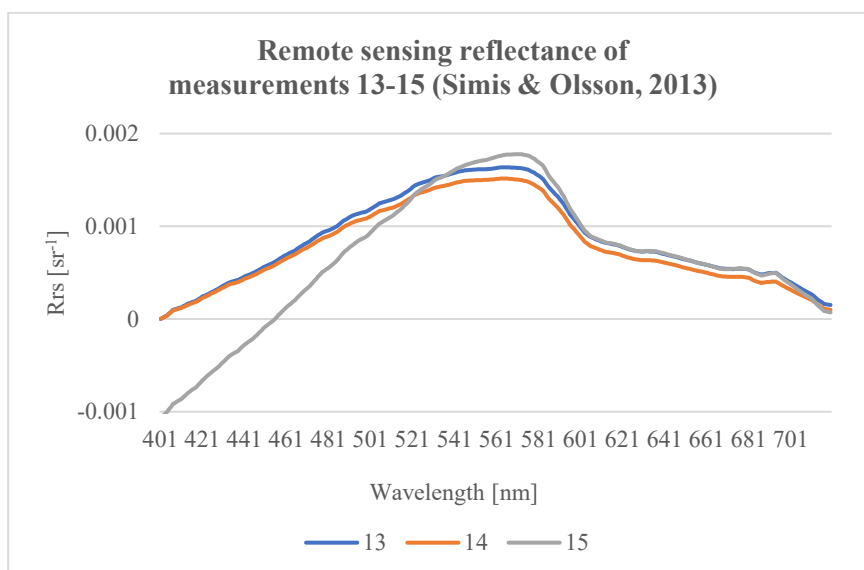
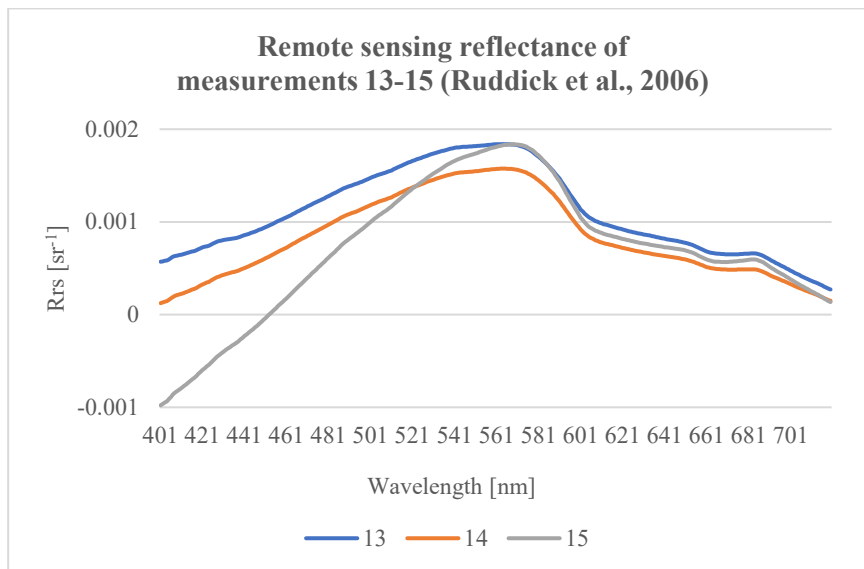
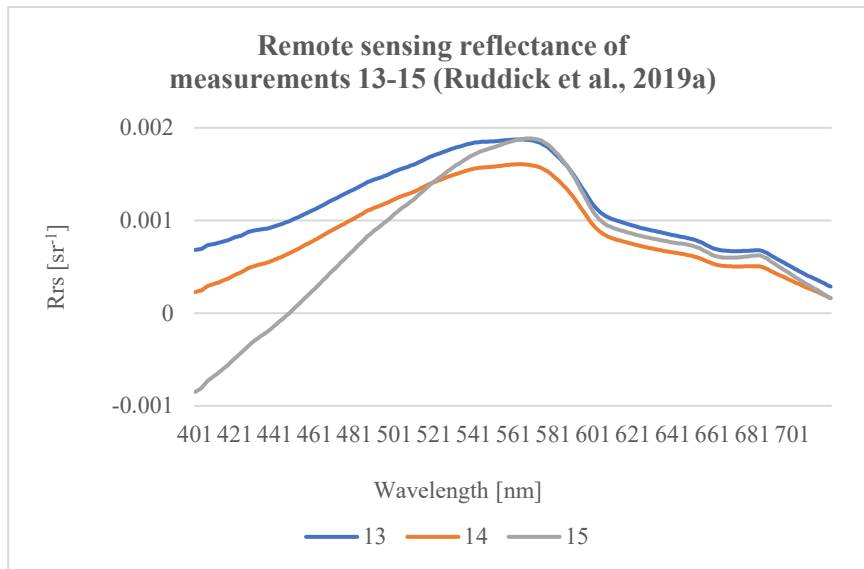
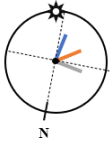


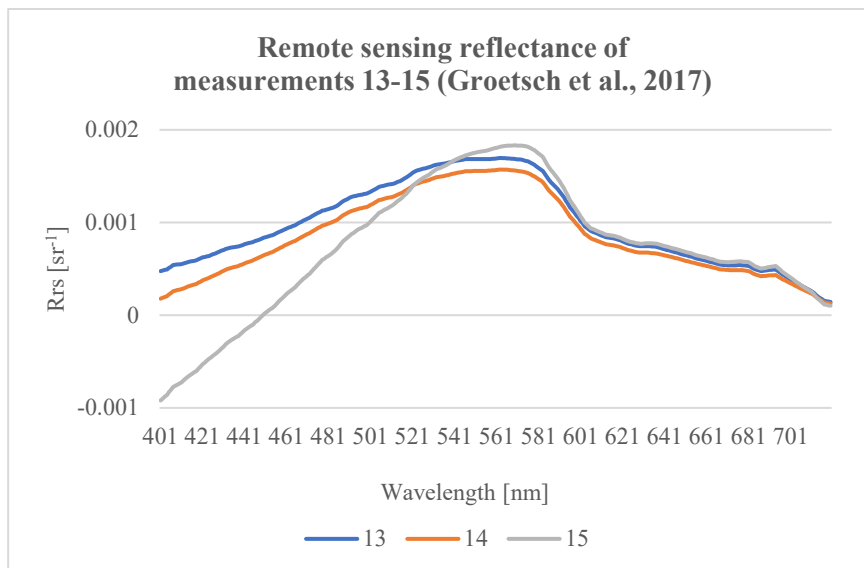
13.3 Processing schemes











Personal Declaration

I hereby declare that the material contained in this thesis is my own original work. Any quotation or paraphrase in this thesis from the published or unpublished work of another individual or institution has been duly acknowledged. I have not submitted this thesis, or any part of it, previously to any institution for assessment purposes.

Zürich, 30. 09. 2020